

GOLD COMPLEXES OBTAINED FROM GOLD YLIDE PREPARATIONS

by

KAROLIEN COETZEE

Thesis presented in fulfilment of the requirements for the degree of



at the

UNIVERSITY OF STELLENBOSCH

Supervisor: Prof H. G. Raubenheimer

Co-supervisor: Dr S. Cronje

April 2005

Declaration

I, the undersigned, hereby declare that the work contained in this thesis is my own original work and that I have not previously in its entirety or in part submitted it at any university for a degree.

Signature:

Date:

OPSOMMING

Hierdie studie behels die sintese en karakterisering van nuwe fosfoniumylid goud(I)-komplekse en ander verbindings wat gedurende koördinasiereaksies vorm. Sulke komplekse kan sinergisme tussen twee farmakologies-aktiewe entiteite (goud(I) en fosfoniumylid) om 'n meer aktiewe verbinding te vorm meebring.

Vier fosfoniumsoute is berei, $[\text{C}_6\text{H}_5\text{CH}_2\text{PPh}_3]\text{Br}$ (**1**), $[\text{Ph}_3\text{P}(\text{CH}_2)_3\text{PPh}_3]\text{Br}_2$ (**2a**), *p*- $[\{\text{Ph}_3\text{PCH}_2\}_2\text{C}_6\text{H}_4]\text{Br}_2$ (**3a**) en *m*- $[\{\text{Ph}_3\text{PCH}_2\}_2\text{C}_6\text{H}_4]\text{Br}_2$ (**4a**), deur PPh_3 met die ooreenstemmende alkielbromiedes te reageer. Die ^{13}C - en ^1H - KMR-spektra van dié verbindings toon dat 'n aantal kerne in aromatiese ringe magneties onekwivalent is. Normaalweg is die koolstowwe in PPh_3 -eenhede ekwivalent, maar meervoudige, oorvleuelende pieke het nou getoon dat die ooreenstemmende *orto*-, *meta*- en *para*-koolstof sowel as die ooreenstemmende protonkerne in verskillende magnetiese omgewings voorkom. Die kristalstrukture van die soute **3a** en **4a** hierbo is met behulp van X-straal tegnieke bepaal.

Verskillende metodes is gevolg om die fosfoniumsoute te deprotoneer na die ooreenstemmende ylide en om die ylide dan aan goud-bevattende uitgangstowwe te probeer koördineer. Die meeste reaksies het nie-skeibare mengsels gevorm en enkelprodukte kon nie in groot genoeg konsentrasies geïsoleer word om hulle afsonderlik te karakteriseer nie. Kristalle vir X-straal kristalstruktuur bepaling is verkry. Die produk mengsels is gekarakteriseer met behulp van ^1H -, ^{13}C - en ^{31}P - KMR-spektroskopie en massaspektrometrie. Karakteristieke veranderinge in chemiese verskuiwings na laer veldsterktes vir die koolstof en fosfor kerne is waargeneem na koördinasie van die ylide aan Au(I), terwyl die protone na hoër veldsterktes verskuif het.

Die reaksie tussen $(\text{C}_6\text{F}_5)\text{Au}(\text{tbt})$ (tetrahidrotiofeen) en soute **1** – **4a** gevolg deur deprotonering, vorm die goud-ylidkomplekse $[\text{C}_6\text{H}_5\text{CH}(\text{AuC}_6\text{F}_5)\text{PPh}_3]$ (**5**), $[\{\text{Ph}_3\text{PCH}(\text{AuC}_6\text{F}_5)\}_2\text{CH}_2]$ (**6**), *p*- $[\{\text{Ph}_3\text{PCH}(\text{AuC}_6\text{F}_5)\}_2\text{C}_6\text{H}_4]$ (**8**), en *m*- $[\{\text{Ph}_3\text{PCH}(\text{AuC}_6\text{F}_5)\}_2\text{C}_6\text{H}_4]$ (**9**). Die kristalstrukture van komplekse **5** en **9** het al die molekulêre interaksies daarin blootgelê.

Deprotonering van **4a** met n-BuLi, gevolg deur reaksie met (C₆F₅)Au(tht) lewer komplekse **9** en [(Ph₃PCH₂)₂C₆H₄][BrAuC₆F₅]₂ (**10**). Die kristal- en molekulêre struktuur van kompleks **10** is bepaal. Twee aurosikliese verbindings, [μ-((Ph₃PCH)₂CH₂)₂Au₂][BF₄]₂ (**12**) en [μ-((Ph₃PCH)₂C₆H₄)₂Au₂][BF₄]₂ (**13**) is gesintetiseer deur gedeprotoneerde bisyliede verkry van **2b** en **3b** met substitusie van tht aan die ClAu-eenheid te koördineer.

Reaksieprosedures waarin Ag₂O vir deprotonering van die fosfoniumsoute **2a**, **3a** en **4a** gebruik is, het tot mengsels van produkte aanleiding gegee. Enkelkristalle van komplekse [Ph₃PCH(AuC₆F₅)C₆H₄CH₃] (**14**), [C₆F₅Au(tht)] (**15**) en [(C₆F₅)₂Au][(Ph₃PCH₂)₂C₆H₄] (**16**) is geïsoleer uit die reaksies en kristalstruktuurbevestigings is uitgevoer. Die molekulêre struktuur van **15** toon ongewone aurofiliese interaksies en verteenwoordig die eerste voorbeeld van 'n lineêre goudketting; met goud...goud afstande wat sistematies varieër tussen 3.13Å, 3.31Å en 3.20Å.

Sout **2b** is met Ph₃PAu(acac) gereageer om die gewenste produk, [(Ph₃PCH(AuPPh₃))₂CH₂](BF₄)₂ (**19**), saam met [CH₃C(O)C(AuPPh₃)₂C(O)CH₃] (**17**) en ander byprodukte te vorm. Verbinding **17** is as enkelkristalle X-straalkristallografies gekarakteriseer.

Die fluorobifeniel goud(I)-komplekse, 4,4'-[(AuPPh₃)₂C₁₂F₈] (**21**) en 2,2'-[(AuPPh₃)₂C₁₂F₈] (**22**), is gesintetiseer deur koördinasie van AuPPh₃ aan die gelitiseerde 2,2'-dibromooktafluorobifeniel en 4,4'-dibromooktafluorobifeniel respektiewelik. Die molekulêre struktuur van **21** het getoon dat een van die C-Au-P bindingshoeke met 12.5° afwyk van 180°, waarskynlik as gevolg van π-interaksie van die tetrafluorofenielringe en die steriese vereistes van die groot PPh₃-eenhede. Die ander C-Au-P bindingshoek is lineêr [177.9(3)°].

SUMMARY

This investigation comprised the synthesis and characterisation of new Au(I) phosphonium ylide complexes and other compounds formed during coordination reactions. These complexes could exploit the synergism between two pharmacologically active substances (gold complex unit and phosphorus ylide) to furnish an even more active substance.

Four phosphonium salts were prepared, $[\text{C}_6\text{H}_5\text{CH}_2\text{PPh}_3]\text{Br}$ (**1**), $[\text{Ph}_3\text{P}(\text{CH}_2)_3\text{PPh}_3]\text{Br}_2$ (**2a**), *p*- $[\{\text{Ph}_3\text{PCH}_2\}_2\text{C}_6\text{H}_4]\text{Br}_2$ (**3a**) and *m*- $[\{\text{Ph}_3\text{PCH}_2\}_2\text{C}_6\text{H}_4]\text{Br}_2$ (**4a**), by reacting PPh_3 with the corresponding alkylbromides. The ^{13}C and ^1H NMR spectra of the compounds **1** – **4a** indicated that many of the nuclei are magnetically inequivalent. The aromatic units in PPh_3 are normally identical, but multiple, overlapping signals proved that the corresponding *ortho*, *meta* and *para* carbon and proton nuclei are in magnetically different environments from each other. Single crystal structures of salts **3a** and **4a** were determined.

Different methods were followed to deprotonate the phosphonium salts to afford the corresponding ylides and to coordinate the ylides to gold precursor compounds. Most of the reactions yielded inseparable mixtures of products and pure compounds could not be isolated in large enough quantities for characterisation by all physical methods. Sufficient crystals for structure determination by X-ray diffraction were obtained. The product mixtures were characterised by ^1H , ^{13}C and ^{31}P NMR spectroscopy and mass spectrometry. Characteristic downfield chemical shift changes after coordination of the ylides to Au(I) were observed for the carbon and phosphorus nuclei, while the protons displayed upfield shifts.

Reaction of $(\text{C}_6\text{F}_5)\text{Au}(\text{tht})$ with the salts **1** – **4a**, and subsequent deprotonation yielded the gold(I) ylide complexes $[\text{C}_6\text{H}_5\text{CH}(\text{AuC}_6\text{F}_5)\text{PPh}_3]$ (**5**), $[\{\text{Ph}_3\text{PCH}(\text{AuC}_6\text{F}_5)\}_2\text{CH}_2]$ (**6**), *p*- $[\{\text{Ph}_3\text{PCH}(\text{AuC}_6\text{F}_5)\}_2\text{C}_6\text{H}_4]$ (**8**), and *m*- $[\{\text{Ph}_3\text{PCH}(\text{AuC}_6\text{F}_5)\}_2\text{C}_6\text{H}_4]$ (**9**). The crystal and molecular structures of compounds **5** and **9** were determined.

Deprotonation of **4a** with n-BuLi, followed by reaction with (C₆F₅)Au(tht) yielded complexes **9** and [(Ph₃PCH₂)₂C₆H₄][BrAuC₆F₅]₂ (**10**). The crystal structure of compound **10** was determined. Two aurocyclic compounds, [μ-((Ph₃PCH)₂CH₂)₂Au₂][BF₄]₂ (**12**) and [μ-((Ph₃PCH)₂C₆H₄)₂Au₂][BF₄]₂ (**13**) were synthesised by deprotonating salts **2b** and **3b** with n-BuLi and subsequently reacting the corresponding bisylides with ClAu(tht).

Reaction procedures in which Ag₂O was used as deprotonating agent for the phosphonium salts **2a**, **3a** and **4a**, yielded mixtures of products. Single crystals of complexes *m*-[Ph₃PCH(AuC₆F₅)C₆H₄CH₃] (**14**), [C₆F₅Au(tht)] (**15**) and [(C₆F₅)₂Au][(Ph₃PCH₂)₂C₆H₄] (**16**) were isolated from the reaction mixtures and subjected to X-ray crystal structure determination. The molecular structure of **15** exhibited unusual aurophilic interactions and represents the first example of a linear gold chain in which the gold...gold distances systematically alternate between 3.13Å, 3.31Å and 3.20Å.

Salt **2b** was reacted with Ph₃PAu(acac) to afford the desired compound, [(Ph₃PCH(AuPPh₃))₂CH₂](BF₄)₂ (**19**), along with [CH₃C(O)C(AuPPh₃)₂C(O)CH₃] (**17**) and some byproducts. Compound **17** was characterised by single crystal X-ray diffraction.

The fluorobiphenylgold(I) complexes, 4,4'-[(AuPPh₃)₂C₁₂F₈] (**21**) and 2,2'-[(AuPPh₃)₂C₁₂F₈] (**22**) were synthesised by reaction of ClAuPPh₃ with the lithiated 2,2'-dibromooctafluorobiphenyl and 4,4'-dibromooctafluorobiphenyl respectively. The molecular structure of **21** revealed that one of the C–Au–P bond angles deviates from linearity by 12.5°, probably as a result of π-stacking of the tetrafluorophenyl rings and steric requirements of the bulky PPh₃ units. The other C–Au–P bond angle is linear [177.9(3)°].

Francois

ACKNOWLEDGEMENTS

I would like to express my sincerest gratitude to all who have guided, advised and supported me during the presented study. In particular I would like to thank the following people and institutions:

Our Heavenly Father for countless blessings.

My family, Francois and his parents for their prayers, love and support.

Stephanie for extra trouble gone through, understanding, sacrifices and encouragement to do my best.

Prof Raubenheimer for guidance and support.

Elsa Malherbe and Jean McKenzie for the recording of excellent NMR spectra. In particular I would like to thank Jean for the interpretation of complicated coupling patterns of signals in the NMR spectra.

Mr B. Barnard, Prof L. J. Barbour and Dr C. Esterhuizen for the recording of crystal data and patient support in solving some of the structures.

Dr C. Meyer and Mr J. S. Malherbe for advice on the synthesis of the phosphonium salts.

All my colleagues who worked with me in the laboratory during this study. You made this study a pleasant journey.

Mintek and the NRF for financial support.

ABBREVIATIONS

Å		Angström (10^{-10} m)
acac		Acetylacetonato
Bu		Butyl
Δ		Difference between two values
Et		Ethyl
L		Ligand
M		Metal
M ⁺		Molecular ion
Me		Methyl
MS		Mass Spectrometry
m/z		Mass/charge
NMR		Nuclear Magnetic Resonance
NMR:	δ	Chemical shift in ppm
	br	Broad
	d	Doublet
	dd	Doublet of doublets
	dm	Doublet of multiplets
	ddm	Doublet of doublet of multiplets
	J	Coupling constant
	m	Multiplet
	s	Singlet
	t	Triplet
Ph		Phenyl
PPh ₃		Triphenylphosphine
ppm		Parts per million
R		Alkyl/Aryl group

THF

Tetrahydrofuran

tth

Tetrahydrothiophene

Different aspects of the work in this study have been presented in the form of:

Presentations and lectures:

Two presentations at Mintek's Gold biomedical research and development presentation days, 19 June 2003 and 11 June 2004.

A lecture presented by Prof. H. G. Raubenheimer at various European Universities: Gold chemistry: unique and challenging.

Posters:

A poster at the SACI Inorganic Chemistry Conference in Pretoria, 8 – 11 June 2003 and the Cape organometallic symposium at Morgenhof, Stellenbosch, 30 October 2003. Gold(I) usage in medicine, U. E. I. Horvath, W. F. Gabrielli, K. Coetzee, S. Cronje, M. Esterhuizen and H. G. Raubenheimer.

A poster at the Cape Organometallic Symposium in Cape Town at the Waterfront, 28 October 2004. Gold(I) a versatile coordination center, U. E. I. Horvath, W. F. Gabrielli, K. Coetzee, T. K. Hagos, S. Cronje and H. G. Raubenheimer

CONTENTS

OPSOMMING	i
SUMMARY	iii
ACKNOWLEDGEMENTS	vi
ABBREVIATIONS	vii
CONTENTS	x

CHAPTER 1

Introduction and aims

1.1	Introduction	1
1.2	Phosponium salts as anti-cancer agents	3
1.3	Gold(I) phosphorus ylide complexes	6
1.4	Biphenyl complexes	16
1.5	Aims and objectives of the present investigation	17

CHAPTER 2

Synthesis and characterisation of phosphonium precursors and gold(I) compounds

2.1	Introduction	19
2.2	Results and discussion	20
2.2.1	Preparation of benzyltriphenylphosphoniumbromide (1), 1,3-bis(triphenylphosphino)propanedibromide (2a), [1,4-phenylenebis(methylene)bis(triphenylphosphonium)]di- bromide (3a) and [1,3-phenylenebis(methylene)bis(triphenyl- phosphonium)]dibromide (4a)	22
2.2.2	Spectroscopic characterisation of compounds 1 - 4a	24
2.2.3	Preparation of [Ph ₃ P(Ph)CHAu(C ₆ F ₅)] (5), [Ph ₃ PCH(AuC ₆ F ₅)CH ₂ CH(AuC ₆ F ₅)PPh ₃] (6), <i>p</i> -[(C ₆ F ₅)AuCH(PPh ₃)C ₆ H ₄ CH(PPh ₃)Au(C ₆ F ₅)] (8) and <i>m</i> -[(C ₆ F ₅)AuCH(PPh ₃)C ₆ H ₄ CH(PPh ₃)Au(C ₆ F ₅)] (9)	31
2.2.4	Spectroscopic characterisation of compounds 5 - 9	34

2.2.5	Preparation of $[\text{Ph}_3\text{PCH}(\text{AuC}_6\text{F}_5)\text{C}_6\text{H}_4\text{CH}(\text{AuC}_6\text{F}_5)\text{PPh}_3]$ (9), by deprotonation of the phosphonium salt 4b with n-BuLi	43
2.2.6	Spectroscopic characterisation of compounds 9 , 10 and 11b	45
2.2.7	Preparation of $[\mu\text{-(Ph}_3\text{PCHCH}_2\text{CHPPh}_3)_2\text{Au}_2][\text{BF}_4]_2$ (12) and $[\mu\text{-(Ph}_3\text{PCHC}_6\text{H}_4\text{CHPPh}_3)_2\text{Au}_2][\text{BF}_4]_2$ (13)	49
2.2.8	Spectroscopic characterisation of compounds 12 and 13	51
2.2.9	Attempted preparation of 9 , and formation of 11a and two other products 14 and 15 , by deprotonation of the phosphonium salt with Ag_2O	57
2.2.10	Spectroscopic characterisation of compounds 9 , 11a , 14 and 15	59
2.2.11	Preparation of 6 , 8 and 9 by deprotonation of the phosphonium salt with Ag_2O	62
2.2.12	Spectroscopic characterisation of the mixture containing compounds 3a , 6 , 9 , 14 and 16	64
2.2.13	Attempted preparation of the dinuclear complex, $[\text{PPh}_3\text{CH}(\text{AuPPh}_3)\text{CH}_2\text{CH}(\text{AuPPh}_3)\text{PPh}_3][\text{BF}_4]_2$ (19)	66
2.2.14	Spectroscopic characterisation of compounds 17 , 18 , 19 and 20	67
2.2.15	Preparation of 4,4'- $[(\text{AuPPh}_3)_2\text{C}_{12}\text{F}_8]$ (21) and 2,2'- $[(\text{AuPPh}_3)_2\text{C}_{12}\text{F}_8]$ (22)	71
2.2.16	Spectroscopic characterisation of compounds 21 and 22	72
2.3	Conclusions and future work	75
2.4	Experimental	79
2.4.1	Materials	79
2.4.2	Preparation of benzyltriphenylphosphoniumbromide (1)	80
2.4.3	Preparation of 1,3-bis(triphenylphosphino)propanedibromide (2a)	80
2.4.4	Preparation of [1,4-phenylenebis(methylene)bistriphenyl- phosphonium]dibromide (3a)	81
2.4.5	Preparation of [1,3-phenylenebis(methylene)bistriphenyl- phosphonium]dibromide (4a)	81
2.4.6	Preparation of $[\text{Ph}_3\text{P}(\text{Ph})\text{CHAu}(\text{C}_6\text{F}_5)]$ (5)	81
2.4.7	Preparation of $[\text{Ph}_3\text{PCH}(\text{AuC}_6\text{F}_5)\text{CH}_2\text{CH}(\text{AuC}_6\text{F}_5)\text{PPh}_3]$ (6) and $[\text{Ph}_3\text{PCH}(\text{AuC}_6\text{F}_5)\text{CH}_2\text{CH}_2\text{PPh}_3]$ (7)	82

2.4.8	Preparation of [<i>p</i> -(C ₆ F ₅)AuCH(PPh ₃)C ₆ H ₄ CH(PPh ₃)Au(C ₆ F ₅)] (8)	82
2.4.9	Preparation of [<i>m</i> -(C ₆ F ₅)AuCH(PPh ₃)C ₆ H ₄ CH(PPh ₃)Au(C ₆ F ₅)] (9)	83
2.4.10	Preparation of 9 , [C ₆ F ₅ AuBr] ₂ [<i>m</i> -Ph ₃ PCH ₂ C ₆ H ₄ CH ₂ PPh ₃] (10) and [<i>m</i> -(C ₆ F ₅)AuCH(PPh ₃)C ₆ H ₄ CH ₂ (PPh ₃)] (11b)	83
2.4.11	Preparation of [μ-(Ph ₃ PCHCH ₂ CHPPh ₃) ₂ Au ₂][BF ₄] ₂ (12)	84
2.4.12	Preparation of [μ-(Ph ₃ PCHC ₆ H ₄ CHPPh ₃) ₂ Au ₂][BF ₄] ₂ (13)	84
2.4.13	Preparation of 9 , 11a , [CH ₃ C ₆ H ₄ CH(AuC ₆ F ₅)PPh ₃] (14) and [(C ₆ F ₅)Au(tht)] _n (15)	85
2.4.14	Preparation of 6 and 14 with Ag ₂ O	85
2.4.15	Preparation of 9 with Ag ₂ O	86
2.4.16	Preparation of [(C ₆ F ₅)Au(C ₆ F ₅)] ₂ [<i>p</i> -Ph ₃ PCH ₂ C ₆ H ₄ CH ₂ PPh ₃] (16)	86
2.4.17	Preparation of [CH ₃ C(O)C(AuPPh ₃) ₂ C(O)CH ₃] (17), [CH ₃ C(O)CH(AuPPh ₃)C(O)CH ₃] (18), [PPh ₃ CH(AuPPh ₃)CH ₂ CH(AuPPh ₃)PPh ₃][BF ₄] ₂ (19) and [Ph ₃ PCH(AuPPh ₃)CH ₂ CH ₂ PPh ₃] (20)	86
2.4.18	Preparation of 4,4'-[(AuPPh ₃) ₂ C ₁₂ F ₈] (21)	87
2.4.19	Preparation of 2,2'-[(AuPPh ₃) ₂ C ₁₂ F ₈] (22), [C ₆ F ₄ (AuPPh ₃)Br] (23) and 2,2'-[(AuPPh ₃)C ₁₂ F ₈ Br] (24)	87

CHAPTER 3

X-ray crystallographic structure determinations

3.1	Introduction	88
3.2	Results and discussion	88
3.2.1	Crystal and molecular structure of [1,4-phenylenebis(methylene)]bis(triphenylphosphonium)- dibromide (3a)	88
3.2.2	Crystal and molecular structure of [1,3-phenylenebis(methylene)]bis(triphenylphosphonium)- dibromide (4a)	93
3.2.3	Crystal and molecular structure of [(C ₆ F ₅)AuCH(Ph)PPh ₃] (5)	97
3.2.4	Crystal and molecular structure of <i>m</i> -[Ph ₃ PCH(C ₆ F ₅ Au)C ₆ H ₄ (AuC ₆ F ₅)CHPPh ₃] (9)	101
3.2.5	Crystal and molecular structure of	

	$[\text{C}_6\text{F}_5\text{AuBr}]_2[m\text{-Ph}_3\text{PCH}_2(\text{C}_6\text{H}_4)\text{CH}_2\text{PPh}_3]$ (10)	104
3.2.6	Crystal and molecular structure of $[\text{C}_6\text{F}_5\text{AuCH}(\text{PPh}_3)(m\text{-Me-C}_6\text{H}_4)]$ (14)	108
3.2.7	Crystal and molecular structure of $[(\text{C}_6\text{F}_5)\text{Au}(\text{SC}_4\text{H}_8)]$ (15)	112
3.2.8	Crystal and molecular structure of $[\text{C}_6\text{F}_5\text{AuC}_6\text{F}_5]_2[p\text{-Ph}_3\text{PCH}_2(\text{C}_6\text{H}_4)\text{CH}_2\text{PPh}_3]$ (16)	115
3.2.9	Crystal and molecular structure of $[(\text{acac})(\text{AuPPh}_3)_2]$ (17)	119
3.2.10	Crystal and molecular structure of $[(\text{C}_6\text{F}_4)\text{AuPPh}_3]_2$ (21)	121
3.3	Conclusions	124
3.4	Experimental	126

CHAPTER 1

Introduction and aims

1.1 Introduction

Organo gold chemistry is an active field of investigation,¹ and the most dynamic topics include studies of weak gold...gold bonding interactions in gold(I) complexes and how these can affect conformations, crystal packing and chemical reactions, as well as studies on the luminescence of gold(I) compounds.² A relationship between the two effects has been suggested, namely that luminescence is likely to be observed when gold...gold interactions are present.³ The synthesis of dinuclear gold(I) complexes has stimulated interest in the study of the weak metal-metal interactions that have been attributed to relativistic effects.⁴ The gold...gold interactions occur in the range 0.25-0.32 nm and are thus shorter than the Van der Waals contact (0.332 nm) or in many cases, the interatomic distance in the metal (0.289 nm). Gold-gold bonding of this nature is most commonly encountered in the coordination chemistry of monovalent gold, where it occurs perpendicular to the principal axis of the linearly two-coordinate gold(I) atoms. It often has a decisive influence on solid-state structures.³

Novel applications of metallic gold as well as its 'inorganic' and organometallic complexes are being established in fields as diverse as electrochemistry, nonlinear optics, catalysis and bioinorganic chemistry. A particularly interesting example of a catalytic application is the use of luminescent gold(I) compounds as photocatalysts.⁵ Developments with relevance to bioinorganic chemistry include the emergence of self-assembled thiolate monolayers on gold as attractive models of organic interfaces, as well as the process of labelling proteins with water soluble gold clusters and subsequent visualisation by electron microscopy, which has

¹ A. Grohmann and H. Schmidbaur, in *Gold, Progress in Chemistry, Biochemistry and Technology*, ed. H. Schmidbaur, John Wiley, Chichester (1999), p 1

² P. Pyykkö, *Angew. Chem. Int. Ed.*, **43** (2004) 4412

³ M. J. Irwin, J. J. Vittal and R. J. Puddephatt, *Organometallics*, **16** (1997) 3541

⁴ H. Schmidbaur, S. Cronje, B. Djordjevic and O. Schuster, *Chem. Phys.*, in press

⁵ D. Li, C. M. Che, H. L. Kwong and V. W. W. Yam, *J. Chem. Soc., Dalton Trans.* (1992) 3325

proven to be an indispensable tool for determining the locations of functional sites in biological macromolecules.⁶

Modern nomenclature uses the term “ylide” for a class of compounds which was first considered by Staudinger in the 1920’s and was later developed by Wittig and his collaborators after World War II. Phosphorus ylides can be classified as phosphine-stabilised carbenes, and may thus constitute the oldest and best-studied class of carbene complexes.⁷ In contrast to the carbene complexes of homologous arsanes or stibanes (arsenic and antimony ylides) or of sulfanes (sulfur ylides), which decompose very easily and act as carbene carriers, the phosphorus-carbene complexes are usually very stable. The ylide formula in the narrow sense emphasizes the dipolar zwitterionic nature involving an onium center at elements like phosphorus, sulfur or arsenic, next to a carbanionic function, which may be at least partially delocalised into suitable substituents. The three important characteristic features of the phosphorus ylides (basicity, donor activity and nucleophilicity) are expressions of the excess charge on the ylidic carbon atom, which is not adequately compensated by the P⁺ center and which expresses itself differently depending on the nature of the reaction partner. Ylide complexes of metals principally constitute organometallic compounds, whose novel metal-carbon bonds lie under the electronic and steric influence of the onium center. Ylides are considered versatile ligands for metals in various oxidation states.⁸

Several methods have been developed for the preparation of phosphorus ylides. These ylides are usually prepared by treatment of a phosphonium salt with a base and the phosphonium salts are usually prepared from the phosphine and alkyl halide. Phosphonium salts can also be prepared by Michael addition of phosphine to activated olefins.⁹

⁶ C. F. Shaw III, in *Gold, Progress in Chemistry, Biochemistry and Technology*, ed. H. Schmidbaur, John Wiley, Chichester (1999), p 260

⁷ H. Schmidbaur, *Angew. Chem. Int. Ed. Engl.*, **22** (1983) 907

⁸ H. Schmidbaur, T. Costa, B. Milewski-Mahria, F. H. Köhler, Y. H. Tsay, C. Krüger, J. Abart and F. E. Wagner, *Organometallics*, **1** (1982) 1266

⁹ A. Grohmann and H. Schmidbaur in *Gold, Progress in Chemistry, Biochemistry and Technology*, ed. H. Schmidbaur, John Wiley, Chichester (1999), p 681

1.2 Phosphonium salts as anti-cancer agents

Delikatny *et al.*¹⁰ recently reported that *p*-(triphenylphosphoniummethyl) benzaldehyde chloride (drug **A**) and [4-(hydrazinocarboxy)-1-butyl] tris-(4-dimethylaminophenyl) phosphonium chloride (drug **B**), induced accumulation of NMR-visible, neutral lipids in cultured human breast cancer cells. Neutral lipid accumulation is a well-known indicator of cell stress and can be induced in tumour cells cultured to high density, exposed to experimental conditions of hypoxia, or treated with chemotherapeutic agents.

Alteration of lipophilicity of aromatic antitumor drugs greatly affects cellular uptake and binding to plasma proteins. Changes to lipophilicity also affect host toxicity, and optimal lipophilicity may be a critical factor in the design of analogues with high anti-tumor activity.¹¹

NMR spectroscopy, histological lipid staining and electron microscopy were used to assess the biochemical and structural changes induced by treating the cultured human breast cell line, HBL-100, with the cationic lipophilic phosphonium salts, drug **A** and drug **B**.¹⁰ The major biochemical change detected by ¹H NMR in drug-treated cells is the significant time- and concentration-dependent increase in lipid acyl chain resonances arising from mobile lipids. The amount of NMR-visible lipids strongly correlates with morphometric measurements of oil red O-staining lipid (a neutral lipid dye, staining nonpolar lipids red and some phospholipids pink), detected in the cytoplasm by light microscopy. Substantial damage to mitochondria and progressive development of lipid droplets accompanied by end-stage autophagic vacuoles, were observed after treatment of HBL-100 cells with drug **B** at the IC₅₀ (concentration of complex that results in 50% growth inhibition).

Tetraphenylphosphonium-based cationic lipophilic phosphonium salts (CLPS) are novel anti-cancer agents with potential utility in the treatment of neoplasia. Tetraphenylphosphonium chloride (TTP) is the parent compound of a series of

¹⁰ E. J. Delikatny, W. A. Cooper, S. Brammah, N. Sathasivam and D. C. Rideout, *Cancer Research*, **62** (2002) 1394

¹¹ M. J. McKeage, S. J. Berners-Price, P. Galettis, R. J. Bowen, W. Brouwer, L. Ding, L. Zhuang and B. C. Baguley, *Cancer Chemother. Pharmacol.*, **46** (2000) 343

CLPS, including drug **A** and the cationic acylhydrazine drug **B**, which have been shown to selectively inhibit the growth of cell lines derived from a wide variety of carcinomas (breast, colon, pancreas, bladder and hypo-pharynx) relative to untransformed cell lines *in vitro* (CV-1 monkey kidney epithelial cells; IEC-18 rat ileal epithelial cells).^{12,13} These drugs are thought to accumulate intracellularly as a function of membrane potential because the collapse of the membrane potential with either valinomycin or high extracellular potassium concentrations reduces both the accumulation and the cytotoxicity of these agents.^{12,13} The high negative plasma membrane potentials characteristic of neoplastic cells are believed to account for the selective accumulation and toxicity of CLPS and the other cationic lipophilic compounds against malignant cells.^{14,15}

Studies of various cationic lipophilic compounds suggest that mitochondrial toxicity provides the basis for the cytotoxicity of these compounds. Inhibition of mitochondrial respiration has been demonstrated in studies of TTP and other lipophilic cationic compounds such as rhodamine 123. Loss of ATP and phosphocreatine, and decreases in the intracellular pH, have also been shown to accompany treatment with cationic lipophilic compounds.^{16,17} It is thought that CLPS, such as drugs **A**, **B** and TTP as well as rhodamine 123, all have similar mechanisms of action, because sensitivity profiles determined with a fixed set of culture cells are closely similar for these agents. Damage to the mitochondria can cause changes in the mitochondrial permeability and the release of apoptotic factors that would ultimately result in cell death. Indeed, the full range of biochemical effects these drugs have on cancer cells have not yet been fully elucidated. It is currently not possible to unequivocally identify the final mediators of CLPS-induced cell death.

HBL-100 cells were treated with drugs **A** and **B** at the IC₅₀, and ¹H NMR spectra were obtained of harvested cells 48 hours after treatment. The ¹H NMR spectra of the untreated cells exhibited a number of broad signals of proteins superimposed

¹² D. Rideout, T. Calogeropoulou, J. S. Jaworski, R. Dagnino and M. R. McCarthy, *Anticancer drug design*, **4** (1989) 265

¹³ D. Rideout, A. Bustamante and J. Patel, *Int. J. Cancer*, **57** (1994) 247

¹⁴ T. J. Lampidis, Y. Hasin, M. J. Weiss and L. B. Chen, *Biomed. Pharmacother.*, **39** (1985) 220

¹⁵ J. S. Modica-Napolitano and J. R. Aprile, *Cancer Res.*, **47** (1987) 4361

¹⁶ A. Viola, N. W. Lutz, C. Maroc, C Chabannon, M. Julliard and P. J. Cozzone, *Int. J. Cancer*, **85** (2000) 733

¹⁷ S. Singer, L. J. Neuringer, W. G. Thilly and L. B. Chen, *Cancer Res.*, **53** (1993) 5808

with a number of narrower resonances of amino acids, creatines, carbohydrates, lactate and choline-containing metabolites, but essentially contained no lipid signals. Spectra of the HBL-100 cells treated with drug **A** or **B** at the IC₅₀ demonstrated substantial increases in NMR-visible lipids, particularly the lipid acyl chain methylene resonance at 1.3 ppm, lipid methyl groups at 0.9 ppm, fatty acyl chain β -methylene at 1.7 ppm and olefinic groups at 5.35 ppm. Detailed resonance assignments for human breast cells have been reported previously.¹⁸

To quantify drug-induced changes, the intensities of lipid resonances were measured relative to signals arising from the external standard, PABA (*p*-aminobenzoic acid), at 6.8 and 7.8 ppm. The peak height and area ratios of the lipid methylene (1.3 ppm) and methyl (0.9 ppm) relative to PABA increased significantly in HBL-100 cells treated with drug **A** or **B** at the IC₅₀ compared with control cells. No statistically significant changes were observed after treatment with drug **A** or **B** at the IC₁₀.

Light microscopic lipid staining techniques were performed to investigate the nature and cellular location of the mobile lipid detected by NMR. HBL-100 cells treated with drugs **A** or **B** displayed a concentration-dependent increase in oil red O-lipid staining in cytoplasmic droplets. In contrast, control HBL-100 cells displayed very few small, scattered cytoplasmic lipid droplets. A comparison of morphometric and spectroscopic data demonstrated that the concentration-dependent increase in cytoplasmic lipids after treatment with either drug **A** or **B** correlated strongly with lipid detected by one-dimensional ¹H NMR.

HBL-100 cells were treated with drug **B** and the treated cells displayed mitochondrial changes, including overall swelling and dense matrix condensations. Mitochondrial cristae were lost, disordered, pushed to the edges and formed doughnut shapes, consistent with previous observations on cationic lipophilic compounds. In some cells mitochondrial damage was extensive. Evidence of necrosis was present with cells showing damaged or missing plasma membranes,

¹⁸ E. J. Delikatny, S. K. Roman, R. Hancock, T. M. Jeitner, C. M. Lander, D. C. Rideout and C. E. Mountford, *Int. J. Cancer*, **67** (1996) 72

swollen endoplasmic reticulum and proteinaceous debris. The control HBL-100 cells showed viable elongated cells with no significant abnormalities.

The medicinal applications of gold are well known and the historical use of gold in medicine and, especially, the gold therapy of rheumatoid arthritis, the mechanism of action of antiarthritic gold drugs, as well as the antitumor and anti-infective properties of gold, have been discussed in great detail by Fricker.^{19,20}

Gold phosphorus ylide complexes are isolobal to phosphonium salts ($\text{Ph}_3\text{PAu}^+ \leftarrow \sigma \rightarrow \text{H}^+$). Ph_3PAu -ylide complexes would exploit the synergism between two pharmacologically active substances to form an even more biologically active substance. A wide variety of gold(I) ylide complexes have been reported, however, very few of these complexes have been tested for biological activity. A series of ionic phosphorus ylide complexes of gold(I) halides have been prepared by the group of Schmidbaur,²¹ and these compounds have been tested in a pharmacological study for possible use in oral arthritis therapy. The complexes are of the type $[(\text{C}_2\text{H}_5)_3\text{PAuCH}_2\text{P}(\text{C}_2\text{H}_5)_3]\text{Cl}$ and $[(\text{R}_3\text{PCH}_2)_2\text{Au}]\text{X}$, where $\text{R} = \text{CH}_3, \text{C}_2\text{H}_5, n\text{-C}_4\text{H}_9, \text{C}_6\text{H}_5$ and $\text{X} = \text{Cl}, \text{Br}$. Some of these compounds showed no effect on Adjuvans-arthritis induced in rats, while others were toxic. One compound was comparable to standard cryotherapeutic agents.

1.3 Gold(I) phosphorus ylide complexes

Vicente *et al.*²² have reported a series of new ylide-, alkynyl-, and mixed alkynyl/ylide-gold(I) complexes in recent years.

The objectives of the work presented by the Vicente group, were to prepare alkynylgold(I) complexes containing ylides to study their nonlinear optical (NLO) properties. These compounds, however, did not show such properties.

¹⁹ S. P. Fricker in *The chemistry of organic derivatives of gold and silver*, ed. S. Patai and Z. Rappoport, John Wiley, Chichester (1999) p 641

²⁰ S. P. Fricker, *Gold Bull.*, **29** (1996) 53

²¹ H. Schmidbaur, J. R. Mandl and A. Wohlleben-Hammer, A. Fügner, *Z. Naturforsch.*, **B33** (1978) 1325

²² J. Vicente, A. R. Singhal and P. G. Jones, *Organometallics*, **21** (2002) 5887

The synthesis of eight new gold(I) complexes with the ligand $C(PPh_3)_2$ and the crystal structure of two of these were reported. The only previously known gold complex with the diylide $C(PPh_3)_2$ is $[AuCl\{C(PPh_3)_2\}]$ (**C**), preliminarily reported by Schmidbaur²³ and obtained by reacting $C(PPh_3)_2$ with $[AuCl(CO)]$. A different way to synthesise **C** and other complexes with this ligand, including the unusual dinuclear complex $[(AuCl)_2\{\mu-C(PPh_3)_2\}]$ (**F**), the first acetylacetonato-ylide gold complex, $[Au(acac)\{C(PPh_3)_2\}]$ (**G**), and the family of alkyne complexes $[Au(C\equiv CR)\{C(PPh_3)_2\}]$ (**I**), were described by the group of Vicente.

Only a few $[Au(C\equiv CR)(ylide)]$ complexes have been prepared, by reacting $[Au(ylide)(tth)ClO_4]$ (tth = tetrahydrothiophene) with $KC\equiv CR$. Two new synthetic methods for these types of compounds were found. One of these methods involved $[Au(acac)\{C(PPh_3)_2\}]$ (**G**), following the method used by the group to previously prepare gold(I) complexes by reacting $[Au(acac)(PR_3)]$ or $[Au(acac)_2]^-$ with acids. The first complexes with the ylide $4-MeC_6H_4S(O)_2CHPPh_3$ and the ylide cation $[HC(PPh_3)_2]^+$, were also isolated.

The synthesis of the triflate salt of the phosphonium cation $[4-MeC_6H_4SO_2CH_2PPh_3]^+$ has been described by Zhdankin,²⁴ starting from $4-MeC_6H_4SO_2CH_2I$, and following a three-step synthetic procedure. Extension of the procedure used for the synthesis of the bisphosphonium salt $[CH_2(PPh_3)_2]Br_2$ provided a new method of synthesis for the above-mentioned compound by heating the same starting material, triphenylphosphine, and triphenylphosphate at 125-130°C for 36 hours. The triflate salt was prepared by reacting the iodide with thallium(I)triflate and the ylide by dehydroiodination of the iodide salt by treatment with *n*-BuLi in THF.

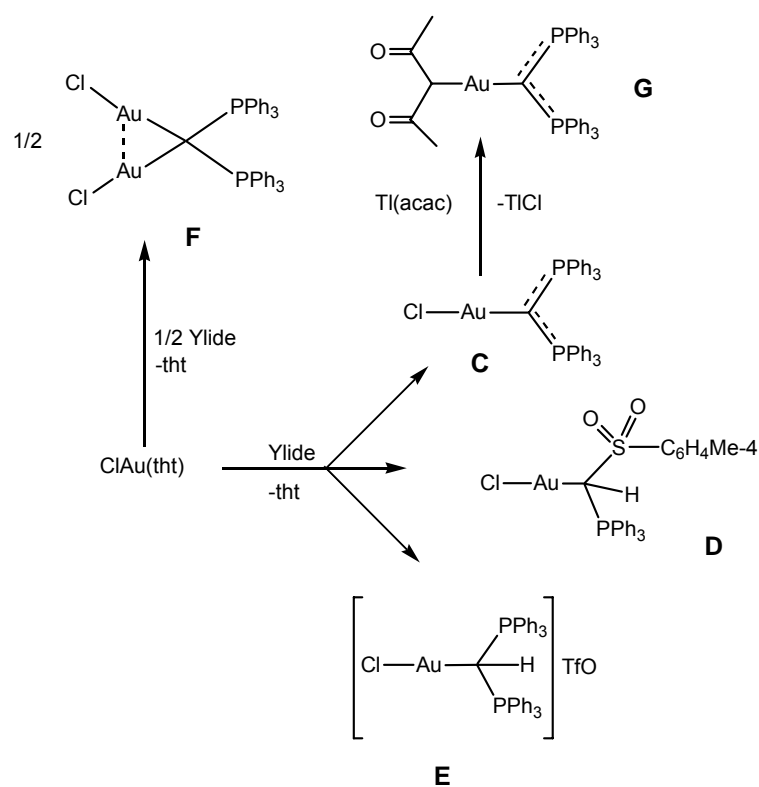
The reaction of $ClAu(tth)$ with the ylide $C(PPh_3)_2$ in THF or with $4-MeC_6H_4SO_2CHPPh_3$ or $[HC(PPh_3)_2]TfO$ in CH_2Cl_2 (1:1 molar ratio) readily afforded the corresponding complexes $[AuCl(ylide)]X_n$ ($n=0$, ylide= $C(PPh_3)_2$ (**C**), $4-MeC_6H_4SO_2CHPPh_3$ (**D**), $n=1$, $X=TfO$, ylide= $[HC(PPh_3)_2]^+$ (**E**)) in good to excellent yields (Scheme 1). Preparation of **C** was attempted on large scale (1g), but a

²³ H. Schmidbaur, C. E. Zybill, G. Müller and C. Krüger, *Angew. Chem., Int. Ed. Engl.*, **22** (1983) 729

²⁴ V. V. Zhdankin, S. A. Erickson and K. J. Hanson, *J. Am. Chem. Soc.*, **119** (1997) 4775

white solid precipitated immediately and turned out to be the dinuclear complex $[(\text{AuCl})_2\{\mu\text{-C}(\text{PPh}_3)_2\}]$ (**F**) (Scheme 1.2). This was confirmed by reacting $[\text{AuCl}(\text{tht})]$ and $\text{C}(\text{PPh}_3)_2$ in a 1:2 molar ratio. The insolubility of **F** and a localised excess of $\text{AuCl}(\text{tht})$ in the 1:1 reaction could explain its unexpected formation in the large-scale synthesis of **C**. These results indicated that the coordinated ylide $\text{C}(\text{PPh}_3)_2$ in **C** retains some basic character after coordination to AuCl , because it replaces the tht ligand of $[\text{ClAu}(\text{tht})]$. Complex **C**, therefore, acts as a ligand.

The reaction of **C** with $\text{Ti}(\text{acac})_3$ in a 1:1.4 molar ratio yields the complex $[\text{Au}(\text{acac})\{\text{C}(\text{PPh}_3)_2\}]$ (**G**), which is the first (acetylacetonato)gold(I) complex with an ylide ligand (Scheme 1.1).

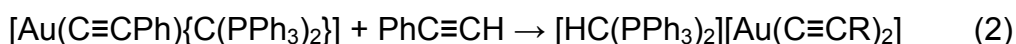
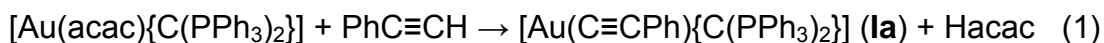


Scheme 1.1

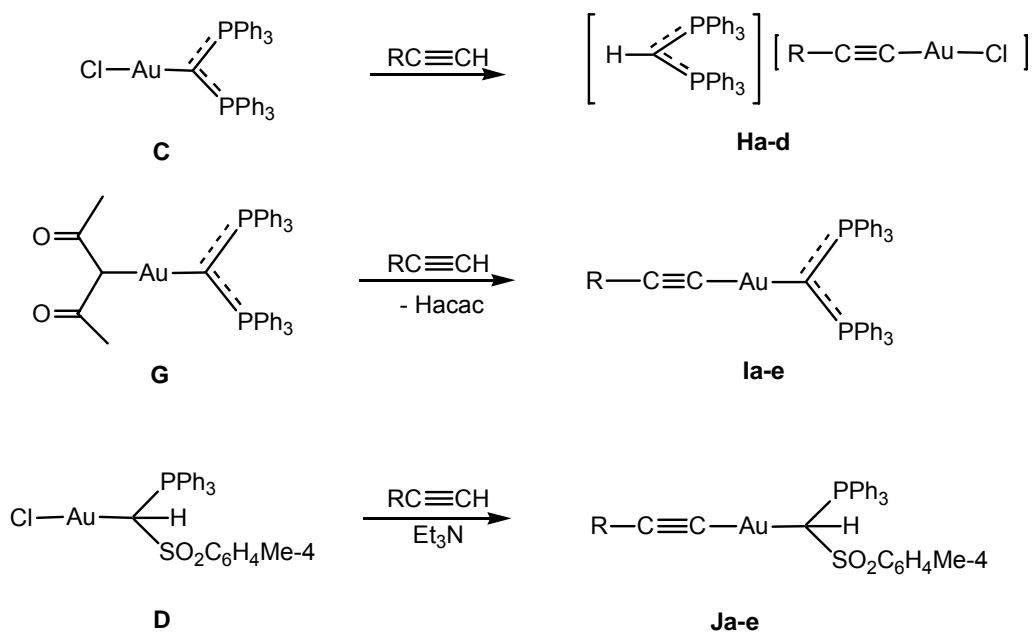
In an attempt to prepare the complexes $[\text{Au}(\text{C}\equiv\text{CR})\{\text{C}(\text{PPh}_3)_2\}]$ ($\text{R}=\text{Ph}$, $4\text{-MeOC}_6\text{H}_4$), **C** was reacted with the corresponding terminal alkynes in the presence of Et_3N (1:1:1 molar ratio). Instead complexes of the type $[\text{HC}(\text{PPh}_3)_2][\text{Au}(\text{C}\equiv\text{CR})\text{Cl}]$ (**H**) were isolated (Scheme 1.3). These results indicated that the basic character of the coordinated ylide, $\text{C}(\text{PPh}_3)_2$ in **C** is better than that of the free Et_3N . Although

Et₃N acts as a catalyst, the complexes [HC(PPh₃)₂][Au(C≡CC₆H₄R-4)Cl] (R=H (**Ha**), CN (**Hb**), OMe (**Hc**), NO₂ (**Hd**)) were prepared in the absence of Et₃N to avoid contamination.

The desired complexes [Au(C≡CC₆H₄R-4){C(PPh₃)₂}] (R=H (**Ia**), CN (**Ib**), OMe (**Ic**), NO₂ (**Id**), C≡CPh (**Ie**)) were prepared by the reaction of [Au(acac){C(PPh₃)₂}] (**G**) with a large excess of alkyne. In order to establish the exact course of the reaction, the reactions were monitored by ³¹P NMR spectroscopy. The first reaction comprises deprotonation of PhC≡CH with acac and bonding of the C≡CPh unit to Au(I) (equation (1)) to form **Ia**. The excess of the alkyne slowly protonates and replaces the ylide ligand from **Ia** following the reaction in equation 2.



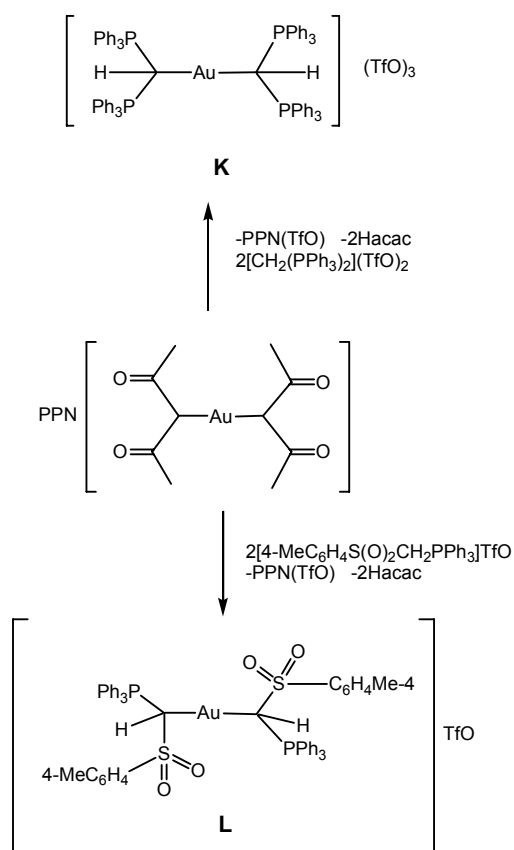
Ylide complex **D** reacts with terminal alkynes in the presence of Et₃N, producing the series of complexes **Ja-e** (Scheme 1.2).



Scheme 1.2

Reactions of $\text{PPN}[\text{Au}(\text{acac})_2]$ ($\text{PPN} = \text{Ph}_3\text{P}=\text{N}^+=\text{PPh}_3$) with the phosphonium salts $[\text{H}_2\text{C}(\text{PPh}_3)_2](\text{TfO})_2$ and $[\text{4-MeC}_6\text{H}_4\text{S}(\text{O})_2\text{CH}_2\text{PPh}_3]\text{TfO}$ in 1:2 stoichiometry afford the cationic complexes **K** and **L** respectively (Scheme 1.3).²² These complexes are white crystalline solids and their ^{31}P NMR spectra in acetone- d_6 show singlets at δ 26.1 and 20.4 respectively, indicating that the phosphorus atoms are equivalent in the complexes.

The molecular structure of the phosphonium salt $[\text{4-MeC}_6\text{H}_4\text{S}(\text{O})_2\text{CH}_2\text{PPh}_3]\text{TfO}$ revealed that the phosphorus and sulfur atoms had distorted tetrahedral geometry. The C-P-C bond angles were similar to those found in the corresponding ylide complexes **D** and **L**. The ylide structure was also solved and it shows that the P-CH bond is intermediate between the single bond in the phosphonium salt and the double bond in the ylide. Hydrogen bonding (2.39-2.57 Å) between the sulfone and triflate oxygen atoms and the phenyl and ylidic hydrogen atoms determines the lattice organisation.



Scheme 1.3

In the molecular structure of the ylide complex **D**, the ligand arrangement around the gold atom is essentially linear, with a C-Au-Cl bond angle of $178.36(11)^\circ$. The molecules of **D** form dimers through C-H \cdots O (2.46 Å) and C-H \cdots Cl (2.56 Å) hydrogen bonds and a weak aurophilic interaction (3.5539(5) Å).

In the dinuclear complex **F**, the gold \cdots gold distance is 3.1432(2) Å, a typical value for aurophilic contact supported by a bridging carbon donor ligand. The Au-C-Au angle ($98.44(11)^\circ$) is narrower than expected for two C_{sp^3} hybrid orbitals.

The ^1H NMR resonance of the methine proton in the ylide complexes **D**, **J** and **L** (4.58-5.32) is intermediate between that of the ylide (2.96 ppm) and that corresponding to the methylene protons of [4-MeC₆H₄S(O)₂CH₂PPh₃]I (6.18 ppm). The same order is observed for the $\delta(^1\text{H})$ value of the methane proton of the ylide cation [HC(PPh₃)₂]⁺ (1.86 - 1.93 ppm in complexes **H**, 1.83 ppm in [CH(PPh₃)₂]Br, and 1.86 ppm in [HC(PPh₃)₂]TfO smaller than in complexes **E**, **K** and **L** (5.58, 5.69 ppm) smaller than in the methylene protons of the phosphonium salt [CH₂(PPh₃)₂](TfO)₂ (6.30 ppm). Therefore, replacement of a proton in a phosphonium salt by a gold moiety increases the shielding of the remaining methane proton.

The $\delta(^{31}\text{P})$ values tend to follow a different order: ylide 4-MeC₆H₄S(O)₂CHPPh₃ (14.8 ppm) < [4-MeC₆H₄S(O)₂CH₂PPh₃]I (17.6 ppm) < complexes **D**, **J** and **L** (20.2 - 21.8 ppm). The same tendency is followed by the $\delta(^{31}\text{P})$ values of the ylide C(PPh₃)₂ (-3.5 ppm) < the ylide cation [HC(PPh₃)₂]⁺ (21.1 ppm in complexes **H**) < ylide complexes **C**, **G** and **I** (14.3 - 16.6 ppm). A different sequence is found for the ylide cation [HC(PPh₃)₂]⁺ (21.1 ppm in complexes **H** and the bromide and triflate salts), which is very similar to that of its phosphonium salts [CH₂(PPh₃)₂]X (X = Br, 20.99 ppm; X = TfO, 20.47 ppm), although both are smaller than the $\delta(^{31}\text{P})$ values in its ylide complexes **E** and **K** (22.1, 26.1 ppm, respectively).

In a separate study Vicente *et al.*²⁵ reported the synthesis of gold(I), gold(III) and silver(I) complexes with ylide ligands derived from carbonylbis(methylenetriphenylphosphonium)diperchlorate.

The acidic character of the methylene protons in the carbonyl-phosphonium salts $[\text{Ph}_3\text{PCH}_2\text{C}(\text{O})\text{R}]^+$ allowed the preparation of dinuclear gold(I) complexes $[(\text{AuL})_2\{\mu\text{-C}(\text{PPh}_3)\text{C}(\text{O})\text{R}\}]^+$ (L = PPh_3 , R = OMe, OEt, Me, Ph, L = AsPPh_3 , R = Me), by reaction of such onium salts with the corresponding $[\text{Au}(\text{acac})\text{L}]$ complexes (1:2) molar ratio. Vicente *et al.* described the synthesis of the new ylide-phosphonium salt $[\text{Ph}_3\text{PCHC}(\text{O})\text{CH}_2\text{PPh}_3]^+$ and the then still unisolated bisylide $(\text{Ph}_3\text{PCH})_2\text{CO}$. The group obtained the gold(I) complexes of the bisylide and one silver(I) complex, by transylidation reactions. This term is used to describe the acid-base reaction between an ylide and an onium salt e.g., $\text{R}_3\text{PCHR}' + [\text{R}''_3\text{PCH}_2\text{R}''']^+ \rightarrow \text{R}''_3\text{PCHR}''' + [\text{R}_3\text{PCH}_2\text{R}]^+$ ¹

The bisylide $(\text{Ph}_3\text{PCH})_2\text{CO}$ belongs to the group of triatomic bridging ligands that are usually designed to promote metal-metal bonds in the synthesis of bimetallic complexes. Some examples of this group of ligands include ligands with a CPC skeleton (anionic ylides) and ligands containing a PCP bridge. Complexes with CCC bridges are very rare.²⁵ Bisylide ligands with a carbon chain between both carbon donor atoms are also very unusual. Such ligands have been explored in the present work.

The reactions of $[\text{M}\{\text{CH}(\text{PPh}_3)\text{C}(\text{O})\text{CH}_3\}_2]\text{ClO}_4$ (M = Ag, Au) with $[(\text{Ph}_3\text{PCH}_2)_2\text{CO}](\text{ClO}_4)_2$ (1:1) in acetone lead to the precipitation of complexes **M** and **N**.^{26,27} Alternative syntheses for complex **N**, were reported separately by Schmidbaur,⁷ Kaska,²⁸ Vicente²⁹ and Usón,³⁰ by ylide transfer reactions, which involve the transfer of an ylide ligand from one metal center to another. In this

²⁵ J. Vicente, M. Chicote, I. Saura-Llamas, P. G. Jones, K. Meyer Bäse and C. F. Erdbrügger, *Organometallics*, **7** (1988) 997

²⁶ J. Vicente, M. T. Chicote, J. A. Cayuelas, J. Fernandez-Baeza, P. G. Jones, G. M. Sheldrick, P. Espinet, *J. Chem. Soc., Dalton Trans.* (1985) 1163

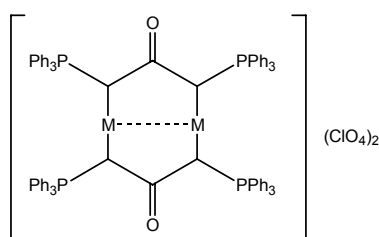
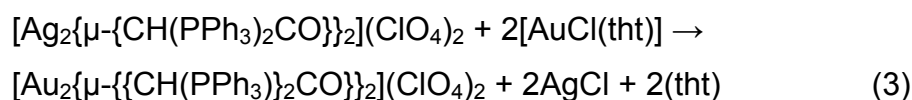
²⁷ J. Vicente, M. T. Chicote, J. Fernandez-Baeza, J. Martin, J. Saura-Llamas, P. G. Jones and L. Turpin, *J. Organomet. Chem.*, **331** (1987) 409

²⁸ W. C Kaska, *Coord. Chem. Rev.*, **48** (1983) 1

²⁹ J. Vicente, M.T. Chicote, J. Fernandez-Baeza, J. Martin, I. Saura-Llamas, L. Turpin and P. G. Jones, *J. Organomet. Chem.*, **331** (1987) 409

³⁰ R. Usón, A. Laguna, M. Laguna, A. Usón and M. C. Gimeno, *Organometallics*, **6** (1987) 982

investigation of the Vicente group, a double ylide transfer from silver to gold (equation 3), occurred, and a better yield of **N** was obtained. The cations contain the eight-membered rings that are a common feature of gold(I) chemistry.³¹ The transannular gold···gold distance, formally non-bonded, at 2.876 Å, is also well known for gold. The C-Au-C angles on the inside of the eight-membered ring deviate considerably from linearity, 170°, presumably to avoid even shorter contacts between the gold atoms. The four carbon atoms bonded to the gold atoms are chiral. Because of the center of inversion, the molecule is in one of the *meso* forms.



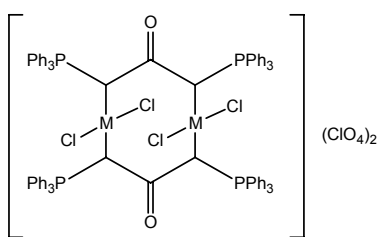
M M = Ag

N M = Au

Scheme 1.4

A suspension of **N** in dichloromethane was treated with a saturated solution of chlorine in carbon tetrachloride to obtain compound **O** as a yellow precipitate. Complex **O** is not stable and decomposed at room temperature to give the starting complex **N** among other products. The chlorination was carried out by slow diffusion of the reacting solutions and the diphosponium salt $[(\text{Ph}_3\text{PCCl}_2)_2\text{CO}][\text{AuCl}_4](\text{ClO}_4)$ (**Oa**) was isolated instead. The crystal structure of **Oa** was obtained and revealed that the cations occupy general positions and that there were two independent $[\text{AuCl}_4]^-$ anions (both lying on centers of symmetry) and one general ClO_4^- anion.

³¹ a) P. G. Jones, *Gold Bull.*, **14** (1981) 102, b) P. G. Jones, *Gold Bull.*, **16** (1983) 114

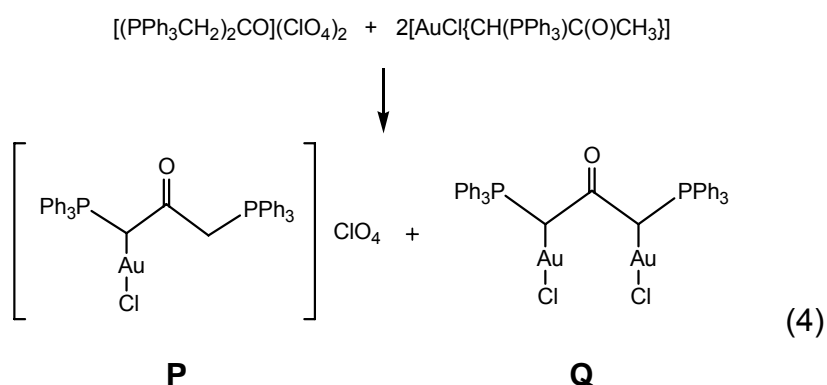


O

Scheme 1.5

The reaction of **N** with PhICl_2 in a 1:1 molar ratio did not afford the desired gold(II) complex $[(\text{AuCl})_2\{\mu\text{-}\{\text{CH}(\text{Ph}_3\text{P})_2\text{CO}\}\}_2](\text{ClO}_4)_2$. Instead, a mixture of **N** and **O** was obtained. It is likely that the coordination sites for the chlorine ligands were too crowded.

The transylidation reaction in equation 3 forms a mixture of products from which, by suitable treatment, **Q** and unreacted phosphonium salt can be isolated as the only pure compounds. The presence of the intermediate **P**, was postulated from IR evidence. This compound was later synthesised by treating the ylide-phosphonium salt $[\text{Ph}_3\text{PCHC}(\text{O})\text{CH}_2\text{PPh}_3]\text{ClO}_4$ with $[\text{AuCl}(\text{tht})]$, but it was always contaminated with trace amounts of $[(\text{Ph}_3\text{PCH}_2)_2\text{CO}](\text{ClO}_4)_2$ and **Q**. These are the products of the intermolecular transylidation reaction of **P**.



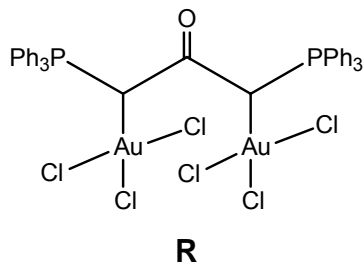
P

Q

Scheme 1.6

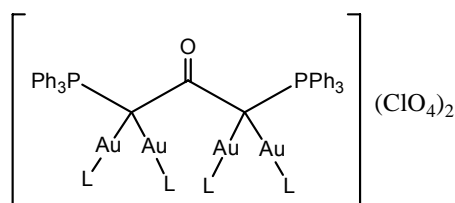
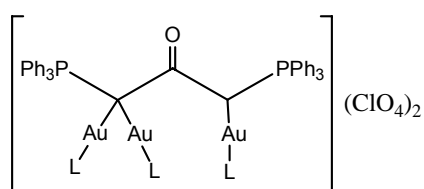
Complex **Q** can also be obtained from the transylidation reaction between **P** and $[\text{AuCl}\{\text{CH}(\text{Ph}_3\text{P})\text{C}(\text{O})\text{CH}_3\}]$. The reaction of **Q** with chlorine gives the gold(III) complex **R**. The reactions between $[(\text{Ph}_3\text{PCH}_2)_2\text{CO}](\text{ClO}_4)_2$ and $[\text{Au}(\text{acac})\text{L}]$ (1:4 molar ratio) yielded the trinuclear complex $[(\text{AuL})_2\{\mu\text{-}\{\text{C}(\text{PPh}_3)\text{C}(\text{O})\text{CH}(\text{PPh}_3)(\text{AuL})\}\}](\text{ClO}_4)_2$ ($\text{L} = \text{PhMe}_2\text{P}$ (**T**)). These complexes are

similar to those previously reported by the same author³² formed by reacting $[\text{Au}(\text{acac})\text{L}]$ ($\text{L} = \text{PPh}_3, \text{AsPh}_3$) and the monophosphonium salts $[\text{Ph}_3\text{PCH}_2\text{COR}]\text{ClO}_4$ ($\text{R} = \text{MeO}, \text{EtO}, \text{Me}, \text{Ph}$), to afford dinuclear $[(\text{AuL})_2(\mu\text{-C}(\text{PPh}_3)\text{C}(\text{O})\text{R})]\text{ClO}_4$ and acetone.



Scheme 1.7

The molecular structures of compounds **S** and **T** were determined. The gold...gold bond lengths are 2.892 Å, 2.862 Å (**S**) and 2.950 and 3.008 Å (**T**), with corresponding Au-C-Au angles of 86.3, 85.9, 88.9 and 91.1°. Short gold...gold contacts have been observed between Au_2 units of **T** and from Au_2 to the single Au atom in **S**. These contacts are significantly longer (3.227 Å in **S** and 3.149, 3.307 and 3.343 Å in **T**) than the assumed three-center bonding interactions. The bond angles P-Au-C all deviate from linear geometry of gold(I) compounds.



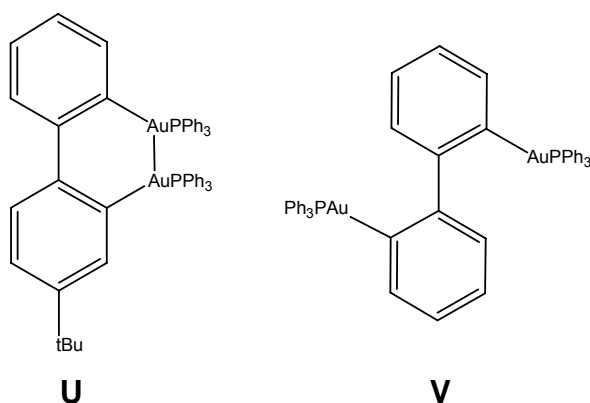
Scheme 1.8

³² a) J. Vicente, M.T. Chicote, J. Cayuelas, J. Fernandez-Baeza, G. M. Sheldrick, P. Espinet and P. G. Jones, *J. Chem. Soc., Dalton Trans.* (1985) 1163 b) J. Vicente, M.T. Chicote, J. Fernandez-Baeza, I. Saura-Llamas and L. Turpin, *J. Organomet. Chem.*, **333** (1987) 129

Limited solubility of complexes **P**, **S** and **T** prevented recording of NMR spectra. The ^{31}P NMR spectrum of **P** shows two doublets, centered at δ 24.4 and 20.8 ($^4J_{\text{PP}} = 9$ Hz). Other signals at δ 19.8 (s) and 25.6 (s) correspond to the presence of the phosphonium salt and **Q**.

1.4 Biphenyl complexes

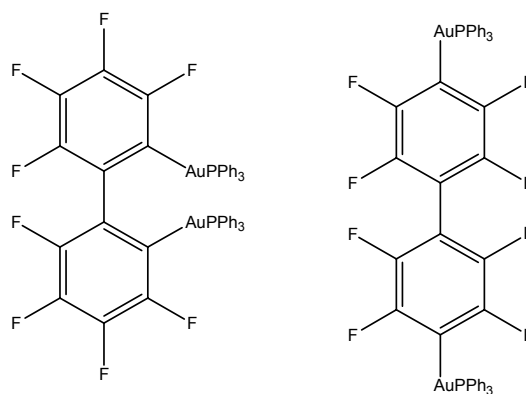
Only two examples of biphenyl gold complexes have been reported thus far (Scheme 1.9),^{33,34} but no fluorobiphenyl complexes with gold are known. We decided to explore this synthetic avenue. Aurophilic interactions occur only in compound **U**, over a distance of 3.17 Å. Despite the bulky triphenylphosphine groups coordinated to the gold(I) in **U**, the gold atoms are orientated towards the same side of the biphenyl rings, making interaction between the gold atoms possible. In the present study the gold precursor compound ClAuPPh_3 was coordinated to 2,2'-dibromooctafluorobiphenyl and in a separate reaction to 4,4'-dibromooctafluorobiphenyl to form dinuclear gold octafluorobiphenyl complexes (Scheme 1.10).



Scheme 1.9

³³ L. G. Kuz'mina, A. V. Churakov and J. A. K. Howard, *Koord. Khim. (Russ.)(Coord. Chem.)*, **24** (1998) 461

³⁴ V. P. Dyadchenko, P. E. Krasik, K. I. Grandberg, L. G. Kuz'mina, N. V. Dvortsova, M. A. Porai-Koshits and E. G. Perevalova, *Metalloorg. Khim. (Russ.)(Organomet. Chem. (USSR))*, **3** (1990) 1260



Scheme 1.10

1.5 Aims and objectives of the present investigation

Gold(I) compounds are well known for the variety of biological activity they display.^{19,20} These applications are widely documented. Phosphonium salts and phosphorus ylides also have proven anti-cancer activity.^{18,35} The aim of this study was to coordinate different phosphorus ylides to suitable gold precursor compounds and to fully characterise these compounds. These complexes would exploit the previously observed synergism between two pharmacologically active substances to form an even more active substance.

Falcão *et al.*³⁶ reported the synergistic effect between auranofin and theophylline, a non-steroidal anti-inflammatory drug, for the treatment of asthma. The group of Sadler³⁷ also suggested a synergism between pharmacologically active substances and Edward³⁸ reported the synergistic effect between auranofin and various corticosteroids, betamethasone dipropionate, flucinolone acetonide and mometasone fluorate, being effective in reducing epidermal hyperplasia and inflammation.

Platinum anti-cancer compounds revealed that multi nuclear compounds exhibit enhanced pharmacological activity with respect to mononuclear compounds.³⁷

³⁵ R. J. Puddephatt, in *Comprehensive Organometallic Chemistry*, eds. G. Wilkinson, F. G. A. Stone and E. W. Abel, Pergamon, Oxford, 1982, p 775

³⁶ A. C. Falcão, M. J. Rocha, M. Almeida and M. M. Caramona, *J. Clinical Pharmacy and Therapeutics*, **25** (2000) 191

³⁷ Z. Guo and P. J. Sadler, *Angew. Chem. Int. Ed.*, **38** (1999) 1512

³⁸ T. R. Edward, Medical Innovations Ltd. (1997) WO 9819683

Analogous to these platinum drugs the present study aimed to incorporate more than one gold(I) nucleus into each new compound.

Phosphonium salts, that would allow us to synthesise and design novel, multi nuclear gold(I) complexes, had to be synthesised, purified and fully characterised. Methods to coordinate these salts to suitable gold(I) precursor compounds in good yields had to be found. The compounds had to be purified and characterised in order to allow testing for biological activity.

Four different phosphonium salts were synthesised and coordinated to suitable gold precursor compounds. Most of the reactions afforded mixtures of products and these mixtures were characterised by ^1H , ^{13}C and ^{31}P NMR as well as mass spectrometry. Fourteen complexes were characterised from the mixtures and seven of these complexes were isolated by fractional crystallisation. The synthetic procedures and ^1H , ^{13}C and ^{31}P NMR, as well as mass spectrometry, and analyses are discussed in Chapter 2, while the crystal structures of the seven isolated complexes, as well as two of the phosphonium salts are discussed in Chapter 3.

From the above-mentioned literature it is evident that gold ylide complexes can be prepared with a variety of gold precursor compounds like $\text{ClAu}(\text{tht})$,³⁹ ClAuPPh_3 ,⁴⁰ $\text{C}_6\text{F}_5\text{Au}(\text{tht})$ ⁴¹ or $(\text{acac})\text{AuPPh}_3$.⁴² The gold precursor compound $(\text{C}_6\text{F}_5)\text{Au}(\text{tht})$ was chosen for most of the reactions in this study, as it prevents the formation of the homoleptic rearrangement product $\text{Ph}_3\text{PAuPPh}_3^+$, which readily forms when the gold ylide complex is unstable.

Very little literature is available on the exact ^{13}C and ^1H NMR signals of each of the phenyl carbon and proton nuclei in the phosphorus ylide gold(I) complexes. Most researchers only report the range in which the phenyl carbon or proton nuclei resonate. We, therefore, embarked on a study to assign such signals in detail.

³⁹ I. Romeo, M. Bardaji, M. C. Gimeno and M. Laguna, *Polyhedron*, **19** (2000) 1837

⁴⁰ H. Schmidbaur, J. R. Mandl, A. Frank and G. Huttner, *Chem. Ber.*, **109** (1976) 466

⁴¹ R. Usón, A. Laguna, M. Laguna and A. Usón, *Inorg. Chim. Acta*, **73** (1983) 63

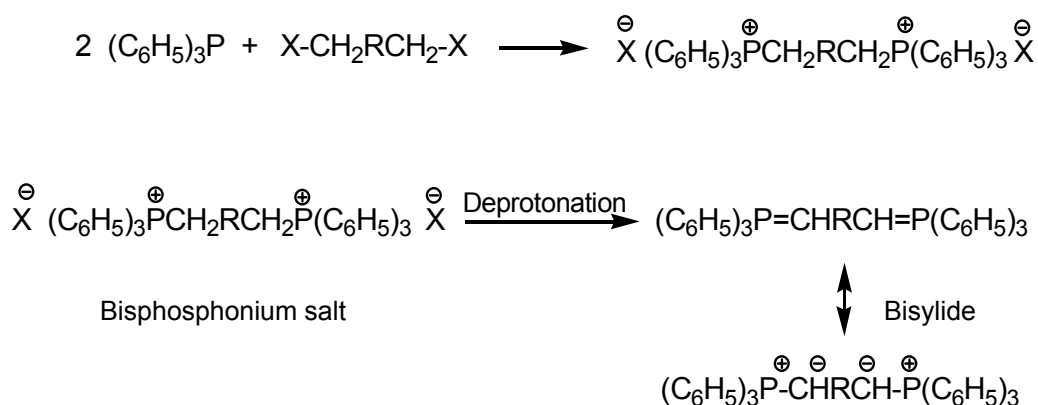
⁴² J. Vicente and M. T. Chicote, *Coord. Chem. Rev.*, **193** (1999) 1143

CHAPTER 2

Synthesis and characterisation of phosphonium precursors and gold(I) compounds

2.1 Introduction

A large number of bisphosphonium salts, including some of the phosphonium salts discussed in this chapter, have been reported in the literature. The coordination of the ylides derived from these salts to metal centres have, however, not been fully investigated. Bisphosphonium salts are deprotonated to form bisphosphonium ylides (Scheme 2.1). Such phosphonium salts are formed *via* the Wittig reactions between the corresponding alkylbromides and triphenylphosphine (Scheme 2.1). The alkylbromides were chosen because they are more readily accessible and the reactivity of the alkylhalides decrease in the series $RCH_2I > RCH_2Br > RCH_2Cl$. The choice of solvent is very important for the formation of bisphosphonium salts since strongly polar solvents, such as nitrobenzene, acetonitrile or dimethylformamide keep the formed monophosphonium salt in solution so that reaction with a second molar equivalent of triphenylphosphine can take place.¹ The use of solvents less polar than these, i.e. diethyl ether, has been unsuccessful.

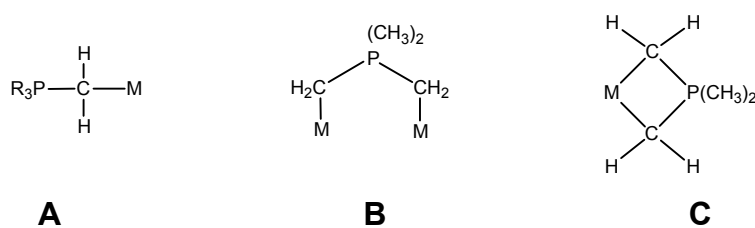


R = Alkyl/Aryl

Scheme 2.1

¹ K. Friedrich and H. Henning, *Chem. Ber.*, **92** (1959) 2756

Organometallic gold(I) compounds are in many instances very unstable. Stabilising ligands make it possible to isolate such compounds. Phosphonium ylides also serve as such stabilising ligands for gold(I). The charge distribution in phosphonium ylides also make them potential ligands for other transition metals. The ylidic carbon is a powerful nucleophilic centre, forming a carbon–metal bond with no metal-ligand backbonding.² Ylides can occur as terminal ligands as in **A** (Scheme 2.2, written without formal charges), as bridging groups (**B**) or as chelating ligands(**C**).³ In this study it was planned to use the ylide ligands as bridging ligands, incorporating two gold(I) nuclei per ligand. This could lead to enhanced biological activity analogous to the dinuclear platinum compounds that showed an increase in biological activity.⁴



Scheme 2.2

2.2 Results and discussion

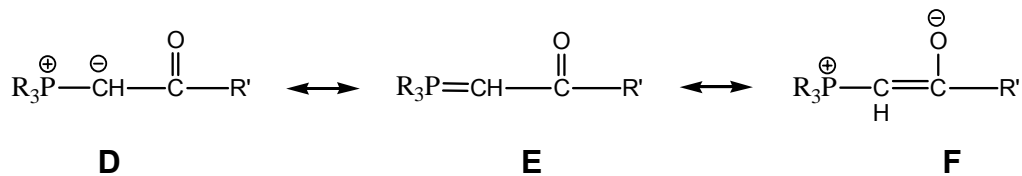
Substitution of coordinated ligands with the ylide, forming a metal-carbon bond, was used as the reaction pathway to form the gold(I) coordination complexes. The ylides can displace the labile coordinated ligands very easily as they are very powerful nucleophiles. The chloride in chloro(tetrahydrothiophene)gold(I) and chloro(triphenylphosphine)gold(I) and the tetrahydrothiophene molecule in (pentafluorophenyl)(tetrahydrothiophene)gold(I) are readily displaced by the ylide ligands. Ylides can be stabilised by a keto, cyano or isocyano group which is able to delocalise the charge density otherwise centered on the ylidic carbon atom. Ylides not stabilised by carbonyl groups were chosen as ligands, as the carbonyl-stabilised ylides are weak bases and sometimes not able to displace already coordinated ligands. Scheme 2.3 shows the resonance structures of a carbonyl-

² R. Navarro and P. Esteban, *J. Chem. Soc., Dalton Trans.* (1999) 4111

³ H. Schmidbaur, *Acc. Chem. Res.*, **8** (1975) 62

⁴ A. M. Pizarro, V. P. Munk, C. Navarro-Ranninger and P. J. Sadler, *Angew. Chem.*, **115** (2003) 5497

stabilised ylide. The contribution of **F** (Scheme 2.3) explains why these ylides have a lower tendency to coordinate through the ylidic-carbon atom, compared to non-stabilised ylides. Stabilised phosphonium salts are also more acidic than non-stabilised phosphonium salts⁵.



Scheme 2.3

In the present study different methods were followed to coordinate the ylides to suitable gold precursor compounds. Four different methods of deprotonation of the phosphonium salts were investigated. *n*-BuLi deprotonated the phosphonium salt but, was not successful in removing all the bromide counterions from the phosphonium salts in the reaction mixture. Bromide ions preferentially coordinated to the gold instead of the ylide. Secondly, Ag₂O was used as a powerful deprotonating agent and simultaneous bromide scavenger, but the formation of water yielded complications. A reaction method, described by Usón *et al.*,⁶ in which the bromide counterion of the phosphonium salt is coordinated to the gold center to form an aurate counterion to the phosphonium salt, which is then subsequently deprotonated with NaH to form the corresponding gold(I)-ylide complex, was most effective. As mentioned in the general introduction, Vicente *et al.*⁷ reported a few compounds in which phosphonium ylides were successfully coordinated to gold(I) using Ph₃PAu(acac) (where acac = acetylacetonato) as starting material. The acac deprotonates the phosphonium salt to form acetylacetonate, while the ylide is coordinated to the gold(I). Coordination of one of the salts (**2**, *vide infra*) to gold(I) was attempted using this reaction method, but was not successful.

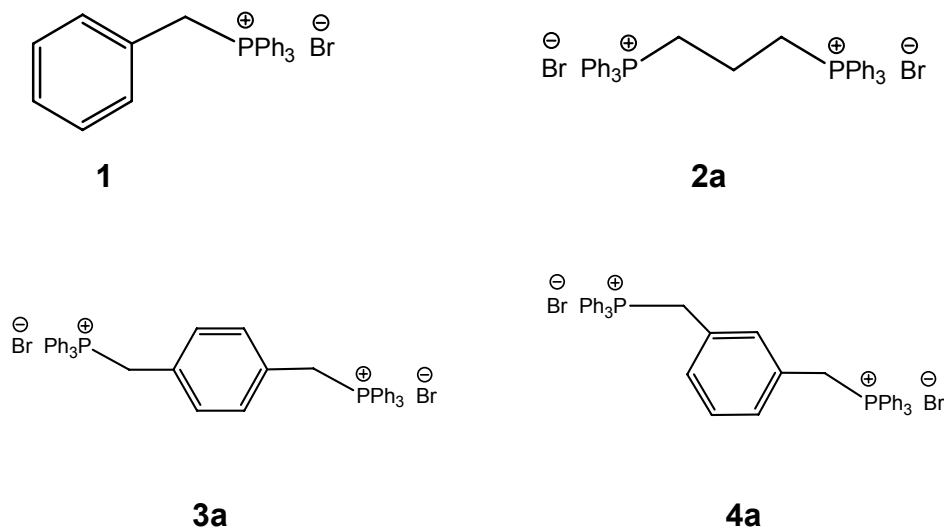
Usón's method is described in sections 2.2.3 and 2.2.4 because the products could be unequivocally characterised and reference to these characterisations are made throughout the discussion of the other procedures.

⁵ J. Vicente, M. T. Chicote, J. A. Cayuelas and J. Fernandez-Baeza, *J. Chem. Soc., Dalton Trans.* (1985) 1163

⁶ R. Usón, A. Laguna and A. Usón, *Inorg. Chim. Acta*, **73** (1983) 63

⁷ J. Vicente, M. T. Chicote, J. A. Cayuelas, J. Fernandez-Baeza, P. G. Jones and G. M. Sheldrick, *J. Chem. Soc., Dalton Trans.* (1985) 1163

Four different phosphonium salts were prepared (Scheme 2.4). Salts **1** and **2a** have no resonance stabilisation, while salts **3a** and **4a** have resonance stabilisation through the phenyl ring. The ylide from salt **1** has previously been coordinated to gold(I),⁶ but no crystal structure could be obtained for the product. The crystal structure of this compound (**5**) was successfully determined in this study (Chapter 3). Ylides derived from salts **2a** – **4a** have not been coordinated to gold before.



Scheme 2.4

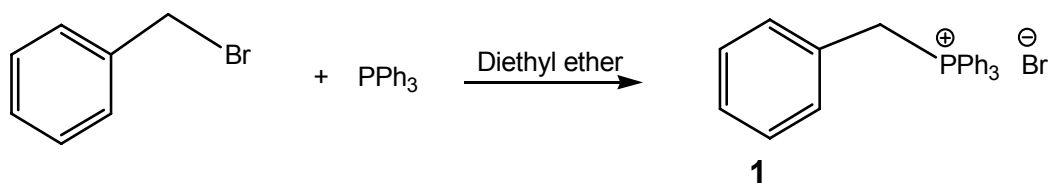
In this study the signals of the ¹H, ¹³C and ³¹P NMR spectra of the formed phosphorus ylide gold(I) complexes were fully assigned and we report the chemical shifts of the *ortho*, *meta* and *para* nuclei of the phenyl rings in the triphenylphosphonium units, as well as the chemical shifts of the central phenyl rings where applicable.

2.2.1 Preparation of benzyltriphenylphosphoniumbromide (**1**), 1,3-bis(triphenylphosphino)propanedibromide (**2a**), [1,4-phenylenebis(methylene)bis(triphenylphosphonium)]dibromide (**3a**) and [1,3-phenylenebis(methylene)bis(triphenylphosphonium)]dibromide (**4a**)

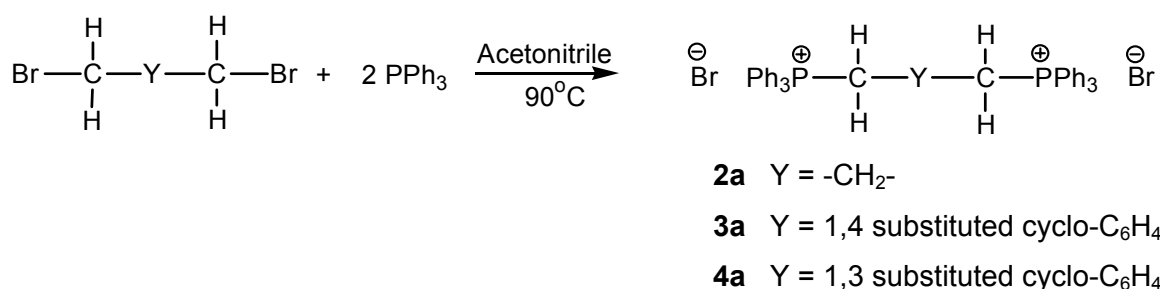
Salt **1** (Scheme 2.5) was prepared by the Wittig reaction between benzylbromide and triphenylphosphine as described by C. M. Garner.⁸ The preparation method was slightly modified. Diethyl ether was used as solvent instead of acetone and

⁸ C. M. Garner, *Techniques and experiments for the advanced organic laboratory*, John Wiley, New York (1997) p79

the mixture was stirred for 5 hours instead of standing for one hour. Salts **2a**, **3a** and **4a** (Scheme 2.6) were also prepared by the Wittig reaction, according to modified procedures described in the literature.⁹ Triphenylphosphine was dissolved in hot acetonitrile and 1,3-dibromopropane (**2a**), α,α' -dibromo-*p*-xylene (**3a**) or α,α' -dibromo-*m*-xylene (**4a**) was added and the suspension was refluxed for 24 hours, whereafter the precipitated salt **2a**, **3a**, or **4a** was filtered off.



Scheme 2.5



Scheme 2.6

The phosphonium salts are thermodynamically very stable with melting points between 240°C and 330°C. The salts should be kept away from oxygen as triphenylphosphine-oxide readily forms. Salt **1** is soluble in chloroform and ethanol. Compound **2a** is soluble in ethanol, chloroform, acetonitrile and insoluble in dichloromethane, while **3a** and **4a** are soluble in ethanol, methanol, chloroform and insoluble in dichloromethane and THF. White crystals suitable for single crystal X-ray diffraction studies were obtained of salts **3a** and **4a** and their molecular structures are discussed in Chapter 3.

⁹ L. Horner, H. Hoffmann, W. Klink, H. Ertel and V. G. Toscano, *Chem. Ber.*, **95** (1962) 581

2.2.2 Spectroscopic characterisation of compounds 1 - 4a

NMR Spectroscopy

The ^1H , ^{13}C and ^{31}P NMR data for compound **1** were recorded in CDCl_3 and are summarised in Table 2.1.

Table 2.1 ^1H , ^{13}C and ^{31}P NMR data for compound **1** in CDCl_3

Assignment	δ / ppm
^1H NMR	
H^7	5.22 (2H, d, $^2J = 14.4$ Hz)
$\text{H}^{3,5}$	7.01 (2H, m)
$\text{H}^{2,6}$	7.03 (2H, m)
H^4	7.14 (m)
H^{meta}	7.55 (6H, m)
H^{ortho}	7.63 (6H, m)
H^{para}	7.70 (3H, m)
^{13}C NMR	
C^7	30.7 (d, $^1J = 46.2$ Hz)
C^{ipso}	117.5 (d, $^1J = 85.8$ Hz)
C^1	126.9 (d, $^2J = 8.8$ Hz)
C^4	128.2 (d, $^5J = 3.8$ Hz)
$\text{C}^{3,5}$	128.6 (d, $^4J = 3.3$ Hz)
C^{ortho}	130.0 (d, $^2J = 12.6$ Hz)
$\text{C}^{2,6}$	131.2 (d, $^3J = 5.6$ Hz)
C^{meta}	134.1 (d, $^3J = 9.7$ Hz)
C^{para}	134.9 (d, $^4J = 2.5$ Hz)
^{31}P NMR	
P	23.8 (s)

The methylene protons appear as a doublet at δ 5.22 in the ^1H NMR spectrum, with a coupling constant of $^2J = 14.4$ Hz.

Protons $\text{H}^{3,5}$, $\text{H}^{2,6}$ and H^4 (Table 2.1) appear as multiplets at δ 7.01, δ 7.03, and δ 7.14 respectively. The *meta*, *ortho* and *para* protons of the phenyl rings in the triphenylphosphonium units also appear as multiplets at δ 7.55, 7.63 and 7.70 respectively.

The methylene carbon in the ^{13}C NMR spectrum resonates as a doublet at δ 30.7 with coupling constant $^1J = 46.2$ Hz, due to coupling between the carbon and phosphorus atoms. The *ipso* carbons of the triphenylphosphonium units form a doublet at δ 117.5, with a coupling constant of $^1J = 85.8$ Hz. All the other signals could be assigned to the phenyl carbons and each carbon signal forms a doublet due to coupling between the phosphorus atom and the carbon atoms.

The phosphorus atom appears as a singlet at δ 23.8 in the ^{31}P NMR spectrum.

The ^1H , ^{13}C and ^{31}P NMR data for compound **2a** were recorded in CDCl_3 and are summarised in Table 2.2. Two dimensional NMR experiments, Gradient Heteronuclear Single Quantum Coherence (gHSQC), were conducted to establish which proton signals are related to which carbon signals.

A multiplet at δ 1.88 is assigned to the protons H^1 (Table 2.2). The protons H^2 form a multiplet at δ 4.59. The *meta* protons of the phenyl rings on the triphenylphosphonium units, form a multiplet at δ 7.58, *ortho* protons are observed at δ 7.68 and the *para* protons at δ 7.88.

Magnetic inequivalence of the carbon atoms in this compound causes coupling which complicates the ^{13}C NMR spectrum. The phenyl rings of the triphenylphosphonium units contain magnetically inequivalent carbon atoms, resulting in multiplets for the *ortho*, *meta* and *para* carbon atoms (δ 130.2, δ 134.1, δ 134.7).¹⁰ This magnetic inequivalence stems from the symmetry of the

¹⁰ D. L. Pavia, G. M. Lampman, G. S. Kriz, in *Introduction to Spectroscopy*, ed. D. L. Pavia, G. M. Lampman, G. S. Kriz, Hartcourt College Publishers, Orlando (2001), p. 258

molecule,¹¹ and results in signals for an AA'XX' spin system with $J_{XX'} = 0$. Spectra of an AA'XX' spin system are always found when a molecule contains two pairs of carbons, such that the carbons within each pair can be imagined to exchange positions by rotation about an axis of symmetry or by reflection at a plane of symmetry.¹¹ Each half of the AA'XX' spectrum can have up to 10 lines, giving rise to the observed multiplets. It is possible, with much labour, to calculate the coupling constants manually, but these calculations are usually performed by simulation or iteration methods.¹² A triplet signal was expected for **C**¹, as it couples to two phosphorus atoms, and a doublet signal for **C**², as both **C**² carbons couple to a phosphorus atom, however, the same magnetic inequivalence is observed. A multiplet at δ 22.4 was assigned to **C**². Carbon **C**¹ appears as a broad singlet (δ 17.8) because, the P-C²-C¹ angles are larger than the preferred 109.5° for effective geminal coupling, and the β -carbon experiences only a small coupling resulting in a slightly broader signal.¹³

The phosphorus atoms give rise to a singlet at δ 25.5 in the ³¹P NMR spectrum. The two phosphorus atoms are chemically equivalent, but are probably not magnetically equivalent, as was suggested by the ¹³C NMR spectrum. The magnetic inequivalence can only be seen when the phosphorus atoms couple to another nucleus. In the ³¹P NMR spectrum they do not couple to another nucleus and, therefore, only a single resonance is observed.

The ¹H, ¹³C and ³¹P NMR data for compound **3a** were recorded in CDCl₃ at 40°C and are summarised in Table 2.3. Two dimensional NMR experiments, gHSQC, were conducted to establish which protons are connected to which carbons.

The methylene protons in **3a** couple to the phosphorus atom to form a doublet at δ 4.62 (¹J_{PH} = 13.6 Hz). The protons on the central phenyl ring display a singlet at δ 6.65. The phenyl protons of the triphenylphosphonium unit display the same coupling pattern as compound **2a**.

¹¹ H. Friebolin, *Basic One- and Two- Dimensional NMR Spectroscopy*, Wiley, Weinheim (1998) p124-125

¹² H. Günther, *Angew. Chem.*, **11** (1972) 961

¹³ D. L. Pavia, G. M. Lampman and G. S. Kriz, *Introduction to Spectroscopy*, Hartcourt College Publishers, Orlando (2001), p. 220

Table 2.2 ^1H , ^{13}C and ^{31}P NMR data for compound **2a** in CDCl_3

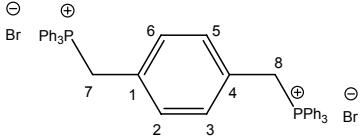
Assignment	δ / ppm
^1H NMR	
H^1	1.88 (2H, m)
H^2	4.59 (4H, m)
H^{meta}	7.58 (12H, m)
H^{para}	7.68 (6H, m)
H^{ortho}	7.88 (12H, m)
^{13}C NMR	
C^1	17.8 (br s)
C^2	22.4 (m)
C^{ipso}	117.8 (d, $^1J = 87.4$ Hz)
C^{ortho}	130.2 (m)
C^{meta}	134.1 (m)
C^{para}	134.7 (m)
^{31}P NMR	
P	25.5 (s)

The methylene carbon in **3a**, couples with the phosphorus atom to form a doublet in the ^{13}C NMR spectrum at δ 29.6 ($^1J = 52.3$ Hz), but fine coupling in both signals of the doublet provides evidence that the methylene carbons are magnetically inequivalent, even though they are chemically equivalent. The magnetic inequivalence of the carbon atoms complicates the splitting patterns of the signals for the central phenyl ring and the phenyl rings on the phosphorus atoms.

The phosphorus atom gives rise to a singlet at δ 28.1 in the ^{31}P NMR spectrum.

Table 2.4 summarises the ^1H , ^{13}C and ^{31}P NMR data for compound **4a**. The data were recorded in CD_2Cl_2 and two dimensional NMR experiments, gHSQC, were conducted to establish which proton signals are related to which carbon signals.

Table 2.3 ^1H , ^{13}C and ^{31}P NMR data for compound **3a** in CDCl_3

	
Assignment	δ / ppm
^1H NMR	
$\text{H}^{7,8}$	4.62 (4H, d, $^2J = 13.6$ Hz)
$\text{H}^{2,3,5,6}$	6.65 (4H, s)
H^{ortho}	7.43 (12H, m)
H^{meta}	7.53 (12H, m)
H^{para}	7.69 (6H, m)
^{13}C NMR	
$\text{C}^{7,8}$	29.6 (dm, $^1J = 52.3$ Hz)
C^{ipso}	117.1 (d, $^1J = 86.9$ Hz)
$\text{C}^{1,4}$	127.8 (m)
C^{ortho}	130.3 (m)
$\text{C}^{2,3,5,6}$	131.7 (br s)
C^{meta}	133.9 (m)
C^{para}	135.4 (br s)
^{31}P NMR	
P	28.1 (s)

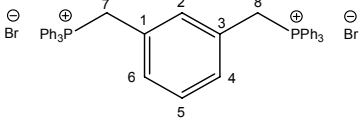
Again the methylene protons display a doublet at δ 5.23 ($^1J_{\text{PH}} = 15.1$ Hz) in the ^1H NMR spectrum of **4a** (Table 2.4). The *ortho*, *meta* and *para* protons of the phenyl rings on the triphenylphosphonium units appear as multiplets at δ 7.43, 7.53 and 7.69 respectively.

In the ^{13}C NMR spectrum of **4a**, the methylene and *ipso* carbon atoms display doublet signals at δ 29.6 ($^1J = 47.5$ Hz) and δ 118.0 ($^1J = 86.3$ Hz). More complicated AA'XX' ($J_{\text{XX}'} = 0$ Hz) splitting patterns are observed for the phenyl rings.

The phosphorus atom has a single signal at δ 23.4 in the ^{31}P NMR spectrum, confirming the theory that the overlapping signals in the ^{13}C NMR spectrum stem

from one compound only, thus exhibiting a magnetic inequivalence between the nuclei and not a structural difference.

Table 2.4 ^1H , ^{13}C and ^{31}P NMR data for compound **4a** in CD_2Cl_2

	
Assignment	δ / ppm
^1H NMR	
$\text{H}^{7,8}$	5.23 (4H, d, $^2J = 15.1$ Hz)
H^2	6.88 (1H, d, $^4J_{\text{PH}} = 7.7$ Hz)
$\text{H}^{4,6}$	7.00 (2H, m)
H^5	7.53 (1H, m)
H^{ortho}	7.60 (12H, m)
H^{meta}	7.71 (12H, m)
H^{para}	7.77 (6H, m)
^{13}C NMR	
$\text{C}^{7,8}$	29.6 (d, $^1J = 47.5$ Hz)
C^{ipso}	118.0 (d, $^1J = 86.3$ Hz)
C^2	129.0 (m, $^3J = 3.2$ Hz)
$\text{C}^{1,3}$	129.2 (m, $^2J = 9.9$ Hz)
C^{ortho}	130.5 (m, $^2J = 13.1$ Hz)
$\text{C}^{6,4}$	131.8 (m, $^3J = 8.6$ Hz)
C^{meta}	134.9 (m, $^3J = 10.2$ Hz)
C^5	135.2 (m, $^4J = 6.2$ Hz)
C^{para}	135.5 (m, $^4J = 1.3$ Hz)
^{31}P NMR	
P	23.4 (s)

Mass spectrometry

The electron impact mass spectrometry (EI-MS) data for compound **1** are summarised in Table 2.5.

Table 2.5 Mass spectrometry data for compound **1**

M/z	Intensity (%)	Fragment ion
353	22	[PhCH ₂ PPh ₃] ⁺
262	100	[PPh ₃] ⁺
183	66	[PPh ₂] ⁺
108	22	[PPh] ⁺
91	9	[PhCH ₂] ⁺

Signals for the anions are not present in the spectrum. The cation at 353, [PhCH₂PPh₃]⁺, and the fragmentation thereof is observed. Triphenylphosphine forms the base peak at m/z 262. Subsequent fragmentation of the triphenylphosphine unit forms fragment ions at 183 ([PPh₂]⁺) and 108 ([PPh]⁺). The benzyl fragment is observed at m/z 91.

The EI-MS data for compound **2a** are summarised in Table 2.6.

Neither the molecular ion, nor the cation is observed. Fragmentation of the triphenylphosphonium unit (base peak, m/z 263) is seen in the fragment ions at m/z 184, 108 and 77.

Table 2.6 Mass spectrometry data for compound **2a**

M/z	Intensity (%)	Fragment ion
263	100	[PPh ₃] ⁺ + H
184	66	[PPh ₂] ⁺
108	32	[PPh] ⁺
77	18	[Ph] ⁺

The EI-MS data for compounds **3a** and **4a** could not be measured because of the very high melting points of these compounds (350°C and 239°C respectively). Electrospray ionisation mass spectrometry (ESI-MS) was used to measure the mass spectra of these compounds. The bombardment of a liquid sample with a primary beam of electrons induces the secondary emission of charged fragments of the molecule. These spectra were recorded in positive mode, therefore, only positively charged fragments are detected.

The ESI-MS data of compound **3a** are summarised in Table 2.7. A 1:1 CHCl₃/methanol mixture was used as matrix in order to favour ionisation.

Table 2.7 Mass spectrometry data for compound **3a**

M/z	Intensity (%)	Fragment ion
365	49	[PPh ₃ CHC ₆ H ₄ CH ₂] ⁺
314	100	[M] ²⁺
262	12	[PPh ₃] ⁺

The cation of **3a** loses a triphenylphosphine group to yield the fragment ion at m/z 365. The doubly charged cation is observed at m/z 314 and the triphenylphosphonium ion at m/z 262.

The ESI-MS data of compound **4a** were recorded in a methanol matrix and are summarised in Table 2.8.

Table 2.8 Mass spectrometry data for compound **4a**

M/z	Intensity (%)	Fragment ion
707	70	[Br][Ph ₃ PCH ₂ C ₆ H ₄ CH ₂ PPh ₃] ⁺
627	70	[Ph ₃ P=CHC ₆ H ₄ CH ₂ PPh ₃] ⁺
315	100	[Ph ₃ PCH ₂ C ₆ H ₄ CH ₂ PPh ₃] ²⁺

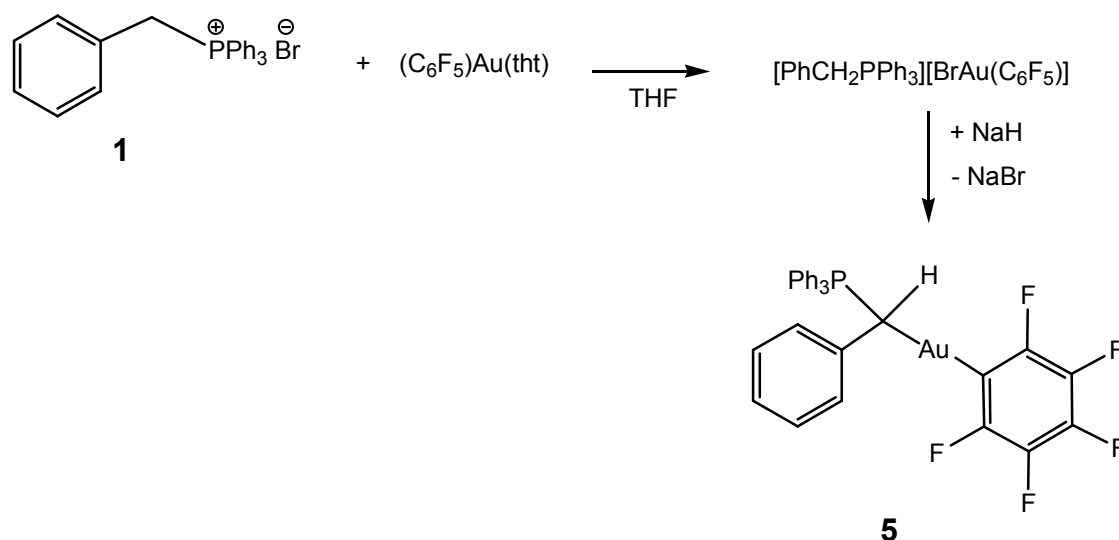
The biscation with one bromide counterion form a peak at m/z 707. Subsequent loss of a proton and the one counterion forms a fragment with m/z 627 and the biscation [Ph₃PCH₂C₆H₄CH₂PPh₃]²⁺ appears as the base peak at m/z 315.

2.2.3 Preparation of [Ph₃P(Ph)CHAu(C₆F₅)] (5**), [Ph₃PCH(Au(C₆F₅))CH₂CH(Au(C₆F₅))PPh₃] (**6**), *p*-[(C₆F₅)AuCH(PPh₃)C₆H₄CH(PPh₃)Au(C₆F₅)] (**8**) and *m*-[(C₆F₅)AuCH(PPh₃)C₆H₄CH(PPh₃)Au(C₆F₅)] (**9**)**

The gold(I) phosphonium ylide coordination complexes **5**, **6**, **8** and **9** were prepared by using a procedure described by Usón *et. al.*⁶ in which the bromide is coordinated to form a phosphine aurate, which is subsequently deprotonated with NaH to form the corresponding gold-ylide complex.

The gold precursor compound (pentafluorophenyl)(tetrahydrothiophene)-gold(I), $(C_6F_5)Au(tht)$, was prepared according to methods described in the literature.¹⁴

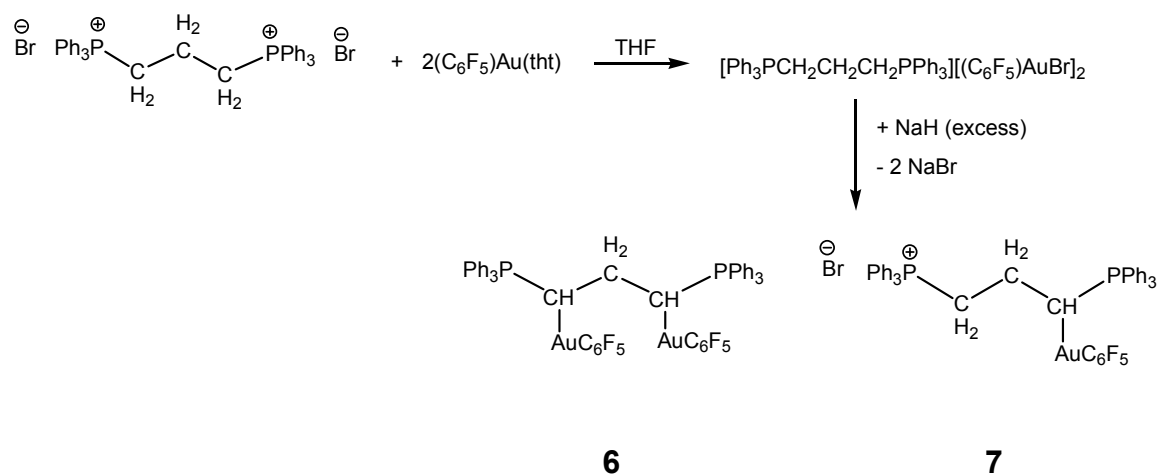
The $(C_6F_5)Au(tht)$ was reacted in a 1:1 molar ratio with benzyltriphenylphosphoniumbromide (**1**) in THF and NaH was used to deprotonate the formed phosphonium salt complex, $[PhCH_2PPh_3][Au(C_6F_5)Br]$, and form the sought-after gold(I)-ylide complex $[Ph_3P(Ph)CHAu(C_6F_5)]$ (**5**) (Scheme 2.7). An extraction with diethyl ether yielded white crystals suitable for single crystal X-ray diffraction studies after crystallisation. The molecular structure of **5** is discussed in Chapter 3. Compound **5** represents the first example of an ylide complex that is stabilised by $C_6F_5^-$.



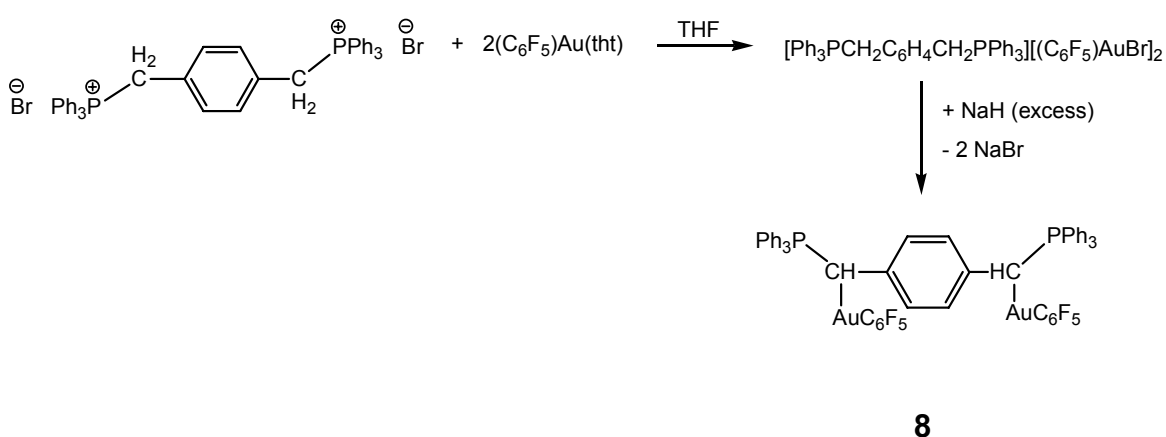
Scheme 2.7

The same procedure was used to prepare compounds **6** (Scheme 2.8) and **8** (Scheme 2.9). The respective phosphonium salts, **2a** and **3a**, were reacted in a 1:2 molar ratio with the gold precursor compound, $(C_6F_5)Au(tht)$. Compounds **6** and **7** could not be isolated and the mixture was characterised. Solvent manipulation was necessary to isolate compound **8**.

¹⁴ R. Usón, A. Laguna and M. Laguna, *Inorg. Synth.*, **26** (1989) 85, b) R. Usón, A. Laguna and M. Laguna, *Inorg. Synth.*, **21** (1982) 72.

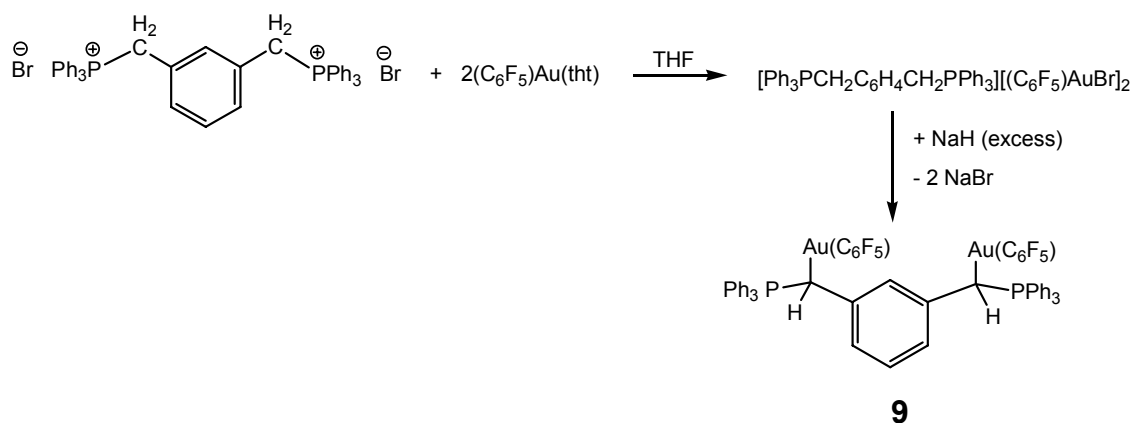


Scheme 2.8



Scheme 2.9

Compound **9** was prepared in a similar, but slightly modified way (Scheme 2.10). Salt **4a** was reacted with $(\text{C}_6\text{F}_5)\text{Au}(\text{tht})$ in a 1:2 (phosphonium salt : gold precursor) molar ratio in THF and after addition of NaH, the suspension was stirred overnight. An extraction with diethyl ether removed the unreacted phosphonium salt and crystals suitable for a crystal structure determination were obtained from a solution of **9** in CH_2Cl_2 layered with pentane after three days at 4°C .



Scheme 2.10

The sought-after gold ylide complexes were isolated from these reactions, whereas in the reaction procedures where the phosphonium salts are deprotonated first to obtain the ylides which were then coordinated to gold, only a stable gold bromide compound forms as the product (Section 2.2.5).

2.2.4 Spectroscopic characterisation of compounds 5 - 9

NMR Spectroscopy

The ^1H , ^{13}C and ^{31}P NMR data for compound **5** recorded in CDCl_3 are summarised in Table 2.9.

The carbon signals corresponding to the pentafluorophenyl carbon atoms display no change after coordination of the ylide to gold(I). No coupling between the phosphorus and the fluorine atoms is observed, as the signals appear the same as in the ^{13}C NMR spectrum of the gold precursor compound, $\text{C}_6\text{F}_5\text{Au}(\text{tht})$. The splitting pattern observed is, therefore, due to carbon to fluorine coupling.

The ylidic proton (H^7 , Table 2.9) in **5** displays an upfield shift of 1.3 ppm after coordination, in comparison with the uncoordinated ligand (**1**).

The ylidic carbon (C^7) displays a downfield shift of 4.7 ppm, after coordination to gold. The *ipso* carbons of the triphenylphosphonium units display a downfield shift of 7.7 ppm, and C^1 an upfield shift of 2 ppm. Carbon C^4 displays a significant

downfield shift of 5.8 ppm. The *para* carbons also display a small upfield shift of 1.6 ppm. All coupling constants are as expected for carbon-phosphorus coupling.

Table 2.9 ^1H , ^{13}C and ^{31}P NMR data for compound **5** in CDCl_3

Assignment	δ / ppm
^1H NMR	
H^7	3.92 (1H, d, $^2J = 13.6$ Hz)
H^{2-6}	7.00 (5H, m)
H^{meta}	7.50 (6H, m)
H^{para}	7.63 (3H, m)
H^{ortho}	7.75 (6H, m)
^{13}C NMR	
C^7	35.4 (dm, $^1J = 31.6$ Hz)
C^1	124.9 (d, $^2J = 3.8$ Hz)
C^{ipso}	125.2 (d, $^1J = 84.1$ Hz)
$\text{C}^{3,5}$	128.6 (d, $^4J = 2.9$ Hz)
C^{ortho}	129.4 (d, $^2J = 11.7$ Hz)
$\text{C}^{2,6}$	130.2 (d, $^3J = 8.0$ Hz)
C^8	132.3 (m)
C^{para}	133.3 (d, $^4J = 2.9$ Hz)
C^4	134.0 (d, $^4J = 7.3$ Hz)
C^{meta}	134.2 (d, $^3J = 8.9$ Hz)
C^{10}	137.1 (dm, $^1J = 232.2$ Hz)
C^{11}	138.7 (dm, $^1J = 244.3$ Hz)
C^9	148.9 (ddm, $^1J = 225.8$ Hz, $J = 26.2$ Hz)
^{31}P NMR	
P	26.21 (s)

The phosphorus signal displays a downfield shift $\Delta\delta$ 2.4 after coordination of the deprotonated phosphonium salt to the gold(I), because of the deshielding influence of the metal on the phosphorus atom.

All these changes in the chemical shifts after coordination of the deprotonated phosphonium salt to the gold(I), correspond well with observed changes in chemical shifts reported by Vicente *et al.*,¹⁵ as mentioned in the general introduction.

The ¹H, ¹³C and ³¹P NMR data for compound **6** were recorded in CDCl₃ and are summarised in Table 2.10.

The ¹H, ¹³C and ³¹P NMR spectra reveal that a mono-coordinated compound (**7**) formed, since two phosphorus signals (coupled with each other) of equal intensity are observed in the ³¹P NMR spectrum and two sets of *ipso*, *ortho*, *meta* and *para* carbon signals of equal intensity for the phenyl rings of the triphenylphosphonium units are observed. One of these sets of signals is very similar to the free phosphonium salt signals, while the other set of signals differs significantly from these. A smaller amount (30%) of the desired, double coordinated compound (**6**) formed as shown by the third set of signals similar to the signals for each type of carbon, proton and phosphorus nucleus in the phosphonium salt, but slightly shifted as expected.

In the ¹H NMR spectrum the signal corresponding to **H**¹ of the gold(I) coordinated side of compound **7** displays a downfield shift of 0.97 ppm, while **H**² displays an insignificant shift $\Delta\delta$ 0.6 downfield, after coordination of the ylide derived from the phosphonium salt to gold. In **6**, the chemical shift of **H**¹ shifted 0.5 ppm downfield, while **H**² shifted 2 ppm upfield. The proton signals of the triphenylphosphonium units of both these compounds did not change much after coordination took place.

After coordination of the ylide derived from salt **2a**, the carbon signal for **C**¹ in **7** in the ¹³C NMR spectrum, displays a downfield shift of 5.5 ppm, while the signal for the two **C**² carbons overlap and show a downfield shift of 4 ppm. In **6**, **C**¹ shows a downfield shift $\Delta\delta$ 4 and **C**² a downfield shift $\Delta\delta$ 4.1. The triphenylphosphonium unit of the gold(I) coordinated side of **7** exhibits an *ipso* signal with a downfield shift of 6.2 ppm, while the *meta*, *ortho* and *para* carbon signals display no significant change in chemical shift after coordination to gold. The *ipso* carbons of

¹⁵ J. Vicente, A. R. Singhal and P. G. Jones, *Organometallics*, **21** (2002) 5887

6, present a downfield shift of 6.6 ppm, while the *ortho*, *meta* and *para* carbon shifts stayed the same as in the uncoordinated phosphonium salt.

Table 2.10 ^1H , ^{13}C and ^{31}P NMR data for compound **6** and **7** in CDCl_3

Assignment	δ / ppm	δ / ppm
<div style="display: flex; justify-content: space-around; align-items: center;"> <div style="text-align: center;"> <p>6</p> </div> <div style="text-align: center;"> <p>7</p> </div> </div>		
^1H NMR		
H ¹	2.36 (2H, m)	2.85 (2H, m)
H ²	2.55 (2H, m)	2.63 (1H, m)
H ³		4.04 (2H, m)
H ^{meta}	7.30 (12H, m)	7.53 (12H, m)
H ^{para}	7.55 (6H, m)	7.65 (6H, m)
H ^{ortho}	7.90 (12H, m)	7.78 (12H, m)
^{13}C NMR		
C ¹	21.8 (br s)	23.3 (br s)
C ²	26.5 (m)	26.4 (m)
C ³		22.1 (m)
C ^{ipso}	124.4 (d, $^1J = 84.5$ Hz)	117.6 (d, $^1J = 86.7$ Hz)
C ^{ortho}	131.0 (m)	124.0 (d, $^1J = 84.5$ Hz)
		129.6 (d, $^2J = 12.0$ Hz)
		130.7 (d, $^2J = 12.8$ Hz)
C ^{ipso} C ₆ F ₅	132.8 (m)	131.87 (m)
C ^{meta}	133.8 (m)	133.3 (d, $^3J = 9.0$ Hz)
		133.5 (d, $^3J = 8.3$ Hz)
C ^{para}	133.1 (m)	133.6 (m)
		135.5 (d, $^4J = 3.0$ Hz)
C ^{meta} C ₆ F ₅	136.5 (dm, $J_{\text{CF}} = 246.3$ Hz)	137.7 (dm, $J_{\text{CF}} = 259.5$ Hz)
C ^{para} C ₆ F ₅	138.5 (dm, $J_{\text{CF}} = 251.2$ Hz)	138.1 (dm, $J_{\text{CF}} = 255.3$ Hz)
C ^{ortho} C ₆ F ₅	148.6 (ddm, $J_{\text{CF}} = 225.2$ Hz, $J_{\text{CF}} = 29.3$ Hz)	149.0 (ddm, $J_{\text{CF}} = 223.2$ Hz, $J_{\text{CF}} = 30.6$ Hz)
^{31}P NMR		
P	29.3 (s)	22.6 (d, $^4J = 14.6$ Hz), 29.3 (d, $^4J = 10.9$ Hz)

The phosphorus atom, of the gold(I) coordinated side of complex **7**, presents a phosphorus signal with a downfield shift of 3.8 ppm in the ^{31}P NMR spectrum, while the phosphorus signal of **6**, shifted $\Delta\delta$ 3.8 downfield after coordination to the gold.

The ^1H , ^{13}C and ^{31}P NMR data for compound **8** were recorded in THF-d8, as it is poorly soluble in dichloromethane and DMSO and insoluble in most other solvents, such as diethyl ether, pentane and hexane. The ^1H , ^{13}C and ^{31}P NMR data for **8** in THF-d8 are summarised in Table 2.11.

In compound **8**, four diastereomeric structures (DD, LL, DL and LD) are possible as a result of the two different conformations (D and L) that each of the two chiral centra (the two ylidic carbons) may allow. These four diastereomers give two different, but very similar sets of NMR signals for each type of carbon, proton or phosphorus atom in the spectra. The DD and LL isomers have one set of signals and the DL and LD another. For compound **8**, two chemical shifts per carbon, proton and phosphorus atom type are reported, one corresponding to each set of diastereomers. From the NMR spectra (^{13}C , ^1H and ^{31}P) it is evident that one of these sets of diastereomers is formed in a larger percentage (60%) than the other (40%).

The ^{31}P NMR spectrum displays two singlet signals corresponding to the two sets of diastereomers at δ 26.12 and δ 26.32 and no coupling between the phosphorus atoms are observed.

In the ^1H NMR spectrum the two protons H^7 and H^8 exhibit a doublet at δ 4.00 (for the one set of diastereomers) and a doublet at δ 4.04 (for the other set of diastereomers) with proton-phosphorus coupling constants of 13.4 Hz and 13.5 Hz respectively. The central phenyl ring protons are all chemically equivalent and display a broad singlet for each set of the diastereomers at δ 6.68 and δ 6.72. The two sets of signals for the phenyl protons of the triphenylphosphonium units are very similar and overlap with each other to form multiplets.

Table 2.11 ^1H , ^{13}C and ^{31}P NMR data for compound **8** in THF-d8

Assignment	δ / ppm
^1H NMR	
$\text{H}^{7,8}$	4.00 (2H, d, $^1J = 13.4$ Hz) 4.04 (2H, d, $^1J = 13.5$ Hz)
$\text{H}^{2,3,5,6}$	6.68 (4H, br s) 6.72 (4H, br s)
H^{ortho}	7.52 (24H, m)
H^{para}	7.66 (12H, m)
H^{meta}	7.83 (24H, m)
^{13}C NMR	
$\text{C}^{7,8}$	34.9 (m) 35.3 (m)
C^{ipso}	126.4, 126.5 (two dd, $^1J = 85.3$ Hz, $^9J = 1.5$ Hz)
C^{ortho}	130.2 (m)
$\text{C}^{1,4}$	131.2 (m) 131.4 (m)
C^{para}	134.1 (br s)
C^{meta}	135.3 (m)
$\text{C}^{2,3,5,6}$	137.0 (m) 137.2 (m)
^{31}P NMR	
P	26.12 (s), 26.32 (s)

In the ^{13}C NMR spectrum the two ylidic carbons in each set of diastereomers are equal and the two sets of diastereomers give rise to two multiplets at δ 34.9 and δ 35.3. A doublet for each set of diastereomers is expected, but due to the magnetic inequivalence, each of these ylidic carbons gives rise to a multiplet signal, similar to the signals in the free phosphonium salt. Six signals in the range 125.8 -127.0 were assigned to the *ipso* carbons of the phenyl rings of the triphenylphosphonium units. A doublet for each of the two sets of diastereomers is observed. Each

doublet exhibits long range coupling to the other phosphorus atom, due to the chemical inequivalence of the phosphorus atoms. Within **8**, some carbon atoms of the phenyl rings of the two triphenylphosphonium units (on either side of the central phenyl ring) are chemically equivalent and display one multiplet each for the *ortho*, *meta* and *para* carbons.

The sample concentration was too low (due to insolubility of the compound), to observe the signals of the AuC₆F₅ units in the ¹³C NMR.

The spectra of **8** and **3a** were recorded in different solvents and are not comparable.

The ¹H, ¹³C and ³¹P NMR data for compound **9** were recorded in CD₂Cl₂ and are summarised in Table 2.12.

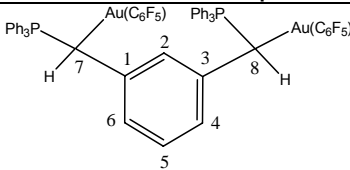
From the ¹³C, ¹H and ³¹P NMR spectra it follows that compound **9** does not form diastereomers, as there is only one signal for each type of carbon, proton or phosphorus atom. The same pattern of overlapping doublets, as a result of the magnetic inequivalence of C^{meta} and C^{ortho} (in the phenyl ring of the triphenylphosphonium unit), was visible as previously mentioned for complex **8** and the free phosphonium salt, **4a**.

The sample concentration was too low to observe the carbon signals for the pentafluorophenyl groups, as a result of poor solubility of compound **9**.

The ³¹P NMR spectrum displays one single resonance at δ 25.6, providing further evidence that no diastereomers are involved. The magnetic inequivalence of the phosphorus atoms is only visible when they couple to another nucleus, therefore, only a singlet is observed in the ³¹P NMR spectrum.

After coordination of the deprotonated salt **4a** to the gold, the chemical shift of the ylidic protons show an upfield shift of 1.5 ppm. The central phenyl ring protons resonate at higher field strength, Δδ 0.1 - 0.4.

Table 2.12 ^1H , ^{13}C and ^{31}P NMR data for compound **9** in CD_2Cl_2

Assignment	δ / ppm
	
^1H NMR	
$\text{H}^{7,8}$	3.77 (2H, d, $^2J = 13.9$ Hz)
$\text{H}^{6/4}$	6.61 (2H, m)
$\text{H}^{2,5}$	6.74 (2H, m)
H^{meta}	7.46 (12H, m)
H^{para}	7.60 (6H, m)
H^{ortho}	7.70 (12H, m)
^{13}C NMR	
$\text{C}^{7,8}$	35.6 (d, $^1J = 36.0$ Hz)
C^{ipso}	125.4 (d, $^1J = 84.4$ Hz)
C^2	126.9 (t, $^3J = 5.5$ Hz)
$\text{C}^{1,3}$	129.1 (m)
C^{ortho}	129.8 (m)
$\text{C}^{4/6}$	132.3 (m)
C^{para}	133.7 (m)
C^{meta}	134.5 (m)
C^5	140.4 (t, $^4J = 4.8$ Hz)
^{31}P NMR	
P	25.6 (s)

The ylidic carbons exhibit a downfield shift of 6 ppm in their chemical shifts after coordination of the ylide to gold. The *ipso* carbons of the triphenylphosphonium groups, display a downfield shift of 7.4 ppm. The chemical shifts of the central phenyl ring carbon atoms resonate at higher field strength, $\Delta\delta$ 2.1 - 5.2, while the triphenylphosphonium carbon atoms did not show a significant change in their chemical shifts.

Mass spectrometry

The electron impact mass spectrometry data for compound **5** are summarised in Table 2.13.

A small peak for the molecular ion is observed at 716. The peak equal in mass to the cation of the phosphonium salt (**1**) at m/z 352, is the base peak.

Table 2.13 EI-MS data for compound **5**

M/z	Intensity (%)	Fragment ion
716	3	$[M]^+$
459	3	$[AuPPh_3]^+$
352	100	$[PhCH_2PPh_3]^+$
275	6	$[PPh_3CH_2]^+$
262	40	$[PPh_3]^+$
183	60	$[PPh_2]^+$
167	38	$[C_6F_5]^+$
91	24	$[PhCH_2]^+$

Compounds **6** - **9** have molecular masses higher than 1000 and were, therefore, analysed using electrospray ionisation mass spectrometry (ESI-MS).

The mass spectrometry data for compound **6** were recorded from the crude mixture in a dichloromethane matrix and are summarised in Table 2.14.

Table 2.14 ESI-MS data recorded from the crude mixture of the reaction of **6**

M/z	Intensity (%)	Fragment ion
1373	35	$[M]^+$ of 6 + CH_2Cl_2
1293	15	$[M]^+$ of 6
929	100	$[M]^+$ of 7
761	95	$[Ph_3PCH(Au)CH_2CH_2CH_2PPh_3]^+$

The molecular ion of **6** forms a peak at m/z 1293. The base peak is formed by the compound **7** at m/z 929. The molecular ion of **6** associated with one dichloromethane molecule formed a fragment at m/z 1373.

The mass spectrometry data for compound **8** are summarised in Table 2.15. Dichloromethane was used as matrix.

Table 2.15 Mass spectrometry data for compound **8**

M/z	Intensity (%)	Fragment ion
1354	15	$[M]^+$
991	100	$[\text{Ph}_3\text{PCH}(\text{AuC}_6\text{F}_5)\text{C}_6\text{H}_4\text{CH}_2\text{PPh}_3]^+$
313	15	$[\text{Ph}_3\text{PAuC}_6\text{F}_5]^+$

The molecular ion was observed at m/z 1354 and the mono-coordinated compound formed the base peak at m/z 991.

The mass spectrometry data for compound **9** were recorded in a chloroform matrix and are summarised in Table 2.16.

The biscation of the phosphonium salt (**4a**) associated with one molecule of CHCl_3 to give the base peak at m/z 372. A peak at m/z 358 was assigned to the product of a homoleptic rearrangement, $[\text{PPh}_3\text{AuPPh}_3]^+$.

Table 2.16 Mass spectrometry data for compound **9**

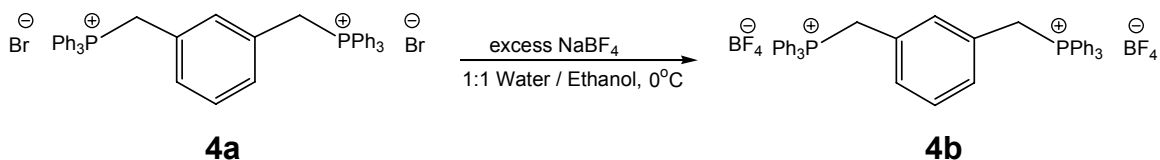
M/z	Intensity (%)	Fragment ion
372	100	$[\text{Ph}_3\text{PCH}_2\text{C}_6\text{H}_4\text{CH}_2\text{PPh}_3]^{2+} + \text{CHCl}_3$
358	18	$[\text{Ph}_3\text{PAuPPh}_3]^+$

2.2.5 Preparation of $[\text{Ph}_3\text{PCH}(\text{AuC}_6\text{F}_5)\text{C}_6\text{H}_4\text{CH}(\text{AuC}_6\text{F}_5)\text{PPh}_3]$ (**9**), by deprotonation of the phosphonium salt **4b** with *n*-BuLi

Gold has a very great affinity for bromide and the bromide ion usually coordinates to the gold instead of the ylide. Thus the bromide counterions of the phosphonium

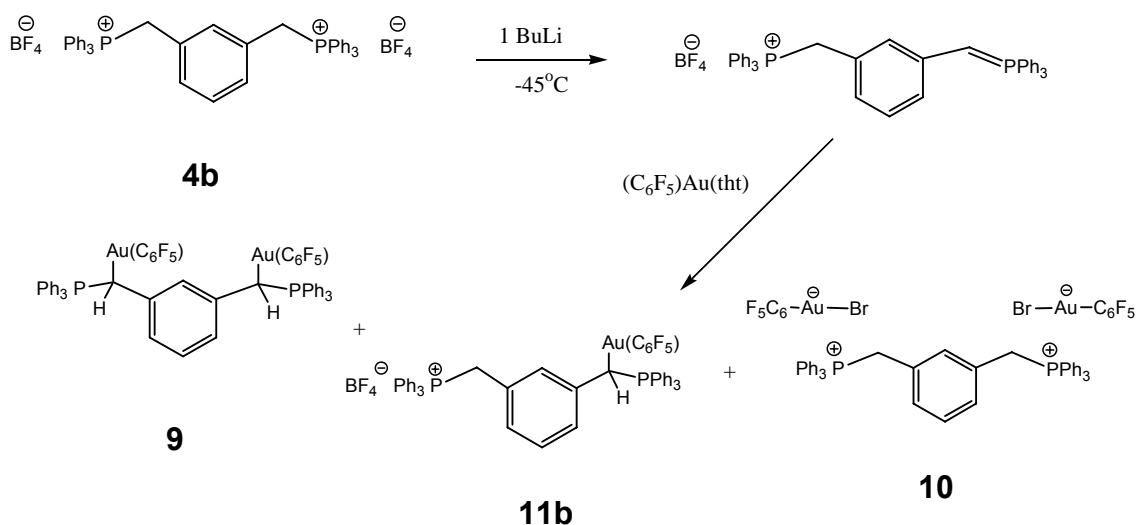
salts were replaced with BF_4^- . This is important if the phosphonium salt is to be deprotonated with *n*-BuLi and subsequently reacted with $\text{C}_6\text{F}_5\text{Au}(\text{tht})$. The bromide ions are displaced with tetrafluoroborate because the BF_4^- ions are larger than the bromide ions and prefer the bulky phosphonium cation instead of the sodium ion.

In order to substitute the bromide counterions of the phosphonium salts with tetrafluoroborate, an excess of sodiumtetrafluoroborate was dissolved in a 1:1 water/ethanol mixture. The phosphonium salt was added to this, yielding a clear solution, and stirred for two hours at 0°C . The phosphonium salt with tetrafluoroborate counterions (**4b**) formed a white precipitate, which was filtered off and dried under vacuum. It was then recrystallised from hot ethanol (Scheme 2.11).



Scheme 2.11

The neutral ylide obtained from deprotonating **4b** with one molar equivalent of *n*-BuLi, was then reacted in a 1:1 molar ratio with $(\text{C}_6\text{F}_5)\text{Au}(\text{tht})$.¹⁴ Thin layer chromatography showed that a mixture of about five products formed. Solvent manipulation was carried out to try and isolate compound **11b**. However, the compounds could not be separated. Crystals suitable for single crystal X-ray diffraction were crystallised from a solution of the crude mixture in CH_2Cl_2 and the structure of compound **10** is described in Chapter 3. From the single crystal X-ray analysis it was clear that displacement of the bromide counterions was not complete and instead the bromide coordinated to the gold and not the ylide. From the NMR spectra of the mixture of products it was clear that compound **10** was the main product and the desired mono-coordinated gold compound (**11b**) was the byproduct (15%). A small amount (10%) of the double coordinated compound (**9**) also formed. Subsequently, an aurate counterion for the phosphonium salt was formed and deprotonation of this phosphonium salt formed the ylide complexes as described in Section 2.2.3.



Scheme 2.12

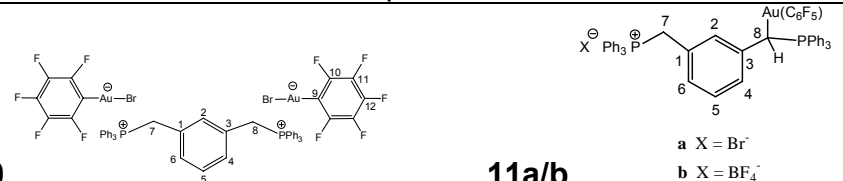
2.2.6 Spectroscopic characterisation of compounds **9**, **10** and **11a/b**

NMR Spectroscopy

The ^1H , ^{13}C and ^{31}P NMR data of the crude mixture were recorded in CD_2Cl_2 since the compounds could not be separated. The data for **10** and **11a/b** are summarised in Table 2.17. The ^1H , ^{13}C and ^{31}P NMR signals for compound **9** are assigned as in Table 2.12.

The NMR spectra were assigned empirically, making use of coupling constants and proton signal integrals, to assign the different resonances to the correct compounds. This was necessary as all three products formed were extremely similar and most of the signals overlapped, especially in the phenyl region. Because compound **10** formed in a very large ratio compared to compound **9** and **11b**, the largest intensity resonances were assigned to compound **10**. Throughout the spectra, similar signals with smaller intensity were observed and these were empirically assigned to compounds **9** and **11a/b**. Compound **9** is present in a slightly larger concentration than **11b**.

Table 2.17 ^1H , ^{13}C and ^{31}P NMR data for compounds **10** and **11a/b** in CD_2Cl_2

Assignment	δ / ppm	δ / ppm
		
<p>10 11a/b</p> <p style="margin-left: 200px;">a X = Br⁻ b X = BF₄⁻</p>		
^1H NMR		
H ^{7,8}	4.53 (4H, d, $^2J = 14.5$ Hz)	3.70 (1H, d, $^2J = 13.2$ Hz) 4.35 (2H, d, $^2J = 13.0$ Hz)
H ^{4/6}	6.79 (2H, m)	6.61 (1H, m)
H ^{4/6}		6.62 (1H, m)
H ²	6.90 (1H, m)	6.51 (1H, m)
H ⁵	6.99 (1H, m)	6.68 (1H, m)
H ^{ortho}	7.49 (12H, m)	7.49 (12H, m)
H ^{meta}	7.65 (12H, m)	7.65 (12H, m)
H ^{para}	7.80 (6H, m)	7.80 (6H, m)
^{13}C NMR		
C ⁷	35.4 (m)	31.3 (m)
C ⁸		32.0 (m)
C ^{ipso}	117.0 (d, $^1J = 86.5$ Hz)	117.1 (d, $^1J = 86.2$ Hz) 125.0 (d, $^1J = 84.2$ Hz)
C ²	128.6 (m)	127.3 (m)
C ^{1,3}	129.5 (m)	130.0 (m)
C ^{ortho}	130.8 (m)	129.8 (d, $^2J = 11.8$ Hz)
C ^{6,4}	131.4 (m)	133.5 (m)
C ^{meta}	134.3 (m)	134.3 (m)
C ⁹	134.6 (m)	
C ^{para}	136.0 (m)	135.9 (d, $^4J = 3.0$ Hz)
C ¹¹	137.8 (dm, $J_{\text{CF}} = 238.3$ Hz)	
C ¹²	140.4 (dm, $J_{\text{CF}} = 230.8$ Hz)	
C ⁵	142.0 (m)	142.0 (m)
C ¹⁰	149.2 (dm, $J_{\text{CF}} = 225.5$ Hz)	
^{31}P NMR		
P	22.8 (s)	25.2 (br s), 25.6 (br s)

The protons **H**⁷ and **H**⁸ in compound **10** form a doublet at δ 4.53 ($^2J_{\text{PH}} = 14.5$ Hz) as expected. The protons **H**⁷ and **H**⁸ in compound **11b** form two different doublet resonances, as expected, one at δ 3.70 ($^2J_{\text{PH}} = 13.2$ Hz) and the other one at δ 4.35 ($^2J_{\text{PH}} = 13.0$ Hz). All the different phenyl protons overlap to form complicated coupling patterns assigned as multiplets. The protons of the central phenyl rings however resonate in the range δ 6.51- δ 7.01 and the triphenylphosphonium protons are observed between δ 7.39- δ 7.85.

The ylidic carbon signals for compound **10** form a multiplet at δ 35.1. Compound **11b** again displays two different ylidic carbon signals one multiplet at δ 31.3 and the other one at δ 32.0. Magnetic inequivalence of the *ortho* and *meta* carbons of the triphenylphosphonium units result in multiplet signals. Again the phenyl carbon signals overlap and are assigned as in Table 2.17. The chemical shifts of the carbon signals corresponding to the pentafluorophenyl groups are very similar to the same chemical shifts in the gold precursor compound C₆F₅Au(tht).

The ³¹P NMR spectrum gives further proof of four chemically inequivalent phosphorus atoms, consistent with the three products formed. Compound **10** exhibits a singlet of high intensity at δ 22.8, compound **9** a singlet at δ 25.6 and compound **11b** broad singlets (of much lower intensity) at δ 23.4 and 22.4. The broad singlets corresponding to compound **11b** arise from the two different phosphorus atoms that couple with one another. These atoms are too far apart, therefore, the coupling is too small to split the signals into doublets, resulting only in the broadening of these signals.

The proton signals for compounds **9**, **10** and **11b** show an upfield shift, with respect to the proton chemical shifts of **4b**. Protons **H**⁷ and **H**⁸ in compound **10** present an upfield shift of on average 0.7 ppm after formation of the aurate counterions, and the central phenyl ring protons an upfield shift between $\Delta\delta$ 0.02 - 0.6. The chemical shifts of the triphenylphosphonium protons did not change much. Protons **H**⁷ and **H**⁸ in compound **11b** display a very large upfield shift after coordination of one of the ylidic carbons to gold. The uncoordinated side of **11b** shifted 0.9 ppm upfield and the coordinated side shifted 1.53 ppm upfield. The

central phenyl ring protons show upfield shifts between 0.4 and 0.9 ppm. The triphenylphosphonium protons did not shift much.

The ylidic carbon atoms in compound **10** exhibit a downfield shift of Δ 5.8 ppm, the carbon-phosphorus coupling constant decreased by 12.2 Hz. Both the coordinated and uncoordinated ylidic carbons in compound **11b** display downfield shifts, the coupling constant of the one side increased with only 1 Hz, while the coupling constant of the other side decreased by 22.8 Hz. The central phenyl ring carbons in **10** and **11b** exhibit upfield shifts for carbons C^2 of 0.4 and 1.7 ppm respectively and downfield shifts for C^5 of 6.8 ppm for **10** and **11b**. Carbons C^1 and C^3 in **10** and **11b** occur downfield 0.3 and 0.8 ppm from the positions in the precursor. The *ipso* carbons in compound **10** moved somewhat upfield ($\Delta\delta$ 1), without a significant change in their coupling constants. The uncoordinated side of compound **11b** now has an *ipso* carbon signal 0.9 ppm upfield from the precursor shifts, while the coordinated side show a downfield chemical shift of $\Delta\delta$ 7.0. The chemical shifts of the triphenylphosphonium carbons did not change much after coordination of the ylide.

Mass spectrometry

As mentioned before, **9**, **10** and **11b** could not be separated, thus the mass spectrometry data were recorded of the crude mixture. Compound **9** has a relative molecular mass of more than 1000 and the cation of compound **10** 628 without the two aurate anions and a molecular mass of 1072, when the two aurate anions are included. Compound **11b** has a molecular mass of 991. Mass spectrometry data were collected using EI-MS as well as ESI-MS. For the ESI-MS chloroform was used as matrix. The ESI-MS data for compounds **9**, **10** and **11b** are summarised in Table 2.18 and the EI-MS data for the same compounds in Table 2.19.

The fragment corresponding to the cation of **4b** or **10** (the same ion) is seen in the ESI-MS at m/z 627. The cation of **11b** is seen at m/z 715 in the ESI-MS spectrum. There is also a fragment corresponding to the molecular mass of the counterion of compound **10**. Thus, overall enough proof of the formation of products **10** and **11b**.

Table 2.18 ESI-MS data for the mixture of **9**, **10** and **11b**

M/z	Intensity (%)	Fragment ion
1159	9	$[M]^+$ of 11b + $[\text{HC}_6\text{F}_5]$
991	90	$[M]^+$ of 11b
715	12	$[\text{PPh}_3\text{CH}(\text{AuC}_6\text{F}_5)\text{C}_6\text{H}_4]^+$
627	8	$[\text{Ph}_3\text{PCHC}_6\text{H}_4\text{CH}_2\text{PPh}_3]^+$ 4b/10
366	18	$[\text{AuC}_6\text{F}_5]^+$
314	100	$[\text{Ph}_3\text{PCH}_2\text{C}_6\text{H}_4\text{CH}_2\text{PPh}_3]^{2+}$ 4b/10
262	20	$[\text{PPh}_3]^+$

Table 2.19 EI-MS data for compounds **9**, **10** and **11b**

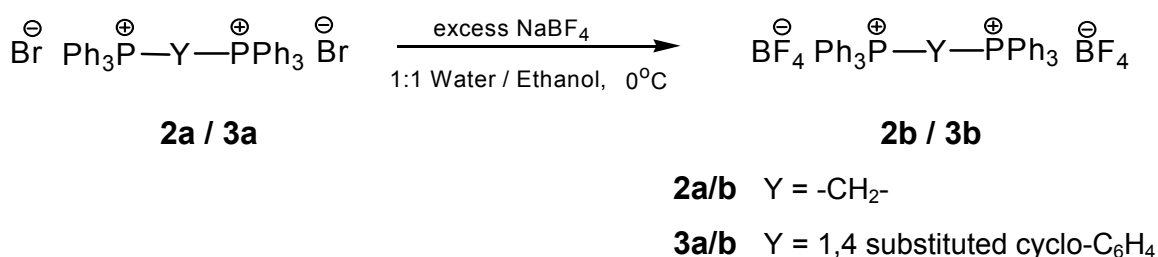
M/z	Intensity (%)	Fragment ion
626	5	$[\text{C}_6\text{F}_5\text{AuPPh}_3]^+$
459	4	$[\text{AuPPh}_3]^+$
364	5	$[\text{AuC}_6\text{F}_5]^+$
262	70	$[\text{PPh}_3]^+$
185	60	$[\text{PPh}_2]^+$
168	100	$[\text{HC}_6\text{F}_5]^+$

2.2.7 Preparation of $[\mu\text{-(Ph}_3\text{PCHCH}_2\text{CHPPh}_3)_2\text{Au}_2][\text{BF}_4]_2$ (**12**) and $[\mu\text{-(Ph}_3\text{PCHC}_6\text{H}_4\text{CHPPh}_3)_2\text{Au}_2][\text{BF}_4]_2$ (**13**)

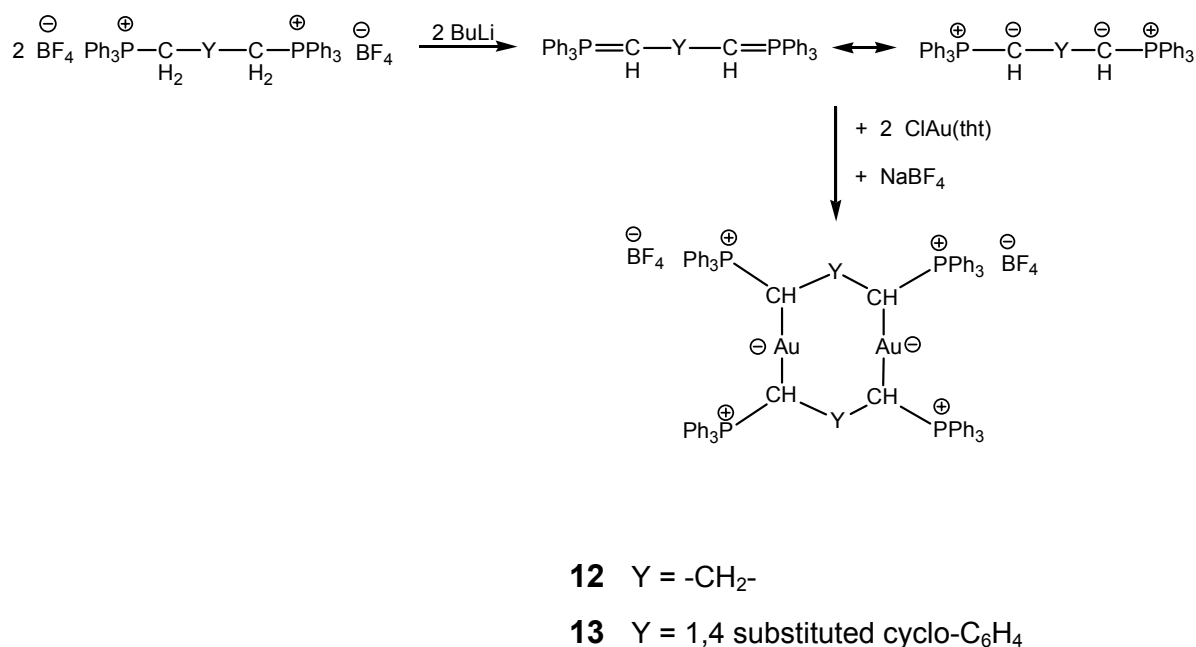
Again, in an attempt to prepare gold(I) ylide complexes, the counterions of the bisphosphonium salts **2a** and **3a** had to be displaced with BF_4^- , in order to avoid preferential coordination by the bromide ion to gold.

The same method, as with salt **4a**, was explored to displace the bromide ions of salts **2a** and **3a** with tetrafluoroborate (Scheme 2.13).

Compounds **12** and **13** were prepared using methods analogous to the methods described in the literature by Schmidbauer *et al.*¹⁶ The ylides obtained from deprotonating salts **2b** and **3b** were reacted in a 1:1 molar ratio with the gold precursor compound chloro(tetrahydrothiophene)gold(I), (tht)AuCl. The (tht)AuCl was prepared according to methods described by Usón *et al.*¹⁷ The bisphosphonium salt was first deprotonated with two molar equivalents of n-BuLi to form the bisylide, and subsequently reacted with one molar equivalent of (tht)AuCl. The formed compounds (**12** and **13**) are thermodynamically very unstable in solution.



Scheme 2.13



Scheme 2.14

¹⁶ a) H. Schmidbauer, J. R. Mandl, A. Frank and G. Huttner, *Chem. Ber.*, **109** (1976) 466, b) H. Schmidbauer and R. Franke, *Chem. Ber.*, **108** (1975) 1321

¹⁷ R. Usón, A. Laguna and M. Laguna, *Inorg. Synth.*, **26** (1989) 86

2.2.8 Spectroscopic characterisation of compounds **12** and **13**

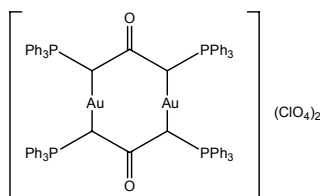
NMR Spectroscopy

The ^1H , ^{13}C and ^{31}P NMR data for compound **12** were recorded in CD_2Cl_2 and are summarised in Table 2.20.

Due to the instability of compound **12** in solution, well resolved ^{13}C and ^1H NMR spectra could not be obtained. It is also not possible to say whether some of the signals are due to decomposition or due to more than one isomer or product formed. Enough information to confirm the formation of compound **12** can, however, be gathered from the spectra.

It is highly unlikely that the 8-membered ring in compound **12** will be rigid in solution, thus a multitude of peaks can be expected for the chemically inequivalent atoms in the NMR spectra. Several conformational isomers as well as equilibria between these isomers can also be expected.

The molecule was modeled in ArgusLab¹⁸ (Figure 2.1) to show the chemical inequivalence of the carbon, proton and phosphorus atoms. The model shows bent C-Au-C angles instead of the expected linear geometry for gold(I) atoms. Compound **12** is very similar to the eight-membered ring complex (Scheme 2.15) reported by Vicente *et al.*,¹⁹ in which the transannular gold...gold distance is 2.88 Å and the geometry of the gold atoms deviate considerably from linearity (170°) to avoid shorter contacts between the gold atoms and to decrease the strain on the ring.

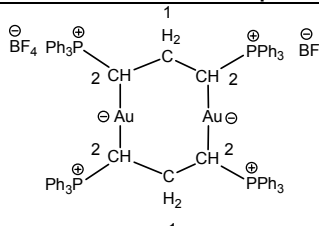


Scheme 2.15

¹⁸ M. A. Thompson, Planaria software LLC, Seattle (1997)

¹⁹ J. Vicente, M. Chicote, I. Saura-Llamas, P. G. Jones, K. Meyer-Bäse and C. F. Erdbrügger, *Organometallics*, **7** (1988) 997

Table 2.20 ^1H , ^{13}C and ^{31}P NMR data for compound **12** in CDCl_3

	
Assignment	δ / ppm
^1H NMR	
H ¹	1.45 (4H, m) 1.65 (4H, m) 1.88 (4H, m) 2.07 (4H, m)
H ²	2.23 (4H, m) 2.52 (4H, m) 2.86 (4H, m) 3.17 (4H, m)
H ^{meta}	7.41 (24H, m)
H ^{ortho}	7.55 (24H, m)
H ^{para}	7.67 (12H, m)
^{13}C NMR	
C ¹	23.2 (m), 24.8 (m)
C ²	29.2 (m), 31.0 (m)
C ^{ipso}	124.3 (m)
C ^{meta}	129.5 (m)
C ^{ortho}	133.2 (m)
C ^{para}	133.2 (m)
^{31}P NMR	
P	22.3 (s), 22.9 (s), 23.3 (s), 27.7 (s)

The signals in the ^{31}P NMR spectrum are all broad, suggesting small coupling amongst the phosphorus atoms. The phosphorus atoms can occupy a number of different positions. They can either be above the plane formed by the 8-membered ring or below this plane or some above the plane, while others are

below. Two sets of four multiplets, observed in the ^1H NMR spectrum, are assigned to H^1 and H^2 of **12**.

The ^1H , ^{13}C and ^{31}P NMR data for compound **13** were recorded in CD_2Cl_2 and are summarised in Table 2.21.

Table 2.21 ^1H , ^{13}C and ^{31}P NMR data for compound **13** in CD_2Cl_2

Assignment	δ / ppm
^1H NMR	
$\text{H}^{7,8}$	4.15 (4H, m) 4.55 (4H, m) 5.17 (4H, m) 5.46 (4H, m)
$\text{H}^{2,3,5,6}$	6.52 (8H, m)
H^{ortho}	7.30 (24H, m)
H^{meta}	7.48 (24H, m)
H^{para}	7.74 (12H, m)
^{13}C NMR	
$\text{C}^{7,8}$	33.5 (m)
C^{ipso}	117.4 (m)
$\text{C}^{1,4}$	124.3 (m)
C^{ortho}	129.6 (m)
C^{para}	132.2 (m)
$\text{C}^{2,3,5,6}$	132.3 (m)
C^{meta}	133.8 (m)
^{31}P NMR	
P	22.7 – 29.8 (m)

A multitude of peaks in the ^{13}C NMR spectrum are observed for C^1 and C^2 . Even if some carbons were chemically equivalent, they could still be magnetically inequivalent, due to the symmetry of the molecule.¹¹ This inequivalence, results in

signals for an AA'XX' spin system as explained on p 26. This would additionally complicate the spectra.

It is impossible to determine any P-C coupling constants, even for the phosphonium phenyl groups.

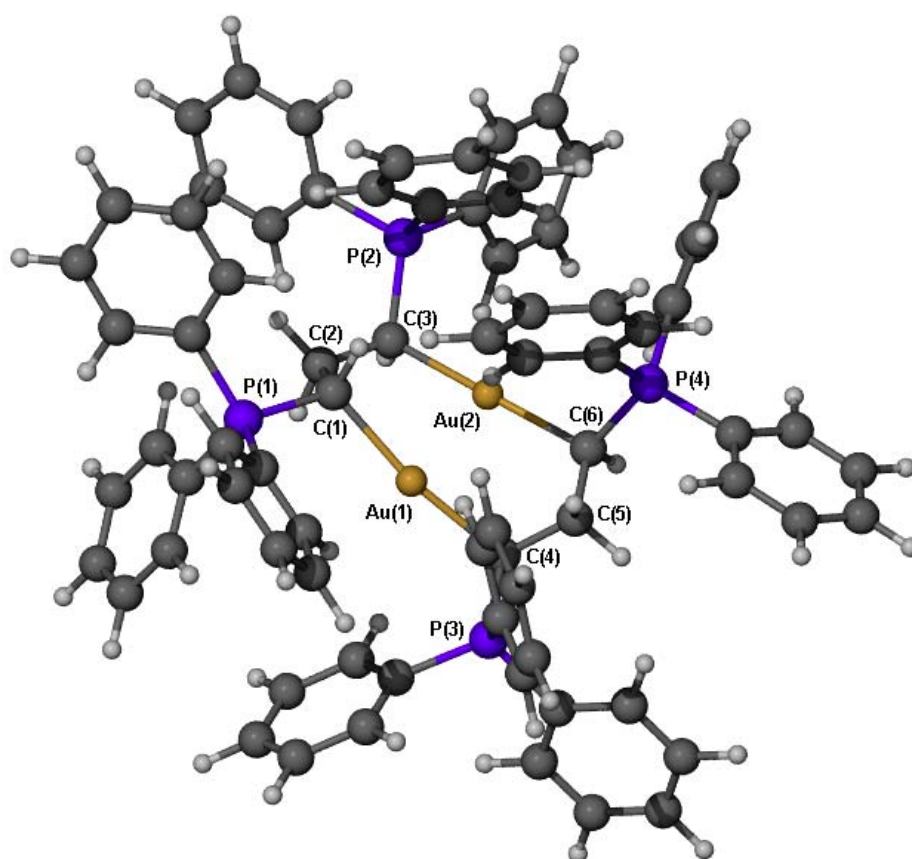


Figure 2.1 ArgusLab model of the non-rigid ring of compound **12**

The complicated NMR spectra of the 14-membered ring compound **13**, suggests a multitude of chemically inequivalent atoms as a result of the non-rigid ring and the possibility of several conformations. A model was built with a molecular modeling set and showed that the 14-membered ring is under a lot of strain. To reduce the strain, the phenyl rings should lie almost flat on top of each other, causing the atoms to be in different chemical environments. As mentioned previously, the molecule was also modeled in ArgusLab¹⁸ (Figure 2.2). Again the non-linear angles shown in the diagram are not unexpected as the molecular determinations of a similar compound (in Scheme 2.13) shows similar, considerable deviation from linearity.

The ^{31}P NMR consists of one large multiplet from 22.7 to 29.8 ppm. The ^{13}C NMR spectrum is also complicated by magnetic inequivalence expressed in more complicated P-C-coupling.¹¹

Compound **13** is even more unstable in solution and from the ^{13}C , ^1H and ^{31}P NMR spectra it is evident that decomposition took place while the spectra were recorded. The spectra were assigned empirically by comparing it to that of the uncoordinated ligand. The poor solubility of **13** resulted in low peak intensity further complicating the assignment of signals.

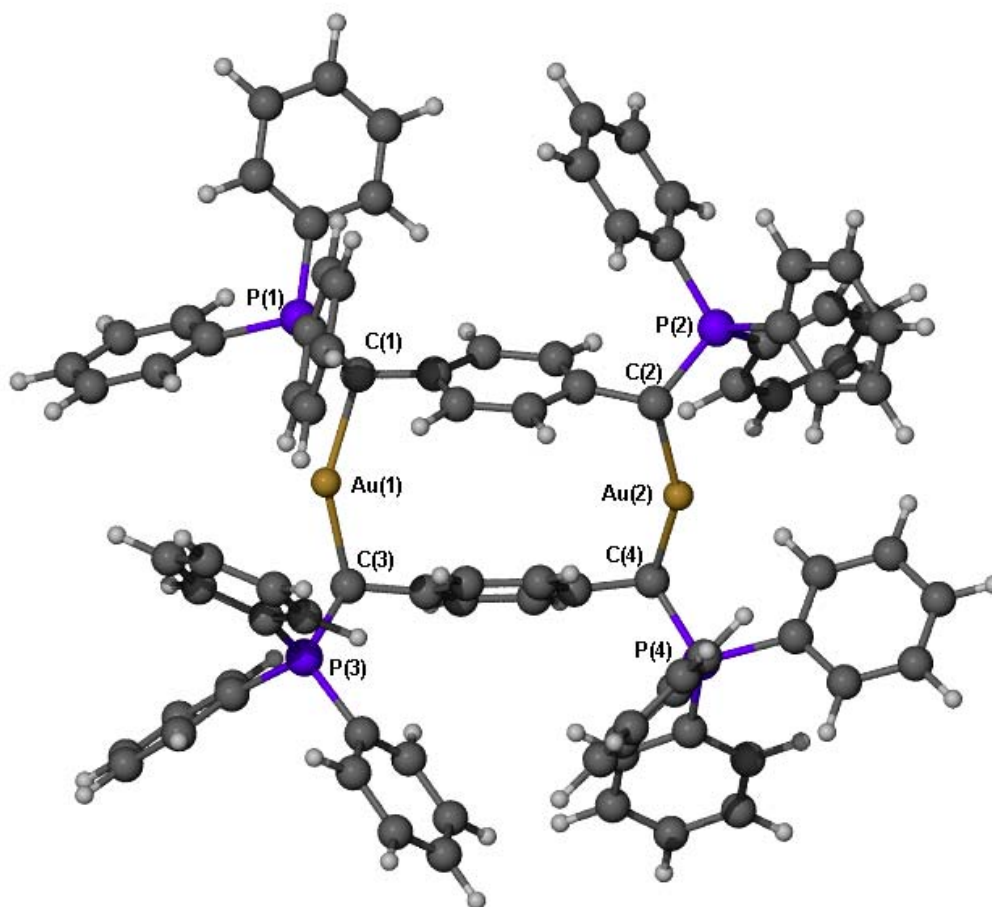


Figure 2.2 ArgusLab model showing the orientation of the central phenyl rings in compound **13**

Mass spectrometry

Both compounds **12** and **13** have relative molecular masses greater than 1000, therefore, the mass spectrometry data were collected using ESI-MS. Acetonitrile was used as matrix for compounds **12** and **13** and the ESI-MS spectra of these compounds are shown in Figures 2.3 and 2.4 respectively.

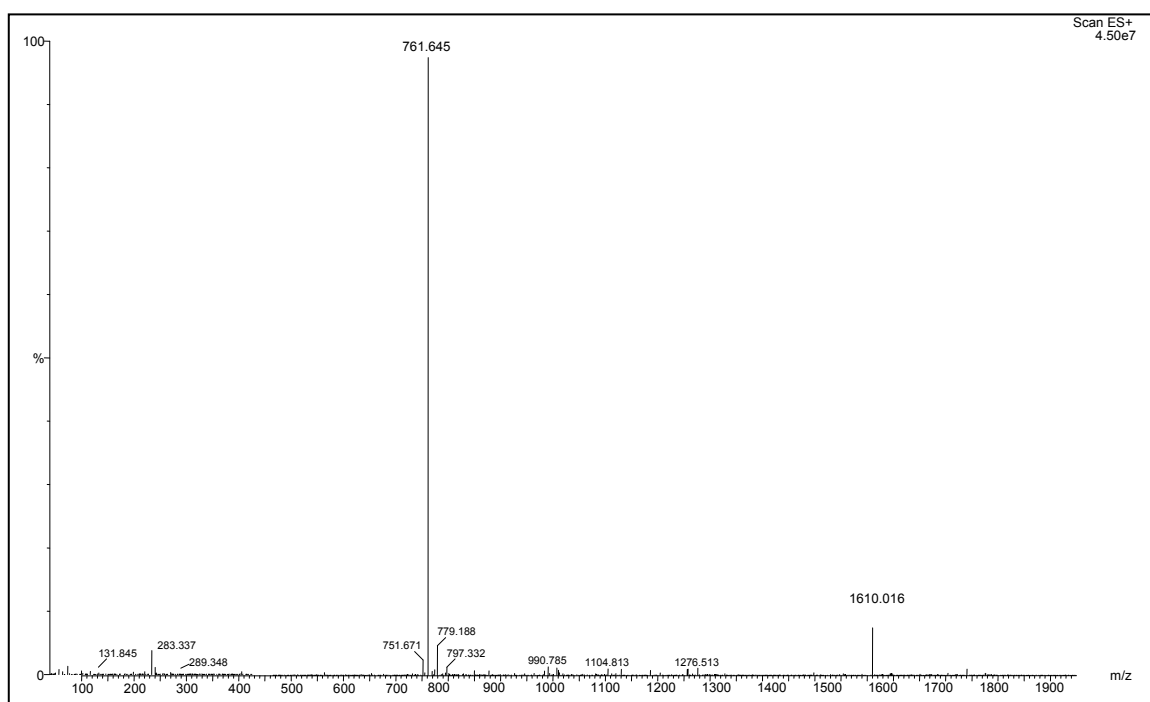


Figure 2.3 ESI-MS spectrum of compound **12**

Table 2.22 ESI-MS data for compound **12**

M/z	Intensity (%)	Fragment ion
761	100	$[\mu\text{-(Ph}_3\text{PCHCH}_2\text{CHPh}_3)_2\text{Au}_2]^{2+}$
1610	10	$[\mu\text{-(Ph}_3\text{PCHCH}_2\text{CHPh}_3)_2\text{Au}_2][\text{BF}_4]^+$

In the ESI-MS spectrum of compound **12**, the base peak at m/z 761 corresponds to the molecular mass of the dinuclear cation. The fragment of m/z 1610 corresponds to the dinuclear cation with one BF_4^- .

Table 2.23 ESI-MS data for compound **13**

M/z	Intensity (%)	Fragment ion
1279	15	$[\text{PPh}_3\text{CH}_2(\text{Au})\text{C}_6\text{H}_4\text{CH}_2(\text{Au})\text{PPh}_3][\text{BF}_4]_2^+ + 2\text{CH}_3\text{CN}$
823	100	$[\mu\text{-(Ph}_3\text{PCHC}_6\text{H}_4\text{CHPh}_3)_2\text{Au}_2]^{2+}$
279	20	Ph_3PO

The ESI-MS spectrum of compound **13** indicates the formation of the dinuclear cation, at m/z 823 (base peak). The m/z value of 1279 corresponds to a cation

associate, $[\text{PPh}_3\text{CH}_2(\text{Au})\text{C}_6\text{H}_4\text{CH}_2(\text{Au})\text{PPh}_3][\text{BF}_4]_2^+ + 2\text{CH}_3\text{CN}$. The fragment at 279 is due to the formation of PPh_3O . A fragment at 381 could not be assigned.

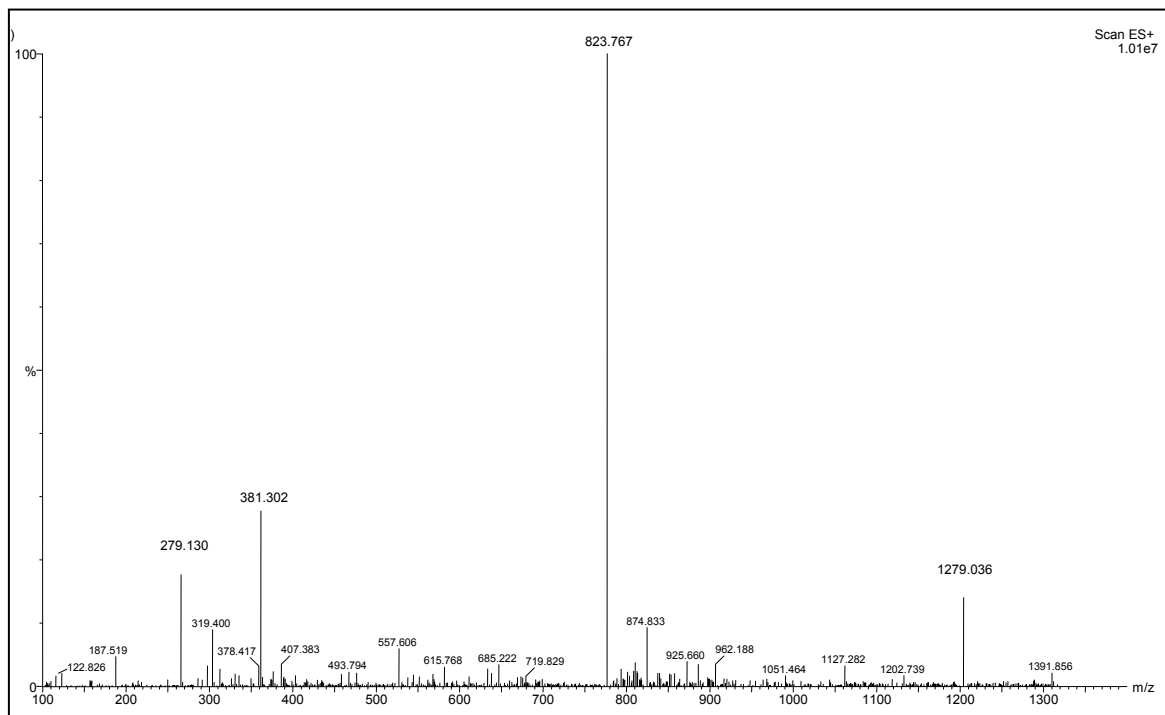


Figure 2.4 ESI-MS spectrum of compound **13**

2.2.9 Attempted preparation of **9**, and formation of **11a** and two other products **14** and **15**, by deprotonation of the phosphonium salt with Ag_2O

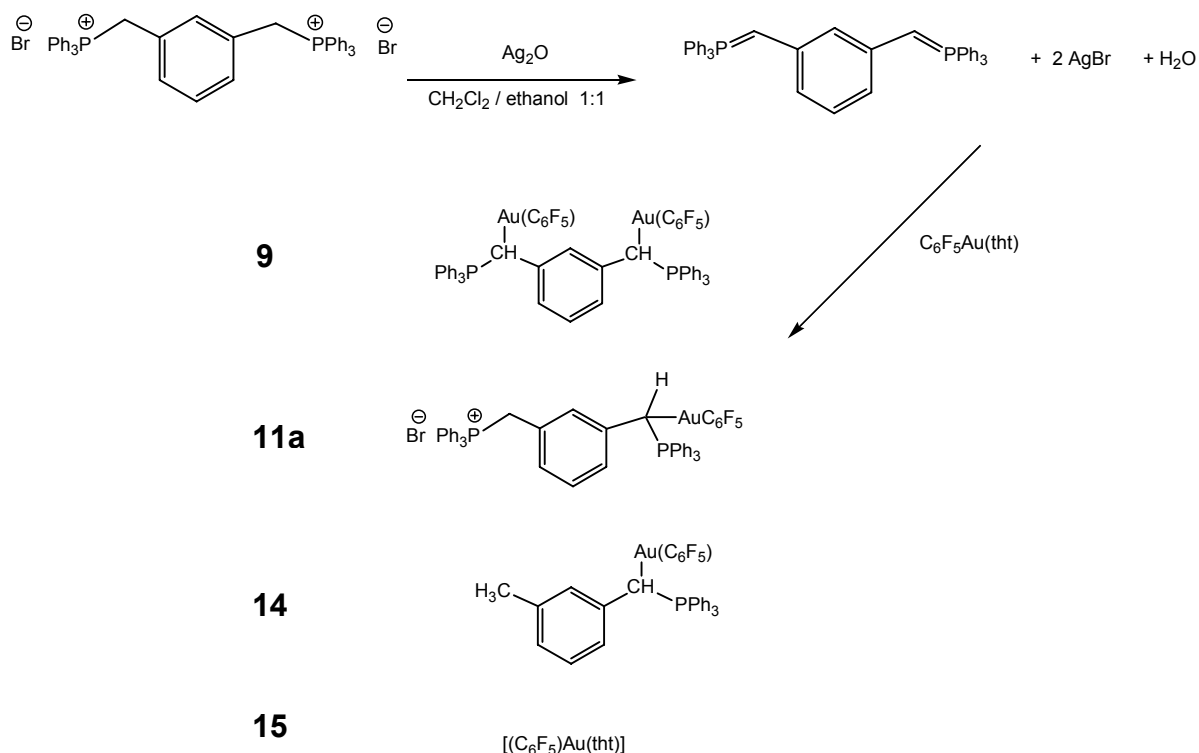
The displacement of the bromide counterions is not always successful with NaBF_4 , and an alternative method of removal of the bromide ions from the reaction mixture was investigated. Wang *et al.*²⁰ used Ag_2O to capture bromide ions from the reaction mixtures to form stable AgBr . Furthermore, Ag_2O is a very powerful deprotonation agent and was used to deprotonate the phosphonium salt, to form the ylide, and simultaneously capture the bromide ions.

One molar equivalent of the phosphonium salt **4a** and one molar equivalent of Ag_2O were suspended in a 1:1 CH_2Cl_2 /ethanol mixture. The deprotonated phosphonium salt was reacted at room temperature with one and a half molar equivalents of $(\text{C}_6\text{F}_5)\text{Au}(\text{tht})$. An extraction with diethyl ether and thereafter with dichloromethane yielded two fractions. Thin layer chromatography showed that

²⁰ J. Wang, C. Y. L. Chen and I. J. B. Lin, *Organometallics*, **18** (1999) 1216

both extracts contained a mixture of three products. A concentrated solution of the ether extract was stored at -14°C for four days and two types of crystals suitable for single crystal X-ray diffraction were obtained. Colourless needles and cubes were submitted to a single crystal X-ray study and the molecular structures of **14** and **15** were determined. A concentrated solution of the dichloromethane extract was also stored at -14°C , but no crystals were obtained.

In the molecular structure of **14** one of the ylide functional groups was displaced by a methyl group. Presumably, the water that forms as byproduct in the deprotonation reaction of the phosphonium salt hydrolyses a 'double bond' between the phosphorus atom and the ylidic carbon to form a methyl group. The molecular structure of **14** is discussed in detail in Chapter 3.



Scheme 2.16

Compound **15** is a widely used starting material and is prepared by reacting lithiated pentafluorophenyl with $\text{ClAu}(\text{tht})$. The crystal structure of compound **15** is discussed in detail in Chapter 3.

2.2.10 Spectroscopic characterisation of compounds **9**, **11a**, **14** and **15**

NMR Spectroscopy

The four products could not be isolated in large enough quantities to spectroscopically investigate them on their own, therefore, the crude mixture was analysed with detailed ^1H , ^{13}C and ^{31}P NMR analysis. The ^1H , ^{13}C and ^{31}P NMR data were recorded in CD_2Cl_2 and are summarised in Table 2.24. The identified NMR signals for compounds **9** (Table 2.12) and **11a** (Table 2.17) have been assigned previously.

The proton H^7 in compound **14**, resonates as a singlet at δ 2.11, while the proton H^8 , forms a doublet at δ 4.63 ($^2J_{\text{PH}} = 14.1$ Hz).

In the ^{13}C NMR spectrum of **14**, the singlet at δ 20.9 is assigned to C^7 and a multiplet at δ 33.7 is assigned to C^8 . The *ipso* carbons of the phenyl rings at the triphenylphosphonium unit form a doublet at δ 125.5 ($J_{\text{PC}} = 84.2$ Hz), as expected. The central phenyl ring carbons couple to the phosphorus atom to form doublets for each type of carbon as assigned in Table 2.24. The chemical shifts of the carbon atoms are assigned empirically by measuring the coupling constants of the carbon-phosphorus coupling.

The ^{31}P NMR spectrum displays a singlet at δ 25.7 corresponding to the phosphorus atom in **14**.

In the proton spectrum of **15** (Table 2.25), a broad singlet at δ 2.11 (4H) is due to the hydrogens on the β -carbons in the tht ring, $(\text{C}_6\text{F}_5)\text{Au}(\text{SCH}_2\text{CH}_2\text{CH}_2\text{CH}_2)$, and the broad singlet at δ 3.31 (4H) to the hydrogens on the α -carbons in the same ring.

In the ^{13}C spectrum of **15**, a singlet at δ 31.0 belongs to the β -carbons and a broad singlet at δ 39.0 to the α -carbons in the tht ring of compound **15**. A doublet of doublets of multiplets at δ 149.8 ($J_{\text{CF}} = 221.1$ Hz, $J_{\text{CF}} = 30.4$ Hz) was assigned to $\text{C}^{\text{ortho}} \text{C}_6\text{F}_5$, a doublet of multiplets at δ 139.4 ($J_{\text{CF}} = 252.6$ Hz) is assigned to C^{para}

C_6F_5 , a doublet of multiplets at δ 137.4 ($J_{CF} = 225.1$ Hz) to $C^{meta} C_6F_5$ and a triplet of multiplets at δ 116.1 ($J_{CF} = 53.1$) was assigned to $C^{ipso} C_6F_5$.

Table 2.24 1H , ^{13}C and ^{31}P NMR data for compound **14** in CD_2Cl_2

Assignment	δ / ppm
1H NMR	
H^7	2.11 (3H, s)
H^8	4.63 (1H, d, $^2J = 14.1$ Hz)
$H^{2,4,5,6}$	7.00 (4H, m)
H^{meta}	7.34 (6H, m)
H^{ortho}	7.55 (6H, m)
H^{para}	7.84 (3H, m)
^{13}C NMR	
C^7	20.9 (s)
C^8	33.7 (m)
C^{ipso}	125.5 (d, $^1J = 84.2$ Hz)
C^1	126.2 (d, $^4J = 3.7$ Hz)
C^3	126.6 (d, $^2J = 8.4$ Hz)
C^2	128.3 (d, $^3J = 5.4$ Hz)
C^{ortho}	129.1 (d, $^2J = 12.2$ Hz)
C^6	130.2 (d, $^3J = 3.8$ Hz)
C^4	131.3 (d, $^5J = 8.3$ Hz)
C^{meta}	132.6 (d, $^3J = 9.8$ Hz)
C^5	133.9 (m)
$C^{ipso} C_6F_5$	135.6 (m)
$C^{meta} C_6F_5$	137.0 (dm, $^1J = 77.3$ Hz)
C^{para}	138.7 (d, $^4J = 3.0$ Hz)
$C^{para} C_6F_5$	139.5 (dm, $^1J = 78.0$ Hz)
$C^{ortho} C_6F_5$	149.4 (ddm, $^1J = 224.7$ Hz)
^{31}P NMR	
P	25.7 (s)

Table 2.25 ^1H and ^{13}C NMR data for compound **15** in CD_2Cl_2

[[C ₆ F ₅] ₂ Au(tht)]	
Assignment	δ / ppm
^1H NMR	
(C ₆ F ₅)Au(SCH ₂ CH₂CH₂CH₂)	2.11 (4H, br s)
(C ₆ F ₅)Au(S CH₂CH₂CH₂CH₂)	3.31 (4H, br s)
^{13}C NMR	
(C ₆ F ₅)Au(SCH ₂ CH₂CH₂CH₂)	31.0 (s)
(C ₆ F ₅)Au(S CH₂CH₂CH₂CH₂)	39.0 (br s)
C ^{ipso} C ₆ F ₅	116.1 (tm, J _{CF} = 53.1 Hz)
C ^{meta} C ₆ F ₅	137.4 (dm, J _{CF} = 225.1 Hz)
C ^{para} C ₆ F ₅	139.4 (dm, J _{CF} = 252.6 Hz)
C ^{ortho} C ₆ F ₅	149.8 (ddm, J _{CF} = 221.1 Hz, J _{CF} = 30.4 Hz)

Mass spectrometry

As mentioned, the compounds **9**, **11a**, **14** and **15** could not be separated and the MS data of the crude mixture was recorded. Too few crystals of **14** and **15** were obtained to record MS data of these compounds separately. Compound **9** has a molecular mass greater than 1000, therefore, the mass spectrometry data was collected using ESI-MS. A 1:1 dichloromethane/methanol solvent mixture was used as matrix.

Table 2.26 ESI-MS data for compounds **9**, **11a**, **14** and **15**

M/z	Intensity (%)	Fragment ion
929	100	[M] ⁺ of (14) + 2CH ₂ Cl ₂ + CH ₃ OH
367	8	[AuC ₆ F ₅] ⁺
279	30	Ph ₃ PO

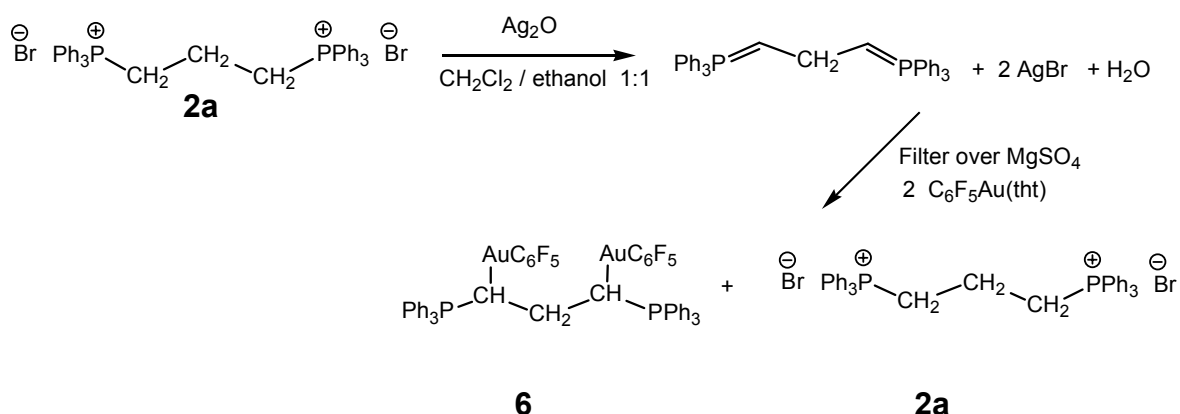
The molecular ion of compound **14**, associated with two dichloromethane molecules and one methanol molecule, form the base peak at m/z 929. The m/z fragment at 367 corresponds to [AuC₆F₅]⁺. The formation of triphenylphosphine-oxide is indicated at m/z 279.

2.2.11 Preparation of **6**, **8** and **9** by deprotonation of the phosphonium salt with Ag_2O

The same preparative method described to prepare compound **14**, was used for compounds **6**, **8** and **9**, but had to be modified slightly in order to prevent the hydrolysis of the double bond in the ylide.

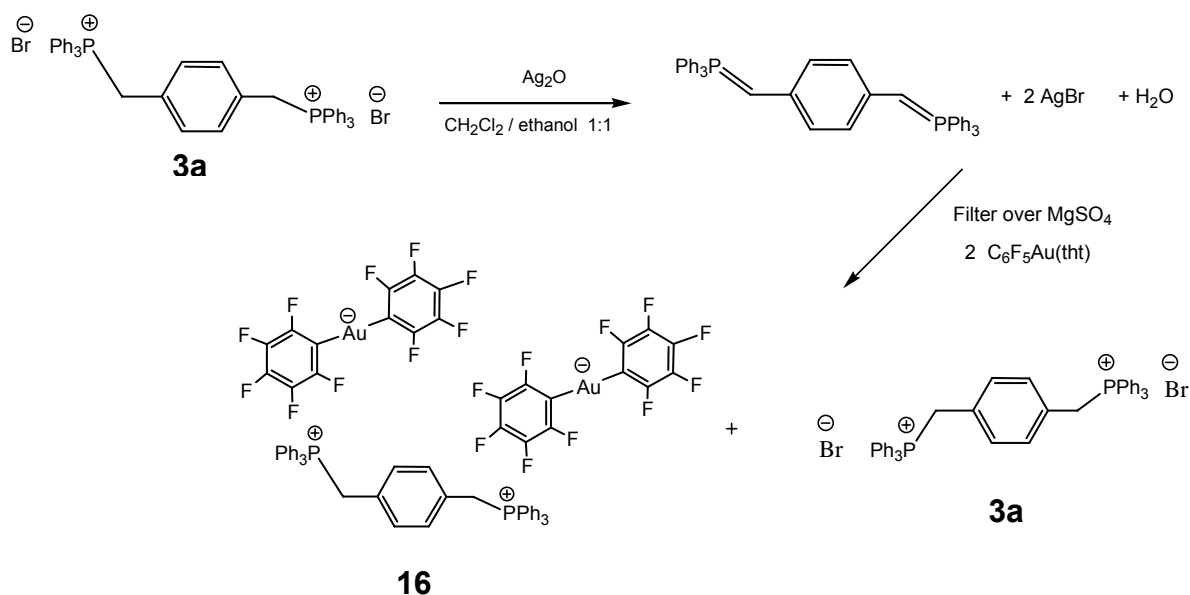
The reaction was performed in a 1:2 [phosphonium salt: $(\text{C}_6\text{F}_5)\text{Au}(\text{tht})$] molar ratio to try and prevent the formation of different products as in the attempted preparation of **9** (Section 2.2.9). The phosphonium salts **2a**, **3a** or **4a** and Ag_2O were separately stirred in 1:1 dichloromethane/ethanol solvent mixtures. The suspensions were filtered through MgSO_4 to remove all the formed water and charged solids (Scheme 2.17 – 2.19). The gold precursor compound, $(\text{C}_6\text{F}_5)\text{Au}(\text{tht})$, was added to this filtrate and decomposition started to occur, so the suspension was filtered through celite.

The residue obtained after stripping of the solvent from the preparation of compound **6**, was first extracted with diethyl ether and subsequently with dichloromethane. The ether extract contained a mixture of three products, while the dichloromethane extract contained only two products. Only the dichloromethane layer was used for further characterisation.



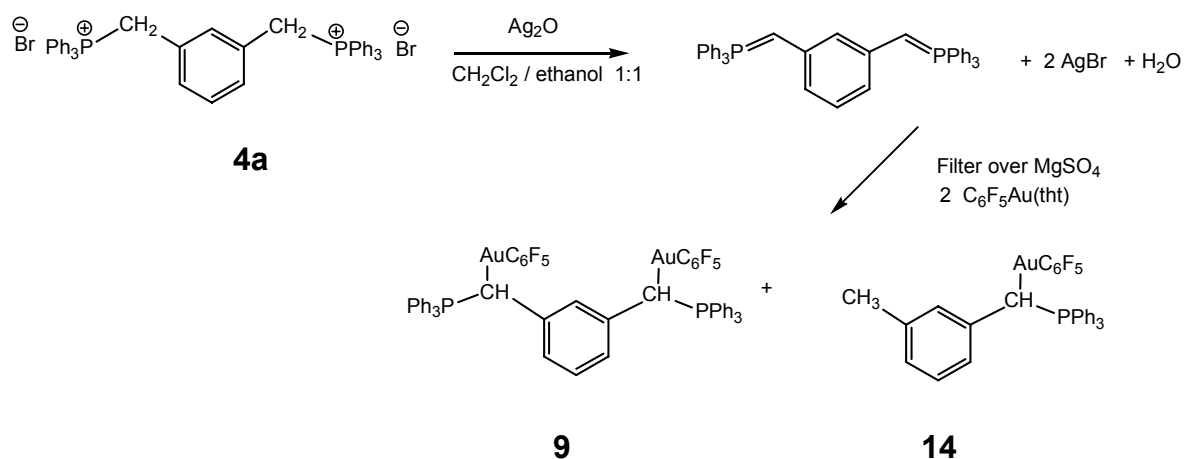
Scheme 2.17

After addition of the $(\text{C}_6\text{F}_5)_3\text{Au}(\text{tbt})$ to the deprotonated **3a**, a white precipitate formed along with some purple colloidal gold. The solvent was removed from the mixture under vacuum and the precipitate redissolved in dichloromethane, filtered through celite and concentrated to dryness. Crystals of **16**, suitable for single crystal X-ray diffraction structure determination, were obtained from a solution of the crude mixture in dichloromethane stored at -14°C for five days. The structure is discussed in Chapter 3. The molecular structure of **16** revealed that deprotonation of phosphonium salt **3a** had not taken place completely in solution and instead, the very stable aurate anion, $[\text{C}_6\text{F}_5\text{AuC}_6\text{F}_5]^-$, formed as counterion to the phosphonium salt (Scheme 2.18).



Scheme 2.18

In the attempted preparation of compound **9**, a colourless oil formed which, after washing three times with diethyl ether, became a white solid. From the ^1H , ^{13}C and ^{31}P NMR spectra it was evident that two products had formed, the desired compound **9**, and a small amount of the hydrolysis product, **14**. Hydrolysis could have taken place before the ylide-mixture was filtered over MgSO_4 to remove the formed water as described in Section 2.2.9.



Scheme 2.19

2.2.12 Spectroscopic characterisation of the mixture containing compounds 3a, 6, 9, 14 and 16

NMR Spectroscopy

The ^1H , ^{13}C and ^{31}P NMR data for compound **6** were recorded in CD_2Cl_2 . The spectra indicated that the reaction did not take place to completion and that only a small amount of **6** had formed, while most of the phosphonium salt was unreacted. Similar spectra as previously discussed and reported in Tables 2.2 and 2.10 were obtained.

The ^1H , ^{13}C and ^{31}P NMR data for the new product compound **16**, were recorded in CD_2Cl_2 and are reported in Table 2.27.

The concentration of the sample was too low to observe the carbon signals for AuC_6F_5 .

In the ^1H NMR spectrum the protons $\text{H}^{7,8}$ appear as a doublet at δ 5.03 ($^2J = 13.8$ Hz). The protons on the central phenyl ring are all chemically equivalent as shown by the broad singlet at δ 6.85.

In the ^{13}C NMR spectrum, $\text{C}^{7,8}$ forms a doublet at δ 31.5 ($^1J = 48.9$ Hz). The magnetic inequivalence and the higher order spin system (AA'XX') cause the central phenyl ring and the triphenylphosphonium phenyl ring carbons to appear as multiplets, as in the free phosphonium salt, **3a**.

Table 2.27 ^1H , ^{13}C and ^{31}P NMR data for **16** in CD_2Cl_2

Assignment	δ / ppm
^1H NMR	
$\text{H}^{7,8}$	5.03 (4H, d, $^2J = 13.8$ Hz)
$\text{H}^{2,3,5,6}$	6.85 (4H, br s)
H^{meta}	7.60 (12H, m)
H^{ortho}	7.64 (12H, m)
H^{para}	7.83 (6H, m)
^{13}C NMR	
$\text{C}^{7,8}$	31.5 (d, $^1J = 48.9$ Hz)
C^{ipso}	117.5 (d, $^1J = 86.3$ Hz)
$\text{C}^{1,4}$	123.3 (m)
C^{ortho}	129.0 (d, $^2J = 12.1$ Hz)
$\text{C}^{2,3,5,6}$	132.4 (m)
C^{meta}	134.6 (m)
C^{para}	136.1 (m)
^{31}P NMR	
P	23.1 (s)

The ^{31}P NMR spectrum displays only one signal, a singlet at δ 23.1 for **16**.

The NMR spectra of compounds **9** and **14** are similar to those obtained before for these compounds (Tables 2.12 and 2.24).

Mass spectrometry

The mass spectra of compounds **6**, **9** and **14** were identical to the previous measurements.

The ESI-MS data for **16** were collected before crystallisation in a chloroform matrix.

Table 2.28 ESI-MS data of the crude mixture of the reaction of **16**

M/z	Intensity (%)	Fragment ion
1159	100	$[\text{C}_6\text{F}_5\text{AuC}_6\text{F}_5][\text{Ph}_3\text{PCH}_2\text{C}_6\text{H}_4\text{CH}_2\text{PPh}_3]^+$
455	50	$[\text{AuPPh}_3]^+$
365	30	$[\text{AuC}_6\text{F}_5]^+$
314	20	$[\text{Ph}_3\text{PCH}_2\text{C}_6\text{H}_4\text{CH}_2\text{PPh}_3]^+$
262	15	$[\text{PPh}_3]^+$

The ESI-MS data clearly confirmed the formation of compound **16**, as the molecular ion without one of the aurate counterions is observed at m/z 1159 (base peak).

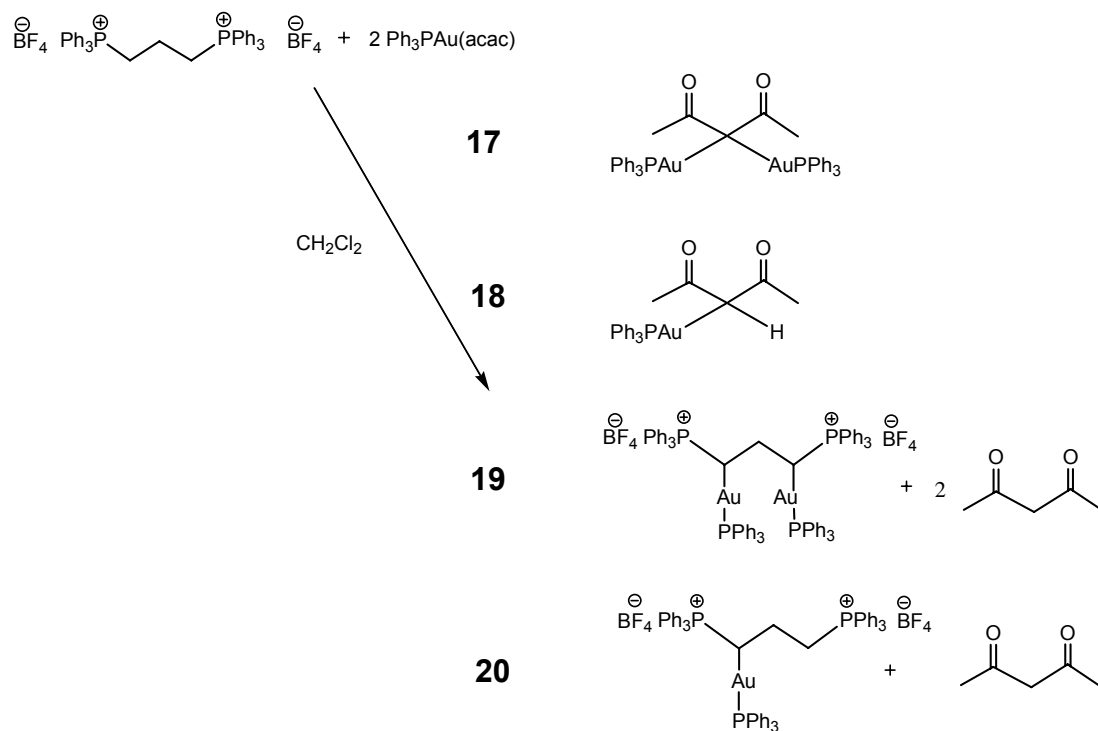
2.2.13 Attempted preparation of the dinuclear complex, $[\text{PPh}_3\text{CH}(\text{AuPPh}_3)\text{CH}_2\text{CH}(\text{AuPPh}_3)\text{PPh}_3][\text{BF}_4]_2$ (**19**)

Vicente *et al.*¹⁹ were very successful in preparing gold(I)-ylide complexes by using $\text{Ph}_3\text{PAu}(\text{acac})$ as starting material (acac = acetylacetonato). When $(\text{acac})\text{AuPPh}_3$ is reacted with phosphonium salts, the acac should deprotonate the phosphonium salt to form acetylacetone, while the ylide coordinates to the vacated site on the gold centre.

The $\text{Ph}_3\text{PAu}(\text{acac})$ was prepared according to methods described in the literature.²¹ One molar equivalent of the bisphosphonium salt **2b** was reacted with two molar equivalents of $\text{Ph}_3\text{PAu}(\text{acac})$. Crystals suitable for single crystal X-ray diffraction studies were obtained from a concentrated solution of the crude product mixture in dichloromethane, layered with diethyl ether. Instead of the expected gold(I)-ylide complex, only a dinuclear (acac)gold(I) complex, **17**, crystallised out. The structure of compound **17** is discussed in Chapter 3.

²¹ J. Vicente and M. Chicote, *Inorg. Synth.*, **32** (1998) 175

After careful analysis of the NMR spectra, it was evident that a mixture of compounds which could not be separated had formed (Scheme 2.20). The mononuclear and dinuclear (acac)gold(I) complexes, **17** (30%) and **18** (25%), as well as the mono- and dinuclear ylide complexes **19** (25%) and **20** (20%).



Scheme 2.20

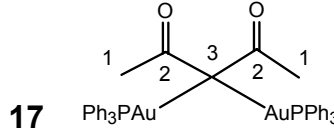
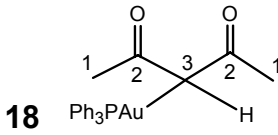
2.2.14 Spectroscopic characterisation of compounds **17**, **18**, **19** and **20**

NMR Spectroscopy

The ^1H , ^{13}C and ^{31}P NMR data of the crude mixture and, the crystals of **17**, were recorded separately in CD_2Cl_2 and are summarised in Tables 2.29 and 2.30. The compounds found are very similar and the signals are assigned by comparing them to the precursor compound signals and by calculating the carbon-phosphorus coupling constants. The spectrum of **17** was recorded from the crystals obtained. Slow decomposition indicated the formation of acetylacetonate and **18**.

In the ^1H NMR spectrum of the mixture, singlets at δ 2.40 and 2.29 correspond to the methyl protons in **17** and **18** respectively. Proton H^3 in **18**, forms a doublet at δ 4.48 ($^3J = 6,0$ Hz) and the protons on the phenyl rings of the triphenylphosphonium units in compounds **17** and **18** overlap to form a multiplet at δ 7.44.

Table 2.29 ^1H , ^{13}C and ^{31}P NMR data for **17** and **18** in CD_2Cl_2

Assignment	δ / ppm	δ / ppm
<div style="display: flex; justify-content: space-around; align-items: center;"> <div style="text-align: center;">  <p>17 Ph_3PAu AuPPh_3</p> </div> <div style="text-align: center;">  <p>18 Ph_3PAu H</p> </div> </div>		
^1H NMR		
H^1	2.40 (6H, s)	2.29 (6H, s)
H^3		4.48 (1H, d, $^3J = 6$ Hz)
$\text{H}^{\text{ortho, meta, para}}$	7.44 (m)	7.44 (m)
^{13}C NMR		
C^1	31.3 (s)	33.1 (s)
C^3	77.1 (m)	77.5 (m)
C^{ipso}	131.1 (d, $^1J = 54.3$ Hz)	129.6 (d, $^1J = 55.9$ Hz)
C^{meta}	129.7 (d, $^3J = 11.4$ Hz)	129.3 (d, $^3J = 11.3$ Hz)
C^{ortho}	134.5 (d, $^2J = 13.7$ Hz)	134.4 (d, $^2J = 14.5$ Hz)
C^{para}	131.5 (br s)	132.1 (d, $^4J = 2.5$ Hz)
C^2	191.6 (s)	202.9 (s)
^{31}P NMR		
P	38.3 (s)	39.9 (s)

In the ^{13}C NMR spectrum the methyl carbon atoms appear as singlet signals at δ 31.3 and δ 33.1 respectively for compounds **17** and **18**. The carbonyl carbons resonate at δ 191.6 for compound **17** and at δ 202.9 for compound **18**.

The phosphorus atoms in **17** resonate as a singlet at δ 38.3 and the phosphorus atom in **18** as a singlet at δ 39.9.

Table 2.30 ^1H , ^{13}C and ^{31}P NMR data for **19** and **20** in CD_2Cl_2

Assignment	δ / ppm	δ / ppm
<div style="display: flex; justify-content: space-around; align-items: center;"> <div style="text-align: center;"> <p>19</p> </div> <div style="text-align: center;"> <p>20</p> </div> </div>		
^1H NMR		
H^3		2.35 (m)
H^1	2.96 (m)	2.96 (m)
H^2	4.20 (m)	3.65 (m)
$\text{H}^{\text{ortho, meta, para}}$	7.40 (m)	7.40 (m)
^{13}C NMR		
C^1	22.2 (m)	33.1 (m)
C^2	26.0 (overlapping doublets, $^1J = 49.7$ Hz)	37.7 (overlapping doublets, $^1J = 49.5$ Hz)
C^3		35.6 (m)
C^{ipso}	123.7 (dm, $^1J = 87.5$ Hz) 123.4 (dm, $^1J = 88.7$ Hz)	117.7 (d, $^1J = 87.7$ Hz) 118.0 (d, $^1J = 86.5$ Hz)
C^{meta}	130.9 (m)	128.9 (dm, $^1J = 55.0$ Hz) 129.9 (d, $^3J = 11.3$ Hz) 130.5 (m)
C^{ortho}	133.5 (m, $^2J = 15.8$ Hz)	134.0 (m) 134.2 (d, $^2J = 13.6$ Hz)
C^{para}	135.6 (m)	134.8 (m) 135.6 (m)
^{31}P NMR		
P	27.1 (s), 41.7 (s)	22.8 (br s), 24.5 (s), 29.3 (br s)

In the ^{13}C NMR spectrum of the crude mixture, two similar doublet signals of equal intensity and with characteristic carbon-phosphorus coupling constants are observed, and assigned to the *ipso* carbons of a compound postulated as **19**, while three other different *ipso* signals are assigned to the *ipso* carbons of a compound postulated as **20**. The *meta* signals of the two different triphenylphosphonium units in compound **19** overlap to give multiplets, and the same pattern is observed for the *ortho* and *para* carbons of **19**. Two of the three

different sets of signals for the triphenylphosphonium units in compound **20** overlap to give multiplet signals.

The ^{31}P NMR spectrum of the crude mixture, displays three different singlet signals of the same intensity, assigned to the phosphorus atoms in compound **20**, and two broad singlets of equal intensity, assigned to the phosphorus atoms in **19**. The broad singlets arise from coupling between the two different phosphorus atoms in **19**. The coupling constant is too small to split the signal into a doublet and, therefore, only broad singlets are seen.

The spectra of the mixture that contained **17** - **20**, however provided substantial evidence that **19** had indeed formed, although in a relatively small quantity and in a still inseparable mixture of other products. No further experiments, using the acac method, were conducted.

Mass spectrometry

The ESI-MS data were recorded of the crude mixture in a CHCl_3 matrix.

Table 2.31 ESI-MS data for compound **17**, **18**, **19** and **20**

M/z	Intensity (%)	Fragment ion
1568	95	$[\text{Ph}_3\text{PCH}(\text{AuPPh}_3)\text{CH}_2\text{CH}(\text{AuPPh}_3)\text{PPh}_3][\text{BF}_4]^+$
1111	100	$[\text{Ph}_3\text{PCH}(\text{AuPPh}_3)\text{CH}_2\text{CH}_2\text{PPh}_3][\text{BF}_4]^+$
1017	95	$[\text{M}]^+$ of 17
741	98	$[\text{Ph}_3\text{PCH}(\text{AuPPh}_3)\text{CH}_2\text{CH}(\text{AuPPh}_3)\text{PPh}_3]^{2+}$
653	99	$[\text{Ph}_3\text{PCH}_2\text{CH}_2\text{CH}_2\text{PPh}_3\text{BF}_4]^+$
512	100	$[\text{Ph}_3\text{PCH}(\text{AuPPh}_3)\text{CH}_2\text{CH}_2\text{PPh}_3]^{2+}$
459	50	$[\text{AuPPh}_3]^+$

From the mass spectrum (Table 2.31) it is evident that the crude mixture contains compounds **17**, **19** and **20**, as the molecular ions of all these compounds are clearly present in the mass spectrum. The cation of **19**, without one counterion, is observed at m/z 1568, the cation of **20**, without one counterion, at m/z 1111 (as the base peak) and the molecular ion of **17** at m/z 1017, could also be assigned. The doubly charged cation of **19**, minus counterions, is observed at m/z 741 and

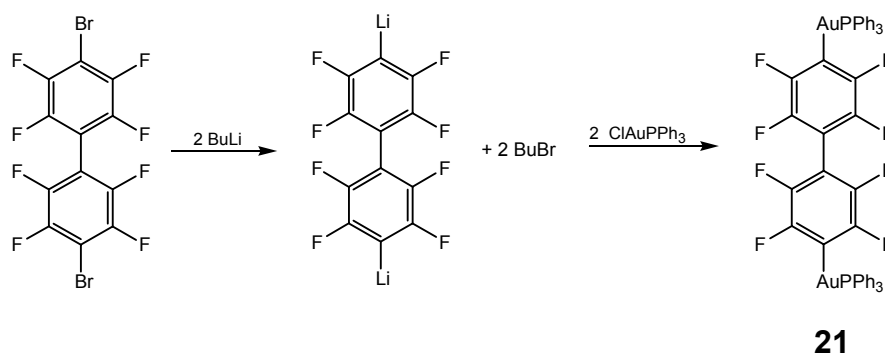
the phosphonium salt **2b**, minus one of its tetrafluoroborate counterions, is observed at m/z 653. A high intensity peak is formed by the doubly positively charged cation of **20** (no counterions).

2.2.15 Preparation of 4,4'-[(AuPPh₃)₂C₁₂F₈] (**21**) and 2,2'-[(AuPPh₃)₂C₁₂F₈] (**22**)

Very few biphenyl compounds have been synthesised up to now and no gold fluorobiphenyl compounds have been reported yet. Compounds 4,4'-[(AuPPh₃)₂C₁₂F₈] (**21**) and 2,2'-[(AuPPh₃)₂C₁₂F₈] (**22**) would be the first fluorobiphenyl compounds isolated.

ClAuPPh₃ was prepared by substitution of tht in ClAu(tht) with triphenylphosphine. Comparison of the characterisation data in the literature²² confirmed the purity of this starting material.

The lithiated 4,4'-dibromooctafluorobiphenyl was reacted with two molar equivalents of ClAuPPh₃. Crystals suitable for single crystal X-ray diffraction studies were obtained after slow diffusion of n-pentane into a solution of **21** in CH₂Cl₂. The structure of **21** is discussed in Chapter 3.



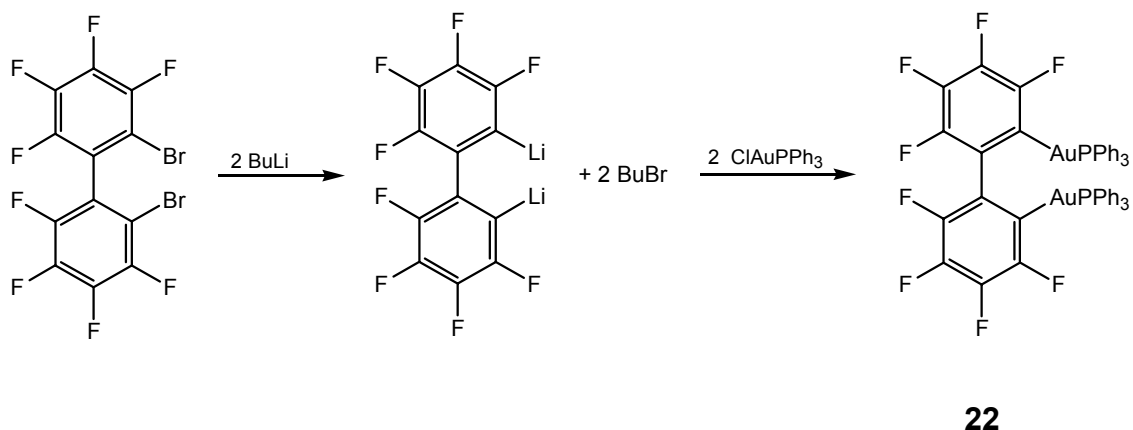
Scheme 2.21

A method described by Filler *et al.*²³ was used to prepare 2,2'-dibromooctafluorobiphenyl.

²² M. Basato, G. Facchin, R. A. Michelin, M. Mozzon, S. Pugliese, P. Sgarbossa and A. Tassan, *Inorg. Chim. Acta*, **356** (2003) 349

²³ R. Filler, A. E. Fiebig and M. Y. Pelister, *J. Org. Chem.*, **45** (1980) 1290

Two molar equivalents of ClAuPPh_3 were reacted with the lithiated 2,2'-dibromooctafluorobiphenyl and while the mixture was stirred at -75°C the compound displayed luminescence. The luminescence was visible while the temperature was slowly raised to room temperature. An oil formed, which after washing with pentane and drying under vacuum turned into a microcrystalline solid.



Scheme 2.22

2.2.16 Spectroscopic characterisation of compounds **21** and **22**

NMR Spectroscopy

The ^1H , ^{13}C and ^{31}P NMR data for compounds **21** and **22** were recorded separately in CD_2Cl_2 and are summarised in Table 2.32. The spectrum of the product mixture of **22** contained the mono-coordinated product and $[\text{BrC}_6\text{F}_4\text{AuPPh}_3]$ (**23**) and the ^1H , ^{13}C and ^{31}P NMR data for these compounds are summarised in Table 2.33.

In the ^1H NMR spectrum of **21**, the *ortho*, *meta* and *para* protons of the triphenylphosphonium units are observed as multiplets at δ 7.54, 7.60 and 7.70 respectively. The proton signals of the triphenylphosphonium protons in **22** overlap to form a multiplet at δ 7.49.

In the ^{13}C NMR spectrum of **22**, the different tetrafluorophenyl carbon signals appear as multiplets with small intensity, as assigned in Table 2.32. Since all

three the compounds in the crude mixture (**22**, **23** and **24**) are very similar the tetrafluorophenyl signals are assigned empirically, as they have very similar chemical shifts. The *ipso* carbons of the triphenylphosphonium units are seen as doublets at δ 130.5 (**21**) and δ 130.8 (**22**), while the *ortho* and *meta* carbon atoms of **22** overlapped with the same carbons of **23** and **24** to form multiplets at δ 129.8 and 134.7.

Table 2.32 ^1H , ^{13}C and ^{31}P NMR data for **21** and **22** in CD_2Cl_2

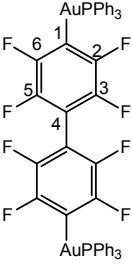
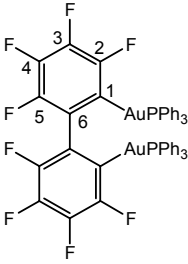
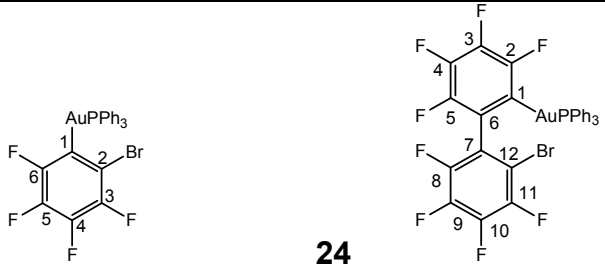
Assignment	δ / ppm	δ / ppm
<div style="display: flex; justify-content: space-around; align-items: center;"> <div style="text-align: center;">  <p>21</p> </div> <div style="text-align: center;">  <p>22</p> </div> </div>		
^1H NMR		
H ^{ortho}	7.54 (12H, m)	
H ^{para}	7.60 (6H, m)	7.49 (30H, m)
H ^{meta}	7.70 (12H, m)	
^{13}C NMR		
C ¹	129.5 (d, $^2J = 10.6$ Hz)	114.2 (m)
C ⁶		126.0 (m)
C ^{ortho}	130.0 (d, $^2J = 11.3$ Hz)	129.8 (m)
C ^{ipso}	130.5 (d, $^1J = 55.1$ Hz)	130.8 (d, $^1J = 34.7$ Hz)
C ^{para}	132.3 (d, $^4J = 2.5$ Hz)	132.3 (d, $^4J = 2.5$ Hz)
C ⁴	134.9 (d, $^5J = 13.6$ Hz)	142.4 (m)
C ^{meta}	135.0 (d, $^3J = 13.8$ Hz)	134.7 (m)
C ³	144.7 (dm, $J_{\text{CF}} = 250.0$ Hz)	138.2 (m)
C ⁵		144.4 (m)
C ²	149.8 (dm, $J_{\text{CF}} = 228.4$ Hz)	148.2 (m)
^{31}P NMR		
P	42.4 (s)	42.8 (s)

Table 2.33 ^1H , ^{13}C and ^{31}P NMR data for **23** and **24** in CD_2Cl_2

Assignment	δ / ppm	δ / ppm
		
^1H NMR		
H^{ortho}		
H^{para}	7.49 (15H, m)	7.49 (15H, m)
H^{meta}		
^{13}C NMR		
C^{12}		11.6 (m)
C^2	107.9 (m)	150.9 (m)
C^1	122.6 (m)	117.6 (m)
C^{ortho}	129.8 (m)	129.8 (m)
C^{ipso}	130.6 (d, $^1J = 38.5$ Hz)	130.4 (d, $^1J = 43.7$ Hz)
C^{para}	131.9 (d, $^4J = 2.3$ Hz)	132.3 (m)
C^{meta}	134.7 (m)	134.7 (m)
C^4	140.2 (m)	140.2 (m)
C^5	140.9 (m)	155.8 (m)
C^6	145.5 (m)	124.6 (m)
C^3	147.5 (m)	138.0 (m)
C^7		123.0 (m)
C^8		155.3 (m)
C^9		156.6 (m)
C^{10}		139.6 (m)
C^{11}		139.0 (m)
^{31}P NMR		
P	40.7 (s)	41.6 (s)

Mass spectrometry

The ESI-MS data for **21** were recorded in a chloroform matrix and are summarised in Table 2.34.

Table 2.34 ESI-MS data for compound **21**

M/z	Intensity (%)	Fragment ion
1673	10	$[M]^+ + [AuPPh_3]^+$
1215	15	$[M]^+$
721	100	$[Ph_3PAuPPh_3]^+$
459	18	$[AuPPh_3]^+$

The molecular ion of **21** is observed at m/z 1215 and the base peak fragment corresponds to the homoleptic rearrangement product $[Ph_3PAuPPh_3]^+$.

The ESI-MS data for compound **22** were recorded in a dichloromethane matrix and is summarised in Table 2.35.

The molecular ion of compound **22** is observed at m/z 1215 and the molecular ion with an additional AuPPh₃ fragment is observed at m/z 1673. The fragment at m/z 953 corresponds to the mass of the molecular ion after the loss of a PPh₃ unit.

Table 2.35 ESI-MS data for compound **22**

M/z	Intensity (%)	Fragment ion
1673	100	$[M]^+ + AuPPh_3$
1215	18	$[M]^+$
953	30	$[M]^+ - PPh_3$
663	80	$[C_6F_4AuPPh_3]^+ + CH_2Cl_2$
611	20	$[C_6F_4AuPPh_3]^+$
279	20	OPPh ₃

2.3 Conclusions and future work

This investigation comprised the synthesis and characterisation of new gold(I) phosphonium ylide complexes and other products formed during these coordination processes. Different methods were used to facilitate the deprotonation of the phosphonium salts to yield the corresponding ylides and subsequent coordination of the ylides to different gold precursor compounds, such as, C₆F₅Au(tht), (tht)AuCl or Ph₃PAuCl.

The deprotonation agents n-BuLi, Ag₂O and NaH were investigated. Deprotonation with n-BuLi proved to be successful in deprotonating the phosphonium salt, but was not successful in removing all the bromide counterions from the reaction mixture. Some bromide ions were left in the reaction mixture and this led to preferential coordination of bromide to the gold instead of the ylide. The Ag₂O was used as a powerful deprotonation agent and simultaneous bromide scavenger. This was a successful method, but led to the formation of a mixture of three or more products which could not be separated. The water that formed as a byproduct during this deprotonation reaction sometimes hydrolysed the ylide functional group and loss of this donor functionality prevented coordination of the ylide to gold. In Usón's procedure, that proved to be the most successful, the bromide counterion of the phosphonium salt is substituted by the gold complex to form an aurate counterion to the phosphonium salt. Subsequent deprotonation of the phosphonium salt with NaH furnishes the corresponding gold(I)-ylide complex. This method formed the desired products and single crystals suitable for X-ray diffraction studies were obtained for **5** and **9**, while the other methods formed mixtures of compounds which could not be separated.

The reaction procedure reported by Vicente *et al.* in which phosphonium ylides were coordinated to gold(I) using Ph₃PAu(acac) as starting material was not successful in our hands. Only small amounts of the phosphonium salt were deprotonated and the reaction procedure yielded a lot of undesired products.

The ¹³C and ¹H NMR spectra of the compounds **1**, **2a**, **3a**, **4a**, **9** and **16**, suggested that there are a large number of nuclei, which from a symmetry viewpoint, seem equivalent, but are magnetically inequivalent. The triphenylphosphonium units were expected to be equal, but multiple, overlapping signals proved that the respective *ortho*, *meta* and *para* carbon and proton nuclei are in magnetically different environments from each other. The ¹³C, ¹H and ³¹P NMR spectra also gave valuable insight into the formation of chiral centres – specifically in compound **8**. In general and in line with Vicente's results, chemical shifts in the NMR spectra show characteristic shift changes after coordination of the deprotonated phosphonium salts to gold(I). The ylidic carbon shifts display a downfield shift of

on average 5 ppm, while the ylidic proton chemical shifts display an upfield shift of on average 1 ppm. In the ^{31}P NMR spectra the phosphorus signals occur downfield $\Delta\delta$ 2.2 after coordination of the deprotonated phosphonium salt to the gold(I), following the same pattern reported by Vicente *et al.* p11. The NMR data are often underreported because of insolubility of the compounds and, therefore, characterisation of the compounds is reliant on single crystal X-ray structure determinations. ^{13}C NMR chemical shifts are not a good indication of the electronic changes that take place upon coordination, as the chemical shift consists of a paramagnetic (σ_p) and diamagnetic (σ_d) compound in the equation $\sigma = \sigma_p + \sigma_d$. In the ^1H NMR spectra σ_p can be ignored because it is too small and, therefore, changes in the ^1H NMR signals reflect deshielding of the nucleus. In the ^{13}C NMR signals σ_p plays a larger role and cannot be ignored. The changes in ^{13}C NMR chemical shifts, therefore, do not necessarily reflect the deshielding of the nucleus.²⁴

The first fluorobiphenylgold(I) complexes have been synthesised (**21** and **22**) in good yields, 60% and 95% respectively, and the molecular structure of one of these (**21**) was obtained. Compound **22** displayed luminescent properties during the reaction procedure. This was not investigated further, but literature suggests that these properties probably arise from gold...gold interactions. This is most easily understood as the emission from a metal-based excited state but emission has also been proposed to occur from $\sigma \rightarrow \pi^*$, $\pi \rightarrow \pi^*$, or LMCT (ligand to metal charge transfer) excited states in different complexes.²⁵

Especially compound **22** if it could be obtained in pure form and high yields opens many new possibilities. Its preparation should receive further attention.

Future work that can complement this study include oxidative addition reactions of halides (X_2) and alkyl halides (RX) to these gold(I) ylide complexes. The possibility to displace both ylidic protons with a suitable gold precursor compound can also be investigated and can possibly lead to the formation of one compound only, instead of mixtures of mono coordinated and double coordinated

²⁴ R. F. Fenske in *Organometallic Compounds, Synthesis, Structures, and Theory*, ed. B. L. Shapiro, Texas A and M University press, Texas (1983) p 305

²⁵ M. J. Irwin, J. J. Vittal and R. J. Puddephatt, *Organometallics*, **16** (1997) 3541

compounds, as was the case in this study. Presently such investigations are hampered by the low yields and unselective preparations. Better experimental procedures are needed.

Very little is known about the far infrared metal vibrations of these types of complexes. Clark and co-workers used Raman spectroscopy to obtain data on the metal-metal stretching vibrations in dimethyl-ylide complexes.²⁶ Their results allowed assignment of the Au-Au and Au-X stretching frequencies in that series. This would be an interesting investigation in compounds such as the C₆F₅Au(tht) forming a polymer chain (**15**) with many gold-gold interactions (Chapter 3).

A brief study of the coordination of the phosphonium salts, mentioned in this chapter, to chromium and iron metal centres was performed, using [BrCr(CO)₅][N(C₂H₅)₄] and [CpFe(CO)₂] as metal precursor compounds. Our brief study was unsuccessful and no coordination took place. This should be investigated further to find a successful synthetic method to obtain coordination compounds.

It is known that ylides have application in the treatment of rheumatoid arthritis²⁷ and recently (2002) Delikatny *et al.*²⁸ discovered that the lipophilic phosphonium salts *p*-(triphenylphosphoniummethyl) benzaldehyde chloride and [4-(hydrazinocarboxy)-1-butyl]tris-(4-dimethyl-aminophenyl)phosphonium chloride induced biochemical and structural changes in the cultured human breast cancer cell line HBL-100. Gold(I) itself is known for application in anti-inflammatory compounds and anti-tumor activity to name a few applications.²⁹ The compounds synthesised in this study might show pharmaceutical activity of some kind and will be investigated, but first, one should be in a position to isolate them purely and in good yields.

²⁶ R. J. H. Clark, J. H. Tocher, J. P. Fackler, R. Neira, H. H. Murray and H. J. Knachel, *J. Organomet. Chem.*, **303** (1986) 437

²⁷ R. J. Puddephatt, in *Comprehensive Organomet. Chemistry*, eds. G. Wilkinson, F. G. A. Stone and E. W. Abel, Pergamon, Oxford, 1982, p 775

²⁸ E. J. Delikatny, W. A. Cooper, S. Brammah, N. Sathasivam and D. C. Rideout, *Cancer Research*, **62** (2002) 1394

²⁹ S. P. Fricker, *Gold Bull.*, **29** (1996) 53

2.4 Experimental

2.4.1 Materials

All reactions were carried out under an inert atmosphere (argon) using standard vacuum-line and Schlenk techniques, to exclude moisture that can hydrolyse the phosphonium salts and decompose the gold complexes. Glassware was dried at $\pm 100^\circ\text{C}$ and cooled down under vacuum before use. Manipulations at low temperature were performed by placing the reaction flask in a propanol bath cooled down with dry ice or liquid nitrogen.

All solvents were dried and purified by conventional methods and freshly distilled from sodium wire, except CH_2Cl_2 , which was distilled from CaH_2 , under nitrogen shortly before use. Before distillation the solvents were dried on 4Å molecular sieves (CH_2Cl_2 , pentane, hexane) or KOH (THF and diethyl ether). All common reagents were used as obtained from commercial suppliers without further purification.

NMR spectra were recorded on a Varian VXR 300 (300 MHz for ^1H , 75.4 MHz for $^{13}\text{C}\{^1\text{H}\}$ and 121.5 MHz for $^{31}\text{P}\{^1\text{H}\}$) or INOVA 600MHz (600 MHz for ^1H , 151 MHz for $^{13}\text{C}\{^1\text{H}\}$ and 243 MHz for $^{31}\text{P}\{^1\text{H}\}$) NMR spectrometer. ^1H and ^{13}C chemical shifts are reported in ppm relative to the ^1H and ^{13}C residue of the deuterated solvents. ^{31}P chemical shifts are reported in ppm (δ) relative to an 85% H_3PO_4 external standard solution. All ^{13}C NMR spectra were recorded overnight, with a one second pulse delay. The electron impact mass spectra were recorded with an AMD 604 instrument and the electron spray ionisation mass spectra were recorded with a VG Quattro instrument. Melting and decomposition points were determined on a Stuart SMP3 instrument.

The n-BuLi (1.6M solution in hexane) was standardised before use according to the procedure reported by Winkle *et al.*³⁰ The 1,3-dibromopropane (Aldrich), benzylbromide (Merck), α,α' -dibromo-*p*-xylene (Fluka), α,α' -dibromo-*m*-xylene (Aldrich), $\text{C}_6\text{F}_5\text{Br}$ (Aldrich), tetrahydrothiophene (Acros), triphenylphosphine

³⁰ M. R. Winkle, J. M. Langsinger and R. C. Ronald, *J. Chem. Soc., Chem. Comm.* (1980) 87

(Aldrich), NaH (Fluka), NaBF₄ (Fluka), 4,4'-dibromooctafluorobiphenyl (Aldrich), silveroxide (Fluka), Tl(acac) (Aldrich) and 1,2-dibromotetrafluorobenzene (Aldrich) were used without further purification. All the gold precursor compounds were prepared according to methods described in the literature.^{14, 17, 21}

2.4.2 Preparation of benzyltriphenylphosphoniumbromide (1)⁸

Triphenylphosphine (16.9 g, 64.3 mmol, 10% excess) in 75 ml of ether was stirred until all the triphenylphosphine had dissolved. Benzylbromide (9.99 g, 58.5 mmol) in 30 ml of ether was added dropwise to this solution. The solution became cloudy and was stirred for 5 hours at room temperature. The suspension was left for two days to precipitate. The precipitate was filtered off and dried *in vacuo*. The salt was recrystallised from hot ethanol. Special precautions were taken to destroy all benzylbromide left in the flasks and funnel used, with ammonium hydroxide, since benzylbromide is a powerful lachrymator.

Yield: 30% (6.32 g)

Melting point: 294 - 296 °C

2.4.3 Preparation of 1,3-bis(triphenylphosphino)propanedibromide (2a)

Triphenylphosphine (6.51 g, 24.8 mmol, 25% excess) in 50 ml acetonitrile was boiled under reflux (90 °C) until all the triphenylphosphine had dissolved. 1,3-Dibromopropane (2.05 g, 9.91 mmol) in 10 ml acetonitrile was added dropwise. This mixture was refluxed for 40 hours, whereafter the suspension was filtered and the white precipitate dried *in vacuo*. The product was recrystallised from hot ethanol, (30 ml). The crystals were filtered off and dried *in vacuo*.

Yield: 25% (1.63 g)

Melting point: 340 - 342 °C.

2.4.4 Preparation of [1,4-phenylenebis(methylene)bistriphenylphosphonium]dibromide (3a)

Triphenylphosphine (11.7 g, 44.8 mmol, 25 % excess) in 100 ml acetonitrile was boiled under reflux (90 °C) until all the PPh₃ had dissolved and α,α'-dibromo-*p*-xylene (5.28 g, 20.1 mmol) in 100 ml acetonitrile was added. The solution became cloudy and was boiled under reflux for 40 hours. The white precipitate that formed was filtered off and dried *in vacuo*. These white crystals were recrystallised from hot chloroform and dried again *in vacuo*.

Yield: 80% (12.4 g)

Melting point: 330 - 332°C

2.4.5 Preparation of [1,3-phenylenebis(methylene)bistriphenylphosphonium]dibromide (4a)

Triphenylphosphine (9.88 g, 37.7 mmol, 25% excess) in 100 ml acetonitrile was boiled under reflux until all the triphenylphosphine had dissolved. To this clear solution (3.97 g, 15.0 mmol) α,α'-dibromo-*m*-xylene in 100 ml acetonitrile was added. The solution remained clear and was boiled under reflux for 24 hours. A white precipitate formed which was filtered off and washed with diethyl ether (3 × 20 ml) and dried under vacuum. The precipitate was recrystallised from hot ethanol.

Yield: 36% (3.86 g)

Melting point: 237 - 239 °C

2.4.6 Preparation of [Ph₃P(Ph)CHAu(C₆F₅)] (5)⁶

Benzyltriphenylphosphoniumbromide (0.890 g, 2.10 mmol) and (C₆F₅)Au(tht) (0.920 g, 1.90 mmol) were suspended in 20 ml of THF and stirred for 40 minutes at room temperature. NaH (0.240 g, 10.0 mmol) in 10 ml THF was added to deprotonate the phosphonium salt to the corresponding ylide. The suspension was stirred for 3 hours at room temperature and filtered through celite. The solvent was removed *in vacuo* and the residue extracted first with diethyl ether and

subsequently with dichloromethane. Crystals suitable for single crystal X-ray diffraction were obtained from a solution of **5** in CH₂Cl₂ at -20°C.

Yield: 70% (1.08 g) with respect to the C₆F₅Au(tht)

Melting point: 128 °C (decomposition)

2.4.7 Preparation of [Ph₃PCH(AuC₆F₅)CH₂CH(AuC₆F₅)PPh₃] (**6**) and [Ph₃PCH(AuC₆F₅)CH₂CH₂PPh₃] (**7**)⁶

A suspension of C₆F₅Au(tht) (0.890 g, 2.02 mmol) and phosphonium salt **2a** (0.730 g, 1.01 mmol) in 20 ml THF was stirred for one hour at room temperature. To this white suspension NaH (0.240 g, 10.1 mmol) in 10 ml THF was added and the mixture was stirred for five hours at room temperature. The white suspension was filtered over celite. A clear filtrate was obtained which upon drying *in vacuo* gave an oil. The oil was extracted sequentially with diethyl ether and dichloromethane, filtered through anhydrous MgSO₄ and dried *in vacuo*. Both layers contained a mixture of products. The diethyl ether layer however contained fewer products as determined by thin layer chromatography and was characterised further.

Yield: 1.31 g (mixture)

2.4.8 Preparation of [(C₆F₅)AuCH(PPh₃)C₆H₄CH(PPh₃)Au(C₆F₅)] (**8**)⁶

A suspension of phosphonium salt **3a** (0.820 g, 1.04 mmol, 1% excess) and C₆F₅Au(tht) (0.930 g, 2.06 mmol) in 20 ml THF was stirred for one hour at room temperature. NaH (0.250 g, 10.4 mmol) in 10 ml THF was added and the mixture was stirred for five hours at room temperature, after which it was filtered over celite. A brown filtrate was obtained and dried *in vacuo*. The residue was extracted sequentially with diethyl ether and dichloromethane, filtered through anhydrous MgSO₄ and dried *in vacuo*. A brown solid stayed behind on the MgSO₄, which was insoluble in CH₂Cl₂, diethyl ether or THF and was discarded. From the NMR spectra it was evident that the dichloromethane extract contained the desired compound.

Yield: 40 % (1.29 g)

Melting point: 135°C (decomposition)

2.4.9 Preparation of $[(C_6F_5)AuCH(PPh_3)C_6H_4CH(PPh_3)Au(C_6F_5)]$ (**9**)⁶

Phosphonium salt **4a** (0.810 g, 1.00 mmol) and $C_6F_5Au(tht)$ (1.10 g, 2.40 mmol) were suspended in 20 ml THF and stirred for one hour at room temperature. A clear solution formed to which NaH (0.250 g, 10.3 mmol) in 10 ml THF was added. The mixture became light yellow and after stirring for one hour the suspension became bright orange. The mixture was stirred overnight as it was believed that the orange colour resulted from suspended free ylide. The next morning the suspension was light yellow again and was filtered over celite to obtain a clear light yellow filtrate. The solvent was removed *in vacuo*. The residue was extracted sequentially with diethyl ether and dichloromethane, filtered through anhydrous $MgSO_4$ and dried *in vacuo*. The diethyl ether layer contained the proposed compound and crystals suitable for single crystal X-ray diffraction studies were obtained from a solution of **9** in CH_2Cl_2 , layered with pentane and stored at -10°C.

Yield: 60% (1.98 g)

Melting point: 120°C (decomposition)

2.4.10 Preparation of **9**, $[C_6F_5AuBr]_2[Ph_3PCH_2C_6H_4CH_2PPh_3]$ (**10**) and $[(C_6F_5)AuCH(PPh_3)C_6H_4CH_2(PPh_3)]$ (**11b**)

Phosphonium salt **4b** (0.880 g, 1.10 mmol) was suspended in 20 ml dry THF and cooled down to -45 °C. n-BuLi (0.600 ml, 1.10 mmol) was added dropwise and the mixture immediately became dark brown as it was stirred at -45°C for 10 minutes. A suspension of $(C_6F_5)Au(tht)$ (0.950 g, 2.10 mmol) in 20 ml dry THF was added to this mixture and was stirred for 10 min at -45 °C, whereafter the temperature was slowly raised to room temperature over one hour. The light brown solution was stirred for four hours at room temperature and filtered over $MgSO_4$. The filtrate was concentrated *in vacuo* to yield a brown oily residue, which was extracted with diethyl ether (3 × 20 ml) and thereafter with dichloromethane (3 × 20 ml). The

dichloromethane extract formed an oil and was layered with hexane and stored at -15 °C for 5 days. A yellow solution formed with a brown oil at the bottom. The yellow solution was removed with a syringe and dried *in vacuo*. Crystals suitable for X-ray diffraction studies were obtained from a solution of the crude mixture in CH₂Cl₂ and the molecular structure of **10** was obtained from these. The ether extract contained a mixture of five compounds and was not characterised further.

Yield: Yield too low (**10**)

Melting point: Yield too low (**10**)

2.4.11 Preparation of $[\mu\text{-(Ph}_3\text{PCHCH}_2\text{CHPh}_3)_2\text{Au}_2][\text{BF}_4]_2$ (**12**)¹⁶

A suspension of phosphonium salt **2b** (1.42 g, 1.90 mmol) in 20 ml THF was cooled down to -30 °C and n-BuLi (2.40 ml, 4.40 mmol) was added dropwise. The mixture turned bright orange. A suspension of ClAu(tht) (0.700 g, 2.20 mmol) and NaBF₄ (0.480 g, 4.40 mmol) in 20 ml THF was added to the ylide suspension and stirred at -30°C for 5 minutes. The temperature was slowly raised to room temperature and decomposition started to take place. The reaction mixture was filtered through MgSO₄ and the solvent removed *in vacuo*. A brown, oily residue formed and an extraction was performed first with diethyl ether and subsequently with dichloromethane. NMR and mass spectra revealed that the desired compound was contained in the dichloromethane extract.

Yield: 60% (1.87 g)

Melting point: 126°C (decomposition)

2.4.12 Preparation of $[\mu\text{-(Ph}_3\text{PCHC}_6\text{H}_4\text{CHPh}_3)_2\text{Au}_2][\text{BF}_4]_2$ (**13**)¹⁶

Compound **13** was prepared in the same manner as **12**, from **3b** (1.50 g, 1.90 mmol), n-BuLi (2.00 ml, 3.70 mmol), (tht)AuCl (0.590 g, 1.90 mmol) and NaBF₄ (0.410 g, 3.70 mmol).

Yield: 55% (1.82 g)

Melting point: 107°C (decomposition)

2.4.13 Preparation of **9**, **11a**, $[\text{CH}_3\text{C}_6\text{H}_4\text{CH}(\text{AuC}_6\text{F}_5)\text{PPh}_3]$ (**14**) and $[(\text{C}_6\text{F}_5)\text{Au}(\text{tht})]_n$ (**15**)

A suspension of phosphonium salt **4a** (0.790 g, 1.00 mmol) and Ag_2O (0.230 g, 1.00 mmol) in a 1:1 ethanol/dichloromethane solvent mixture (60 ml) was stirred for two hours at room temperature. A suspension of $(\text{C}_6\text{F}_5)\text{Au}(\text{tht})$ (0.640 g, 1.40 mmol) in 10 ml dichloromethane was added to the mixture and stirred for two hours. The grey suspension was filtered through MgSO_4 to give a clear, colourless solution. The filtrate was concentrated to dryness to yield a white crystalline powder. Two different types of crystals suitable for single crystal X-ray diffraction studies were obtained from a solution of the crude mixture in diethyl ether stored at -10°C for six days. The molecular structures of **14** and **15** were obtained from these and are discussed in Chapter 3.

Yield: 0.380 g not pure (only enough crystals for structure determination)

Melting point (**14**): Yield too low.

(**15**): $62 - 64^\circ\text{C}$

2.4.14 Preparation of **6** and **14** with Ag_2O

A suspension of salt **2a** (0.730 g, 1.00 mmol) and Ag_2O (0.230 g, 1.00 mmol) in a 1:1 ethanol/dichloromethane mixture was stirred at room temperature for two hours. The suspension was filtered through MgSO_4 to remove all the formed charged solids and the water formed as byproduct. A suspension of $(\text{C}_6\text{F}_5)\text{Au}(\text{tht})$ (0.900 g, 2.00 mmol) in the same solvent mixture was added to the filtrate and stirred for two hours at room temperature. The mixture was filtered through MgSO_4 to yield a colourless oily residue. The residue was first extracted with diethyl ether and subsequently with dichloromethane. The dichloromethane layer contained the least amount of different products and was characterised further.

Yield: 0.650 g (not pure)

2.4.15 Preparation of **9** with Ag₂O

Compound **9** was prepared in the same manner as **6**, with **4a** (1.07 g, 1.40 mmol), Ag₂O (0.320 g, 1.40 mmol) and (C₆F₅)Au(tht) (1.23 g, 2.71 mmol).

Yield: 1.27 g (not pure)

2.4.16 Preparation of [(C₆F₅)Au(C₆F₅)₂][Ph₃PCH₂C₆H₄CH₂PPh₃] (**16**)

The phosphonium salt **3a** (0.370 g, 0.510 mmol) and Ag₂O (0.110 g, 0.510 mmol) were suspended in a 1:1 ethanol/dichloromethane mixture and stirred at 0°C, for only 10 minutes, to try and prevent the hydrolysis of the ylide functional group by the water formed as byproduct in the deprotonation reaction. The suspension was filtered through MgSO₄ first before the (C₆F₅)Au(tht) (0.430 g, 0.910 mmol) was added and the mixture stirred for two hours. The temperature was slowly raised to room temperature. A white precipitate formed and some decomposition took place. The solvent was removed *in vacuo* and the residue redissolved in dichloromethane, filtered through celite and concentrated to dryness. Crystals suitable for single crystal X-ray diffraction studies were obtained from a solution of the crude mixture in dichloromethane. The molecular structure of **16** is discussed in Chapter 3.

Yield: 65 % (0.750 g)

Melting point: 172 °C (decomposition)

2.4.17 Preparation of [CH₃C(O)C(AuPPh₃)₂C(O)CH₃] (**17**), [CH₃C(O)CH(AuPPh₃)C(O)CH₃] (**18**), [PPh₃CH(AuPPh₃)CH₂CH(AuPPh₃)PPh₃][BF₄]₂ (**19**) and [Ph₃PCH(AuPPh₃)CH₂CH₂PPh₃] (**20**)

A suspension of Ph₃PAu(acac) (0.680 g, 1.22 mmol) and salt **2b** (0.400 g, 0.610 mmol) in 30 ml dichloromethane was stirred overnight. The light yellow solution became cloudy and cream coloured and was filtered through celite. The filtrate was concentrated to approximately 1 ml in volume, layered with diethyl ether and

left overnight at -10°C . Crystals suitable for single crystal X-ray diffraction studies were obtained and the molecular structure of **17** is described in Chapter 3.

Yield: 40% (0.490 g)

Melting point: 122.5°C (decomposition)

2.4.18 Preparation of 4,4'-[(AuPPh₃)₂C₁₂F₈] (**21**)

A suspension of 4,4'-dibromooctafluorobiphenyl (0.750 g, 1.60 mmol, 2% excess) in 20 ml diethyl ether was cooled down to -75°C and n-BuLi (1.60 ml, 3.70 mmol) was added dropwise. The mixture was stirred at -75°C for 10 minutes, whereafter the ClAuPPh₃ (1.57 g, 3.17 mmol) was added. The mixture was stirred at -75°C for another 10 minutes before the temperature was slowly (over one hour) raised to room temperature. The suspension was filtered through MgSO₄ and the solvent removed *in vacuo*. Compound **21** was recrystallised from a solution of the crude mixture in diethyl ether. The molecular structure of **21** is described in Chapter 3.

Yield: 60% (1.09 g)

Melting point: 106.7°C (decomposition)

2.4.19 Preparation of 2,2'-[(AuPPh₃)₂C₁₂F₈] (**22**), [C₆F₄(AuPPh₃)Br] (**23**) and 2,2'-[(AuPPh₃)C₁₂F₈Br] (**24**)

Compound **22** was prepared in the same manner as compound **21**, from 2,2'-dibromooctafluorobiphenyl (1.39 g, 3.10 mmol), n-BuLi (2.00 ml, 3.10 mmol), ClAuPPh₃ (2.32 g, 4.70 mmol). No crystals suitable for X-ray diffraction were obtained for compound **22**.

Yield: 1.56 g (not pure)

CHAPTER 3

X-ray crystallographic structure determinations

3.1 Introduction

Coordination of the ylides to the gold precursor compounds led to the formation of mixtures of very similar compounds which could not be separated. Along with instability, this made characterisation of each compound extremely difficult, leaving single crystal X-ray diffraction as the only method of establishing the connectivities in the isolated (sometimes in extremely low yields) compounds unequivocally. With valuable information gained from the crystallographic data, the reaction that had taken place could be determined. This information could not be obtained from NMR studies alone. In some instances, where necessary, this led us to look for alternative reaction procedures.

Au(I) has a complete d-shell and, therefore, ligands like phosphorus ylides donating two electrons to the metal centre obey the VSEPR rules for coordination compounds, forming compounds with linear ($Nc = 2$), trigonal planar ($Nc = 3$) or tetrahedral ($Nc = 4$) geometries. Deviations from these geometries can occur due to steric repulsion of substituents or as a result of solid state effects.¹

In this chapter the crystal and molecular structure of two of the phosphonium salts (**3a** and **4a**) are reported and discussed, as they have not been recorded before. Furthermore, the new gold complexes **5**, **9**, **10**, **14**, **15**, **16**, **17** and **21** are discussed in detail.

3.2 Results and discussion

3.2.1 Crystal and molecular structure of [1,4-phenylenebis(methylene)]bis(triphenylphosphonium)]dibromide (**3a**)

The molecular structure and numbers assigned to the various atoms are shown

¹ P. Schwerdtfeger, H.L. Hermann and H. Schmidbaur, *Inorg. Chem.*, **42** (2003) 1334

in Figure 3.1. Hydrogen atoms on the triphenylphosphonium units are omitted for clarity. Selected bond angles and bond lengths appear in Table 3.1.

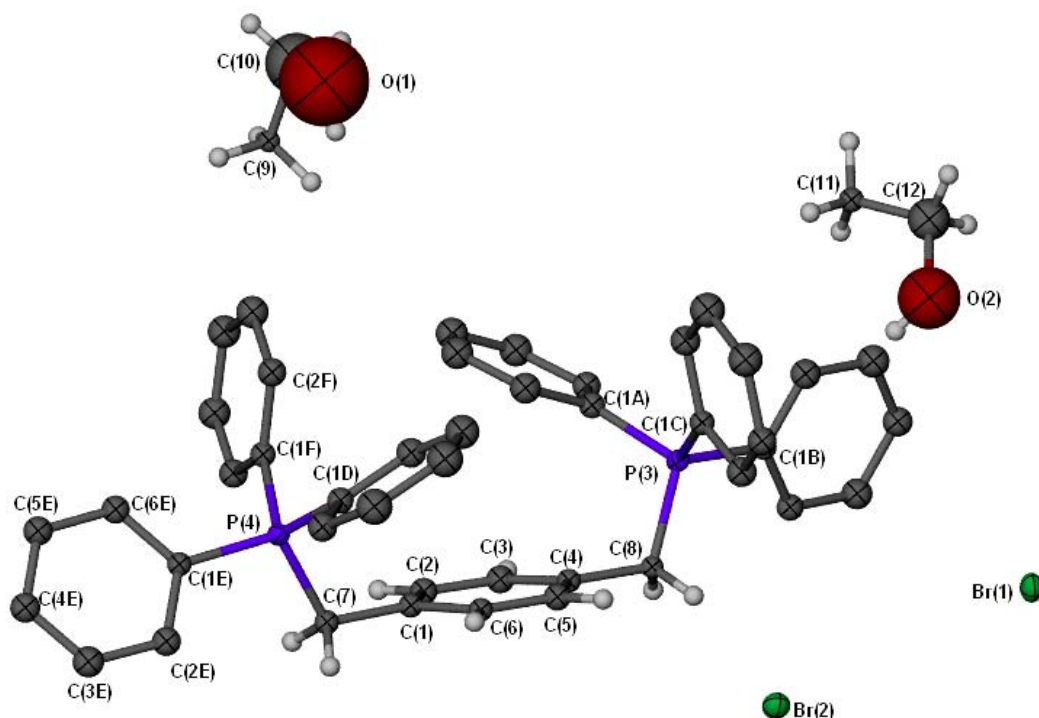
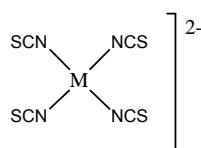
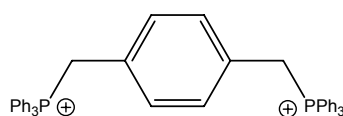


Figure 3.1 Molecular structure of **3a** without hydrogen atoms on the phenyl rings of the triphenylphosphonium units

The bisphosphonium salt **3a**, crystallised in the tetragonal crystal system, space group I41/a, with two ethanol molecules. Crystal lattice arrangement results from short distance interactions between the phosphonium phenyl hydrogen atoms, ethanol carbons and the bromide counterions. These interactions cause both triphenylphosphine groups to lie on the same side of the least-squares plane formed by the phenylenebis(methylene)-ring. Although the molecule is symmetrical, it has no mirror plane perpendicular to the phenylenebis(methylene)-ring, as a result of the steric requirements of the triphenylphosphonium units. The corresponding bond lengths on the two sides of the molecule do not differ significantly. The bond angles on both sides of the molecule are equal except for a non significant difference of 2.3° between one of the corresponding Ph–P–Ph angles. The phosphorus atoms in the triphenylphosphonium units have

tetrahedral symmetry as expected, with the smallest bond angle $106.4(3)^\circ$ and the largest bond angle $111.7(3)^\circ$.

A search of the Cambridge Crystallographic database for similar compounds showed five hits, all cations of compound **3a** crystallised with an anionic coordination complex. Hits **I** - **III** (Scheme 3.1) have similar anions differing only in the metal center, and have the triphenylphosphonium units orientated on the same side of the least-squares plane formed by the phenylenebis(methylene)-ring similar to **3a**. In hits **IV** and **V** (Scheme 3.2) the triphenylphosphonium units are on opposite sides of the plane formed by the phenylenebis(methylene)-ring and these are, therefore, not compared to **3a**.

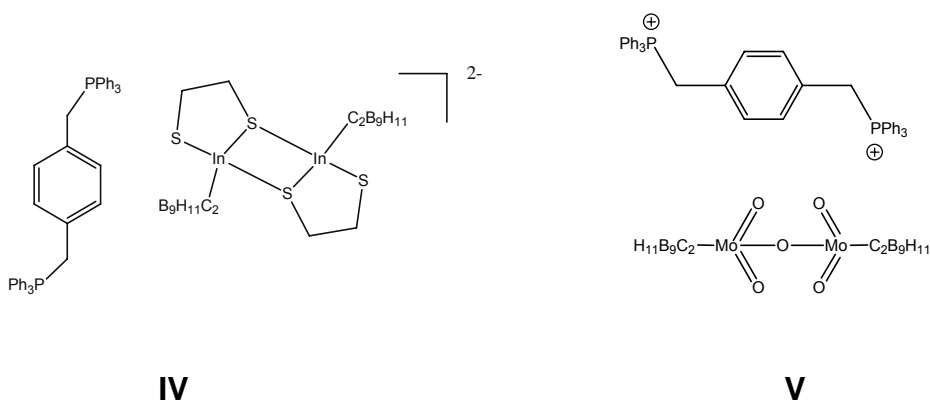


I M = Co

II M = Cu

III M = Ni

Scheme 3.1



Scheme 3.2

A tetraisothiocyanato-cobalt(II) anion co-crystallised with the cation of **3a** and has been described by Reinen *et al.*² Compound **3a** was only compared to **I** because of the better R-factor (5.2%) of **I**.

Table 3.1 Selected bond lengths (Å) and angles (°) for compound **3a**

P(3)–C(1C)	1.792(6)	P(4)–C(1E)	1.791(6)
P(3)–C(1B)	1.798(6)	P(4)–C(1F)	1.797(6)
P(3)–C(1A)	1.798(6)	P(4)–C(1D)	1.804(7)
P(3)–C(8)	1.804(6)	C(1)–C(7)	1.506(8)
P(4)–C(7)	1.810(6)	C(8)–C(4)	1.515(8)
C(1C)–P(3)–C(1B)	109.7(3)	C(1E)–P(4)–C(1D)	110.3(3)
C(1C)–P(3)–C(1A)	108.7(3)	C(1F)–P(4)–C(1D)	111.2(3)
C(1B)–P(3)–C(1A)	109.6(3)	C(1E)–P(4)–C(7)	108.2(3)
C(1C)–P(3)–C(8)	110.5(3)	C(1F)–P(4)–C(7)	111.7(3)
C(1B)–P(3)–C(8)	109.4(3)	C(1D)–P(4)–C(7)	108.9(3)
C(1A)–P(3)–C(8)	108.9(3)	C(1)–C(7)–P(4)	113.7(4)
C(1E)–P(4)–C(1F)	106.4(3)	C(4)–C(8)–P(3)	112.2(4)

The corresponding bond lengths of the cation of **3a** and the cation of **I** do not differ significantly. The majority of the bond angles are the same, except for the P–CH₂–C₆H₄ angles. In structure **I** these two angles (on either side of the central phenyl ring) differ significantly from each other (4.6°), therefore, only one of these angles is similar to the same angle in the cation of **3a**, with the other being 2.9° larger than in **3a**. One of the CH₂–P–Ph angles in **I** is 2° smaller than the corresponding angle in **3a** and one of the Ph–P–Ph angles in **3a** is 1.5° smaller than in **I**. But, overall, there is a good correlation between bond lengths and angles in **3a** and **I**.

Figure 3.3 shows the packing of the unit cell along the c-axis. The unit cell looks very disordered because of the large number (16) of molecules therein. The ethanol molecules and bromide ions arrange themselves in groups which surround the triphenylphosphonium cation. Hydrogen type bonding between H(16) and

² D. Reinen, R. Almann, G. Baum, B. Jacob, U. Kaschuba, W. Massa and G. J. Miller, *Z. Anorg. Allg. Chem.*, **548** (1987) 7

Br(2) and hydrogen atoms on the phenyl rings of the triphenylphosphonium units determine lattice organisation (Figure 3.2, Table 3.2).

Table 3.2 Short distance interactions (Å) in **3a**

Br(1)...H(8)	2.81	Br(2)...H(23)	2.98
Br(1)...H(26)	2.99	Br(2)...H(5)	2.99
Br(1)...H(42)	3.02	Br(2)...H(46)	2.94
Br(1)...H(6)	2.70	Br(2)...H(16)	2.70
Br(1)...H(41)	2.94	H(9)...C(2D)	2.83
Br(1)...H(11)	3.02	H(15)...C(3F)	2.84
Br(2)...H(35)	2.98	C(5B)...H(28)	2.85
Br(2)...H(7)	2.76		

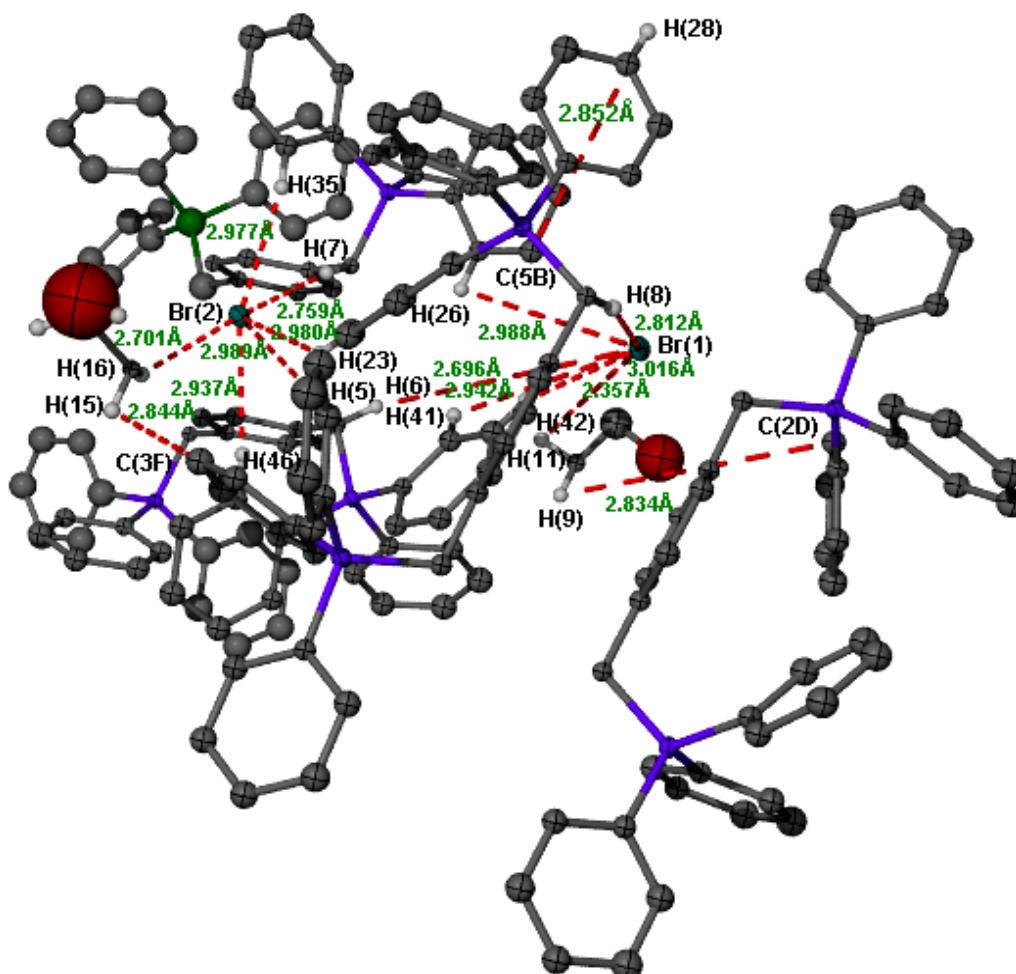


Figure 3.2 Short distance interactions in **3a**, determine lattice organisation. Hydrogen atoms not participating in short distance interactions are omitted.

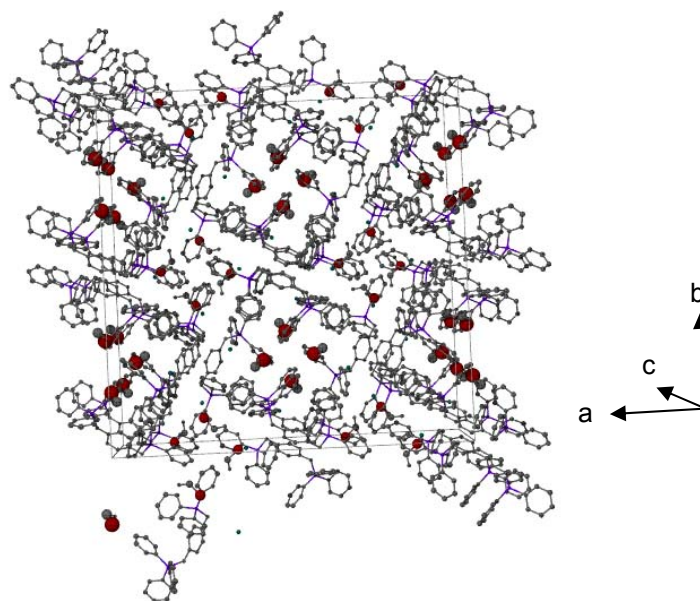


Figure 3.3 Packing of the unit cell of **3a** along the c-axis

3.2.2 Crystal and molecular structure of [1,3-phenylenebis(methylene)]bis(triphenylphosphonium)dibromide (**4a**)

Figure 3.4 shows the molecular structure and numbering of the different atoms of the bisphosphonium salt, **4a**. The hydrogen atoms on the phenyl rings of the triphenylphosphonium units are again omitted for clarity. Table 3.4 contains selected bond lengths and angles of compound **4a**.

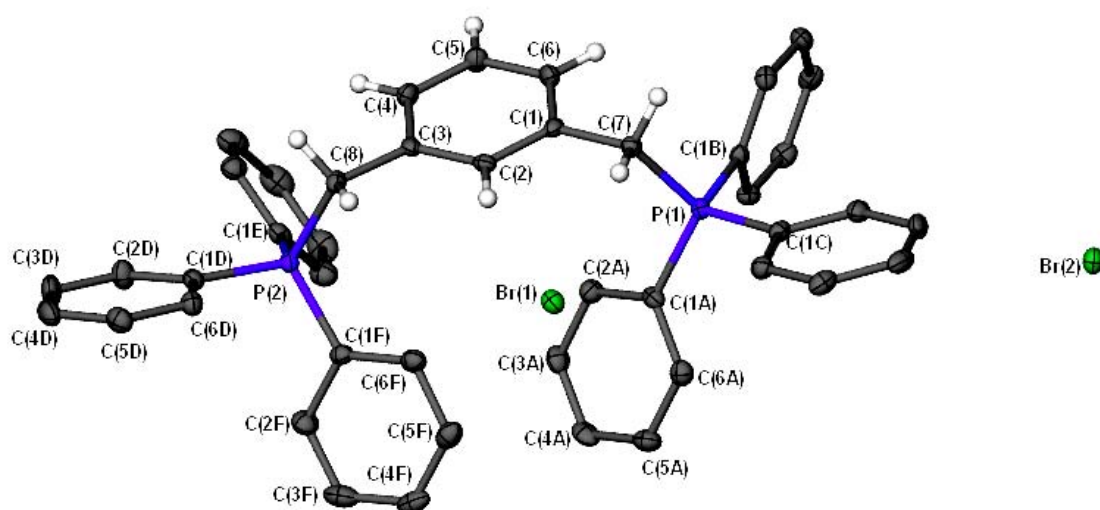


Figure 3.4 Molecular structure of **4a**. Three ethanol molecules that co-crystallised and the hydrogen atoms on the phenyl rings of the triphenylphosphonium units are again omitted for clarity

Compound **4a** crystallised in the triclinic crystal system, space group P-1, with three ethanol molecules. Hydrogen bonds between the hydrogen atoms (in calculated positions) of the hydroxy groups of the ethanol molecules and the bromide ions, short distance interactions between the oxygen atom of the ethanol and calculated hydrogen atoms on the phenyl rings and methylene carbons, as well as interaction between the bromide ions and the phenyl and methylene hydrogen atoms, determine the lattice arrangement (Table 3.3). As in the cation of **3a**, the phenyl rings of the phosphonium units both lie on the same side of the least-squares plane formed by the phenylenebis(methylene)-ring, again probably as a result of hydrogen bonding to the co-crystallised ethanol and bromide anions.

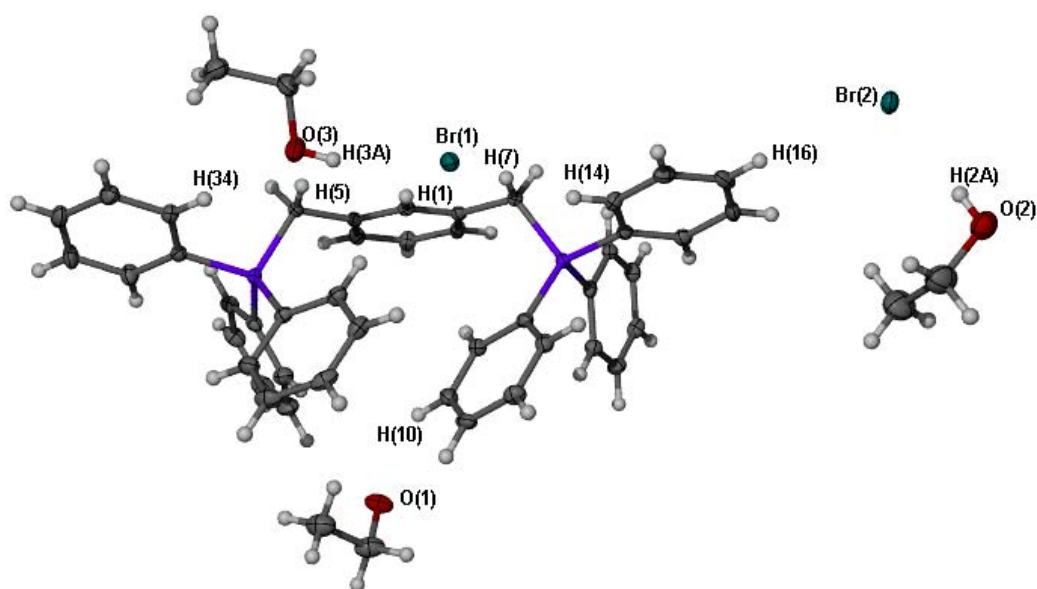


Figure 3.5 POV-ray view of **4a** showing the labels of the atoms that participate in hydrogen bonding and short distance interactions

Table 3.3 Hydrogen bonding (Å) and short distance interactions (Å) in **4a**

H(3A) ... Br(1)	2.47	H(7) ... Br(1)	3.02
O(3) ... H(34)	2.40	H(14) ... Br(1)	2.84
O(3) ... H(5)	2.67	H(16) ... Br(2)	2.94
H(1) ... Br(1)	2.95	H(2A) ... Br(2)	2.54

The structural features of **4a** and **3a** are very similar. Bond distances do not differ significantly. The C(1C)–P(1)–C(7) angle in **4a** is 2.7° smaller than the C(1A)–P(3)–C(8) angle in **3a**. Both the C₆H₄–CH₂–P angles in **4a** are larger than the corresponding angles in **3a** (2.84° and 3.8° respectively). Bond distances on both sides of the phenylenebis(methylene)-ring in **4a** are equal. The bond angles on

the two sides of the phenylenebis(methylene)-ring differ significantly, with C(1A)–P(1)–C(1B), C(1F)–P(2)–C(8), C(1D)–P(2)–C(8) and C(1E)–P(2)–C(1F) larger than the corresponding angle on the other side (Table 3.4). The C(1C)–P(1)–C(1B), C(1E)–P(2)–C(8) and C(1F)–P(2)–C(1D) angles are smaller than the corresponding angles on the other side of the phenylenebis(methylene)-ring (Table 3.4).

Table 3.4 Selected bond lengths (Å) and angles (°) for compound **4a**

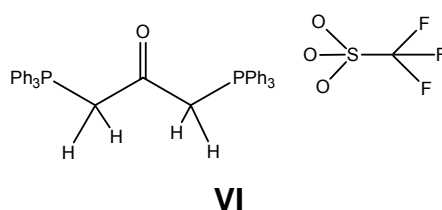
P(1)–C(1A)	1.793(2)	P(2)–C(1F)	1.793(2)
P(1)–C(1C)	1.794(2)	P(2)–C(1D)	1.800(2)
P(1)–C(1B)	1.800(2)	P(2)–C(1E)	1.788(2)
P(1)–C(7)	1.812(2)	C(3)–C(8)	1.520(3)
P(2)–C(8)	1.817(2)	C(7)–C(1)	1.515(3)
C(1A)–P(1)–C(1C)	110.9(1)	C(1F)–P(2)–C(8)	112.8(1)
C(1A)–P(1)–C(1B)	108.3(1)	C(1D)–P(2)–C(8)	107.5(1)
C(1C)–P(1)–C(1B)	109.1(1)	C(1E)–P(2)–C(8)	109.4(1)
C(1E)–P(2)–C(1F)	110.5(1)	C(1A)–P(1)–C(7)	111.7(1)
C(1E)–P(2)–C(1D)	111.0(1)	C(1C)–P(1)–C(7)	106.2(1)
C(1F)–P(2)–C(1D)	105.5(1)	C(1B)–P(1)–C(7)	110.7(1)
C(3)–C(8)–P(2)	116.5(2)	C(1)–C(7)–P(1)	116.0(2)

Only one compound that contains a cation vaguely similar to the cation in **4a** was found in the CCD. The structure of the cation in 1,3-bis(triphenylphosphonium)acetone-bis(trifluoromethanesulfonate) could thus be compared to the cation in **4a**.³

The bond lengths in **VI** are practically equal to the corresponding bond lengths in **4a**. The bond angles in **4a** differ very slightly from the bond angles in **VI**. The C(1C)–P(1)–C(7) angle in **4a** is 0.9° smaller than the corresponding CH₂–P–Ph_{Cipso} angle in **VI**. The C(1F)–P(2)–C(8) angle in **4a** is 2.61° larger than the corresponding CH₂–P–Ph_{Cipso} angle in **VI**. The C(1B)–P(1)–C(7) angle in **4a** is 1.2° larger than the corresponding CH₂–P–Ph_{Cipso} angle in **VI**. The C(1A)–P(1)–

³ A. Bram, H. Burzlaff, D. Hadawi and H. J. Bestmann, *Acta Cryst.*, **C49** (1993) 1409

C(1C) angle is 1.3° smaller and the C(1E)–P(2)–C(1F) angle in **4a** is 1.5° larger than the corresponding Ph_{Cipso}–P–Ph_{Cipso} bond angles in **VI**. The C(1E)–P(2)–C(1D) angle in **4a** is 1.2° smaller than the corresponding Ph_{Cipso}–P–Ph_{Cipso} angle in **VI**. The C(1E)–P(2)–C(1D) angle in **4a** is 3.5° smaller than the corresponding Ph_{Cipso}–P–Ph_{Cipso} angle in **VI**. These very small differences could result from the interactions (Table 3.3) responsible for crystal organisation along with the difference in bonding, i.e. 1,3-substitution on the central phenyl ring as opposed to 1,4-substitution.



Scheme 3.3

Figure 3.6 shows the unit cell packing of **4a**. The molecules arrange themselves with the planes formed by the phenylenebis(methylene)-rings lying diagonally when viewed along the *a*-axis, with the triphenylphosphonium groups lying towards each other in neighbouring molecules. Ethanol molecules and bromide atoms are sandwiched between the planes formed by the phenylenebis(methylene)-rings.

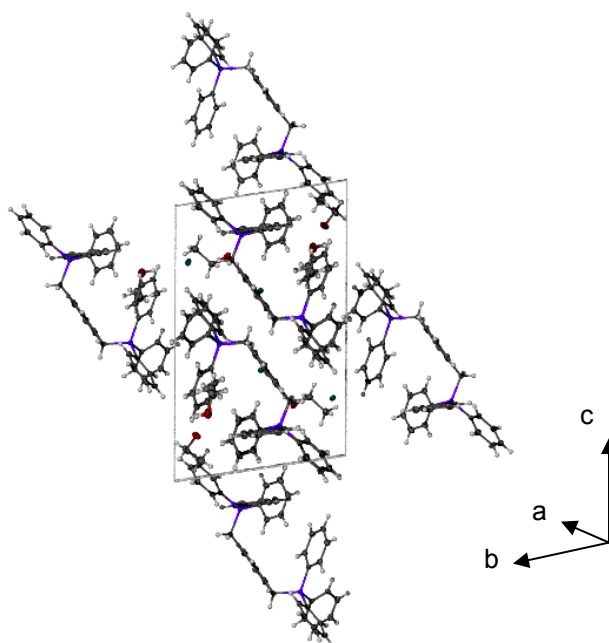


Figure 3.6 Packing diagram of **4a** along the *a*-axis

3.2.3 Crystal and molecular structure of $[(C_6F_5)AuCH(Ph)PPh_3]$ (**5**)

The molecular structure of **5** and the numbers assigned to the atoms in the structure are shown in Figure 3.7. The hydrogen atoms on the phenyl rings of the triphenylphosphonium units are omitted for clarity. Selected angles and bond lengths of **5** are listed in Table 3.5.

Compound **5** crystallised in the orthorhombic crystal system, space group $P2_12_12_1$. No aurophilic interactions are observed. The C(2A)-Au(1)-C(1) angle is practically linear [177.7(5) $^\circ$] as expected for Au(I) compounds. The Au(I)-aryl bond is significantly shorter than the Au(I)-alkyl bond (0.05 Å). The Au(I)-aryl bond length in **IX** (Scheme 3.4) is 2.01(1) and the Au-alkyl bond length in **IX** is 2.09(1) differing significantly by 0.08 Å. The phosphorus atom has the usual tetrahedral configuration with the largest angle C(2B)-P(1)-C(2C), 109.4(5) $^\circ$ and the smallest angle C(2D)-P(1)-C(2B), 105.5(5) $^\circ$.

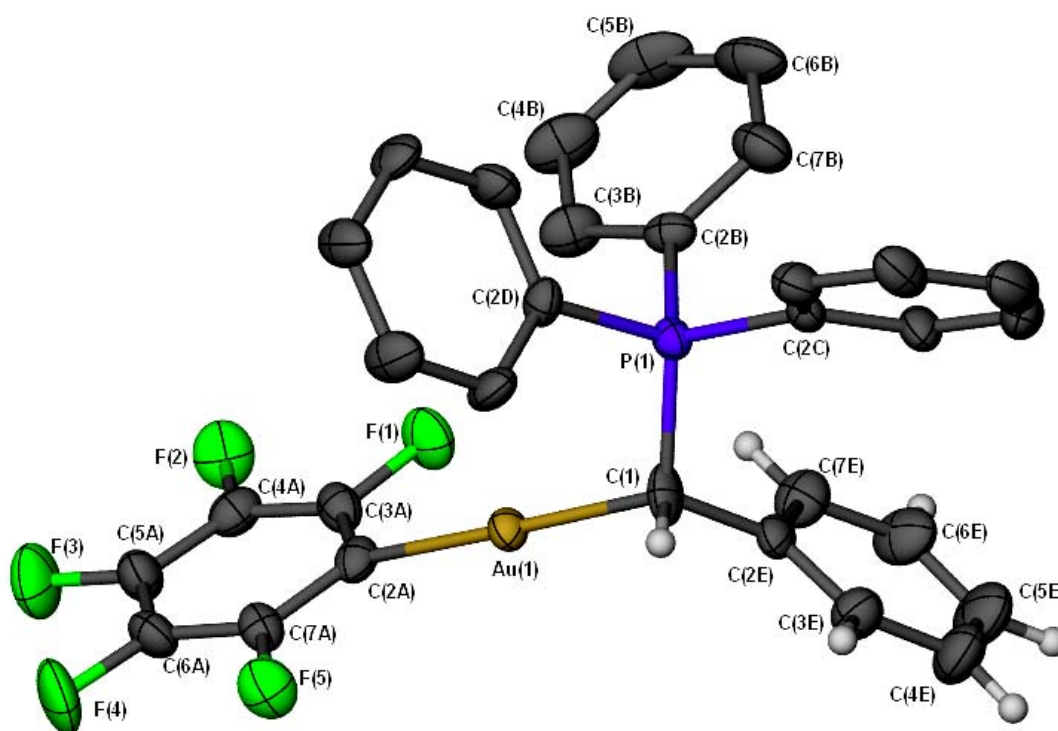


Figure 3.7 Molecular structure of **5** without the hydrogen atoms on the phenyl rings of the triphenylphosphonium units

Compounds containing a structural unit similar to **5** were searched for in the CCD. The phosphonium salt (benzyltriphenylphosphonium) (Scheme 3.4, **VII**) with bromide as counterion was described by Ponnuswamy *et al.* and Hubner *et al.*, and both reported structures were compared to **5** (**VII a** and **b**).⁴

All bond lengths in **5**, are similar to the corresponding bond lengths in **VII a** and **b**. The bond angles in **5** compare well to the bond angles in **VII a** and **b**, except for one of the CH₂–P–Ph angles, which in both latter cases are smaller than in **5** (4.9° and 4.2° respectively) and two of the Ph–P–Ph angles, which in both cases are larger in **VII a** and **b** than in **5** (5.6° and 2.8° respectively and the other angle 3.2° and 2.8° respectively). These small differences in structure possibly result from coordination to gold(I) after deprotonation.

The ylide (deprotonated benzyltriphenylphosphonium) structure (**VIII**, Scheme 3.4) was reported by three different authors, but the structure described by Yufit *et al.*⁵ is compared to **5** as it is the most recent one and had the best R-factor (2.2%).

The C₆H₅–CH[–] bond length in **VIII** (Scheme 3.4) does not differ significantly from the same bond in **5** (0.1 Å shorter than in **5**). As expected the CH[–]–P⁺ bond length however, differs significantly by 0.09 Å (1.7 Å in **VIII** and 1.79(1) Å in **5**) as it has double bond character in **VIII** and single bond character in **5** as a result of coordination to gold. The triphenylphosphonium units display equal bond lengths in both compounds. The C₆H₅–CH–P bond angle in **5** is 13.7° smaller than in **VIII**. This could be due to the double bond character of the CH–P bond in **VIII** forcing the angle to be larger. One of the CH–P–Ph bond angles in **5** are larger (7.9°) and the other two smaller (7.2°, 3.6°) than in **VIII**. The bond angles in the triphenylphosphonium units compare well, with one angle in **5** larger than in **VIII** (3.6°).

The dinuclear gold(I) complexes [(C₆F₅)Au{Ph₂PCH(PPh₂Me)}Au(C₆F₅)]⁶ and [(C₆F₅)₂Au(Ph₂PCHPh₂)Au(C₆F₅)]⁷ (Scheme 3.4, **IX** and **X**) were chosen to

⁴ a) M. N. Ponnuswamy and E. W. Czerwinski, *Acta Crystallogr.*, **C42** (1986) 1019, b) J. Hubner, D. Wulff-Molder, H. Vogt and M. Meisel, *Z. Naturforsch.*, **B52** (1997) 1321

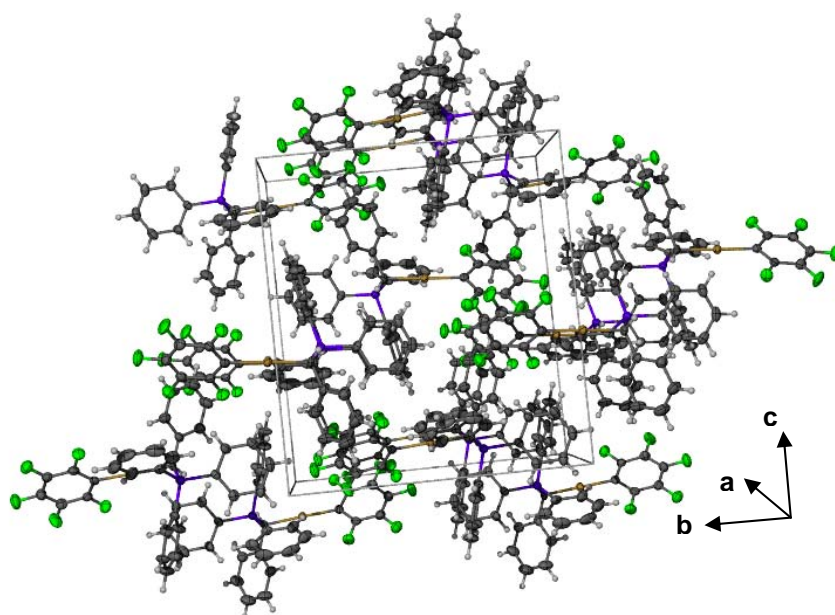
⁵ D. S. Yufit, J. A. K. Howard and M. G. Davidson, *J. Chem. Soc., Perkin Trans.*, **2** (2000) 249

⁶ R. Usón, A. Laguna, M. Laguna, I. Lázaro and A. Morata, *J. Chem. Soc., Dalton Trans.* (1986) 669

Table 3.5 Selected bond lengths (Å) and angles (°) for compound **5**

Au(I)–C(2A)	2.05(1)	C(2C)–P(1)	1.83(1)
Au(I)–C(1)	2.09(1)	C(2D)–P(1)	1.80(1)
P(1)–C(1)	1.79(1)	C(1)–C(2E)	1.50(2)
C(2B)–P(1)	1.81(1)		
C(2A)–Au(1)–C(1)	177.7(5)	C(2D)–P(1)–C(2C)	107.9(5)
C(1)–P(1)–C(2D)	109.4(5)	C(2B)–P(1)–C(2C)	109.4(5)
C(1)–P(1)–C(2B)	114.7(5)	C(2E)–C(1)–P(1)	113.5(9)
C(1)–P(1)–C(2C)	109.7(5)	C(2E)–C(1)–Au(1)	112.5(7)
C(2D)–P(1)–C(2B)	105.5(5)	P(1)–C(1)–Au(1)	110.7(6)

Figures 3.8 and 3.9 show the unit cell packing of **5**. The molecules orientate themselves in layers. The one layer has the pentafluorophenyl groups to one side and the triphenylphosphine groups to the other. The next layer has the two groups in the opposite direction, but with the molecules packed so that the pentafluorophenyl rings lie on top of each other. The triphenylphosphine groups interact with the next three pentafluorophenyl rings over a distance of 2.58 Å through F(2) and H(4) on C(5C). The hydrogen atoms and carbon atoms of neighbouring triphenylphosphine rings interact over a distance of 2.82 Å. The molecules arrange themselves parallel along the b-axis.

**Figure 3.8** Packing diagram of **5** along the a-axis.

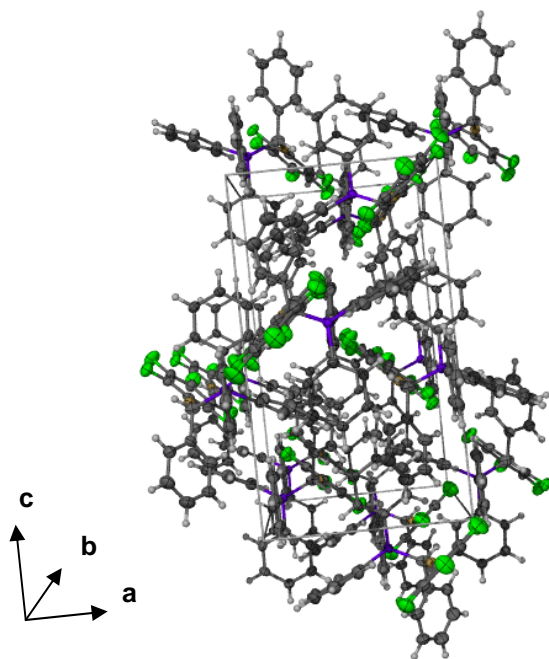


Figure 3.9 Packing of the unit cell of **5** along the b-axis.

3.2.4 Crystal and molecular structure of [Ph₃PCH(C₆F₅Au)C₆H₄(AuC₆F₅)CHPh₃] (**9**)

The molecular structure and numbers assigned to the various atoms in **9** are shown in Figure 3.10. The hydrogen atoms on the phenyl rings of the triphenylphosphonium units and the central phenyl ring are omitted. Table 3.6 contains selected geometrical parameters of compound **9**.

The bisylide gold(I) complex (**9**) crystallised in the triclinic crystal system, space group *P*-1. No aurophilic interactions are seen, due to steric requirements of the bulky triphenylphosphine groups that lie on either side of the least-squares plane formed by the phenylenebis(methylene)-ring, forcing the Au(C₆F₅) units to lie on either side of this plane, too far removed from each other for aurophilic interactions to occur. The C(1B)–Au(2)–C(1) and C(1A)–Au(1)–C(2) bond angles deviate very slightly from linearity by 4° and 5° respectively. The phosphorus atoms in the triphenylphosphonium units have tetrahedral symmetry with the smallest angle C(1D)–P(2)–C(1F), 103.4(3)°, and the largest angle C(1D)–P(2)–C(1E), 111.3(3)°. The corresponding bond lengths on either side of the central phenyl ring are equal. The bond angle C(2)–P(2)–C(1D) is 2.3° smaller than the corresponding angle, C(1)–

P(1)-C(1G), on the other side of the central ring. The C(1D)-P(2)-C(1E) angle is 4° larger than the C(1I)-P(1)-C(1G) angle and the P(2)-C(2)-Au(1) angle is 2.7° larger than the P(1)-C(1)-Au(2) angle. π -Stacking of the C(1B)-C(6B) pentafluorophenyl rings over a distance of 3.38 Å, between C(2B) and C(4B) in neighbouring rings and then also C(4B) and C(2B) in the same rings determine lattice arrangement.

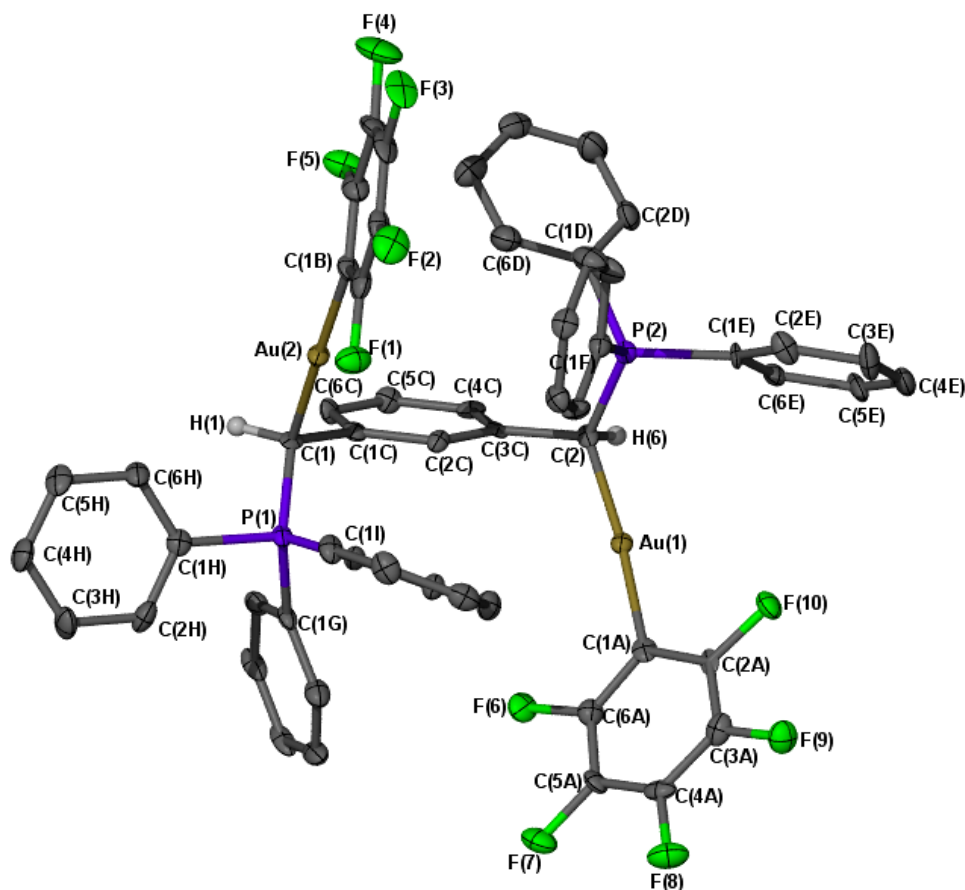


Figure 3.10 Molecular structure of **9** without hydrogen atoms on the phenyl rings of the triphenylphosphonium units and the central phenyl ring

The geometrical parameters of **9** were compared to the corresponding parameters in **4a** to determine the effect of coordination (of the ylidic carbon to gold(I)) on the molecular structure. The structure of **5** was also compared to the structure of **9**, as it contains similar structural units.

All the corresponding bond lengths in **4a** and **9** are equal, except for the two bonds between the phosphorus atoms and the ylidic carbons. The P-CH₂ bonds in **4a**

are both slightly longer than the same bonds in **9** (0.03 Å and 0.04 Å respectively). All bond lengths within the ylide complexes **5** and **9** are equal.

Two of the angles between the ylidic carbon, phosphorus atom and the phenyl rings in the triphenylphosphonium units in **9**, are on average 5° smaller than the corresponding angles in **4a**, while the Ph-P-Ph angles in **4a** are on average 3° larger than the same angles in **9**. The C₆F₅-Au-CH angle in **5** is 2.8° larger than the C(1A)-Au(1)-C(2) angle in **9**. The C(1)-P(1)-C(2B) angle in **5** is 2.7° smaller than the C(2)-P(2)-C(1F) angle in **9**, but overall a good correlation exists between the angles in **5** and **9**.

Table 3.6 Selected bond lengths (Å) and angles (°) for compound **9**

Au(2)-C(1B)	2.037(7)	P(2)-C(1D)	1.794(7)
Au(1)-C(1A)	2.029(7)	P(2)-C(1E)	1.802(6)
Au(2)-C(1)	2.104(6)	P(2)-C(1F)	1.823(7)
Au(1)-C(2)	2.082(7)	P(2)-C(2)	1.780(7)
C(1I)-P(1)	1.809(7)	P(1)-C(1)	1.776(7)
C(1H)-P(1)	1.825(7)	C(3C)-C(2)	1.507(9)
C(1G)-P(1)	1.814(7)	C(1C)-C(1)	1.516(9)
C(1B)-Au(2)-C(1)	175.9(3)	C(1)-P(1)-C(1I)	115.9(3)
C(1A)-Au(1)-C(2)	174.9(3)	C(1)-P(1)-C(1G)	113.1(3)
C(2)-P(2)-C(1D)	110.8(3)	C(1)-P(1)-C(1H)	107.6(3)
C(2)-P(2)-C(1E)	106.8(3)	C(1I)-P(1)-C(1G)	107.3(3)
C(2)-P(2)-C(1F)	117.4(3)	C(1I)-P(1)-C(1H)	107.4(3)
C(1D)-P(2)-C(1E)	111.3(3)	C(1G)-P(1)-C(1H)	104.8(3)
C(1D)-P(2)-C(1F)	103.4(3)	P(2)-C(2)-Au(1)	111.5(3)
C(1E)-P(2)-C(1F)	107.2(3)	P(1)-C(1)-Au(2)	108.8(3)

Figure 3.11 shows the packing of the unit cell of **9**. Hydrogen bonding between F(10) and H(18), on C(3F), and H(19), on C(4F), over a distance of 2.66 Å and 2.62 Å respectively and between F(10) and H(15), on C(3E), over a distance of 2.44 Å, group the molecules in “rings” on each corner of the cell along the a-axis.

These rings are arranged by the π -stacking of the pentafluorophenyl rings through C(2B) and C(4B) of neighbouring rings, as discussed before.

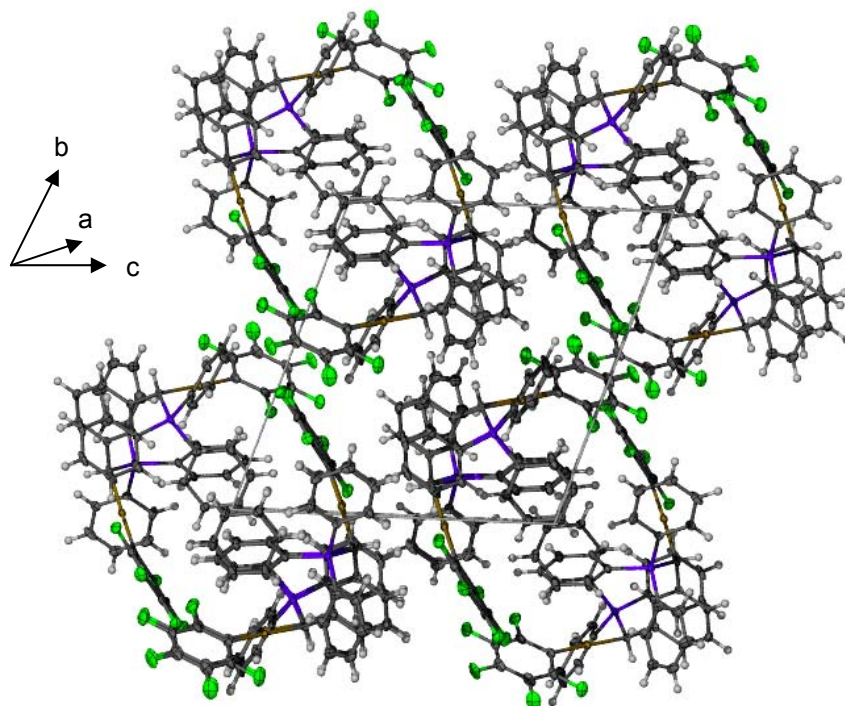


Figure 3.11 Unit cell packing diagram of **9** along the a-axis

3.2.5 Crystal and molecular structure of $[\text{C}_6\text{F}_5\text{AuBr}]_2[\text{Ph}_3\text{PCH}_2(\text{Ph})\text{CH}_2\text{PPh}_3]$ (**10**)

Figure 3.12 shows the molecular structure and numbers assigned to the various atoms in **10**. The hydrogen atoms on the phenyl rings of the triphenylphosphonium units are omitted as well as the second aurate anion and the second dichloromethane molecule that co-crystallised. Selected bond lengths and angles are listed in Table 3.7.

The biscation-bisanion pair (**10**) crystallised in the orthorhombic crystal system, space group *Pba2*. No aurophilic interactions are seen and this time the triphenylphosphine groups lie on either side of the least-squares plane formed by the phenylenebis(methylene)-ring, probably as a result of the steric requirements of the bulky aurate anion. In the structure of **10**, valuable information was gained from the $\text{P-C}_{\text{methylene}}$ bond lengths in order to establish whether or not

deprotonation of the methylene carbon was effected, as this could be a probable cause of failure of the coordination of the gold(I) to the methylene carbon. The bond lengths revealed that deprotonation had not been successful as both P-C_{methylene} bonds were single bonds. The presence of anions as counterions to the phosphonium cations also proved that deprotonation of the methylene carbon did not take place. The triphenylphosphonium phosphorus atom has tetrahedral symmetry, with largest bond angle 111.0(3)° [C(1E) – P(1) – C(1C)] and smallest bond angle 107.7(3)° [C(1E) – P(1) – C(1D)]. The C₆F₅-Au-Br angle is practically linear as expected for Au(I) [177.8(2)°]. All the atoms in the anion of **10** lie in one least-squares plane. The cation in **10** displays a mirror plane perpendicular to the plane formed by the phenylenebis(methylene)-ring, with C(6B) and C(3B) lying in the mirror plane. Thus all bond lengths and angles for corresponding bonds and angles on both sides of the molecule are equal.

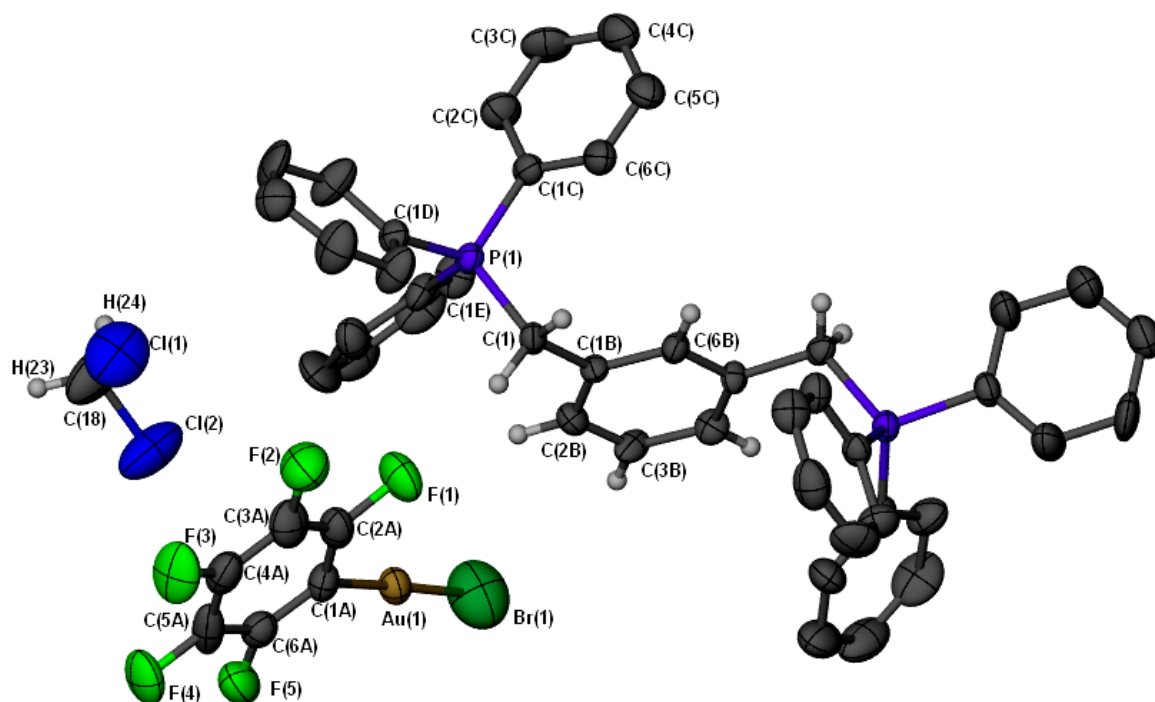
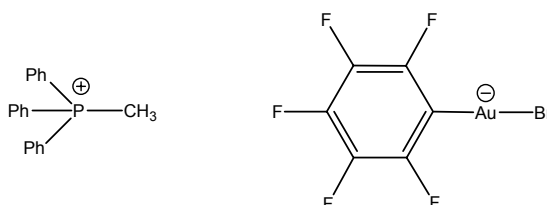


Figure 3.12 Molecular structure of **10**. The hydrogen atoms on the phenyl rings of the triphenylphosphonium units, the second aurate anion and the second dichloromethane molecule that co-crystallised are omitted for clarity.

Table 3.7 Selected bond lengths (Å) and angles (°) for compound **10**

Au(I)–C(1A)	2.013(9)	P(1)–C(1D)	1.801(8)
Au(I)–Br(1)	2.291(3)	P(1)–C(1)	1.812(5)
P(1)–C(1E)	1.780(7)	C(1)–C(1B)	1.520(8)
P(1)–C(1C)	1.798(7)		
C(1A)–Au(1)–Br(1)	177.8(2)	C(1E)–P(1)–C(1)	108.8(4)
C(1E)–P(1)–C(1C)	111.0(3)	C(1C)–P(1)–C(1)	110.8(3)
C(1E)–P(1)–C(1D)	107.7(3)	C(1D)–P(1)–C(1)	108.9(3)
C(1C)–P(1)–C(1D)	109.5(3)	C(1B)–C(1)–P(1)	114.3(4)

Only one compound containing the anion of **10** was found in the CCD. The anion of **10** co-crystallised with $[\text{Ph}_3\text{PCH}_3]^+$ (Scheme 3.5, **XI**)⁸ and the geometrical parameters of the anion in **XI** are compared to the anion of **10**. The cation in **10** is compared to **4a**.

**XI****Scheme 3.5**

The gold-carbon bond distance in **XI** (2.01 Å) compares well with the same bond in **10**. The Au–Br separation in **10** is, however, 0.12 Å shorter than in **XI**. The C–Au–Br bond angle is equal in **10** and **XI** (177.87° in **XI**).

The bond lengths in **10** and **4a** are practically equal. The C(1B)–C(1)–P(1) bond angle in the cation of **10** is slightly smaller than the C(3)–C(8)–P(2) angle in **4a** (2.13°). The (C1)–C(7)–P(1) angle in **4a** is however equal to the C(1B)–C(1)–P(1) angle in **10**. The C(1C)–P(1)–C(7) bond angle in **4a** is 2.8° smaller than the C(1E)–P(1)–C(1) angle in the cation of **10**, while the C(1F)–P(2)–C(8) angle in **4a**

⁸ P. G. Jones and M. D. Villacampa, *Z. Kristallogr.-New Cryst. Struct.*, **212** (1997) 121

is 1.87° larger than the C(1C)–P(1)–C(1) angle in **10**. The C(1F)–P(2)–C(1D) angle in **4a** is 2.2° smaller than the C(1E)–P(1)–C(1D) angle in **10**. The C(1B)–P(1)–C(7) angle in **4a** is 1.78° larger than the C(1D)–P(1)–C(1) angle. Although these small differences were observed, all the other angles in **10** compare well to the corresponding angles in **4a**.

Figure 3.13 shows the packing of the unit cell of **10**. All hydrogen atoms are omitted to clarify the lattice packing pattern. The $[\text{C}_6\text{F}_5\text{AuBr}]$ units arrange themselves parallel to the *c*-axis with the pentafluorophenyl rings of two neighbouring units head to head and the bromides of the next two neighbouring units facing one another. In the *c*-direction, the cation units pack one on each face of the unit cell.

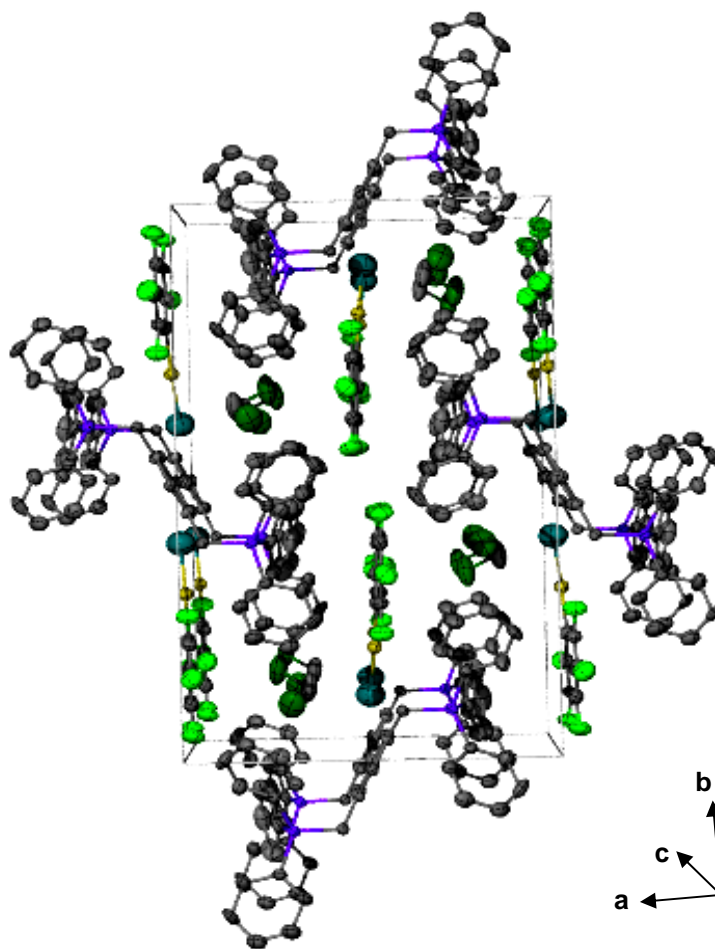


Figure 3.13 Unit cell packing diagram of **10** along the *c*-axis. All hydrogen atoms are omitted to clarify the packing pattern

3.2.6 Crystal and molecular structure of $[\text{C}_6\text{F}_5\text{AuCH}(\text{PPh}_3)(m\text{-Me-C}_6\text{H}_4)]$ (**14**)

The molecular structure of **14** and the numbers assigned to the atoms are shown in Figure 3.14. The hydrogen atoms on the phenyl rings of the triphenylphosphonium units, as well as the hydrogen atoms on the diethyl ether molecule are omitted for clarity. Table 3.11 contains selected bond lengths and angles of **14**.

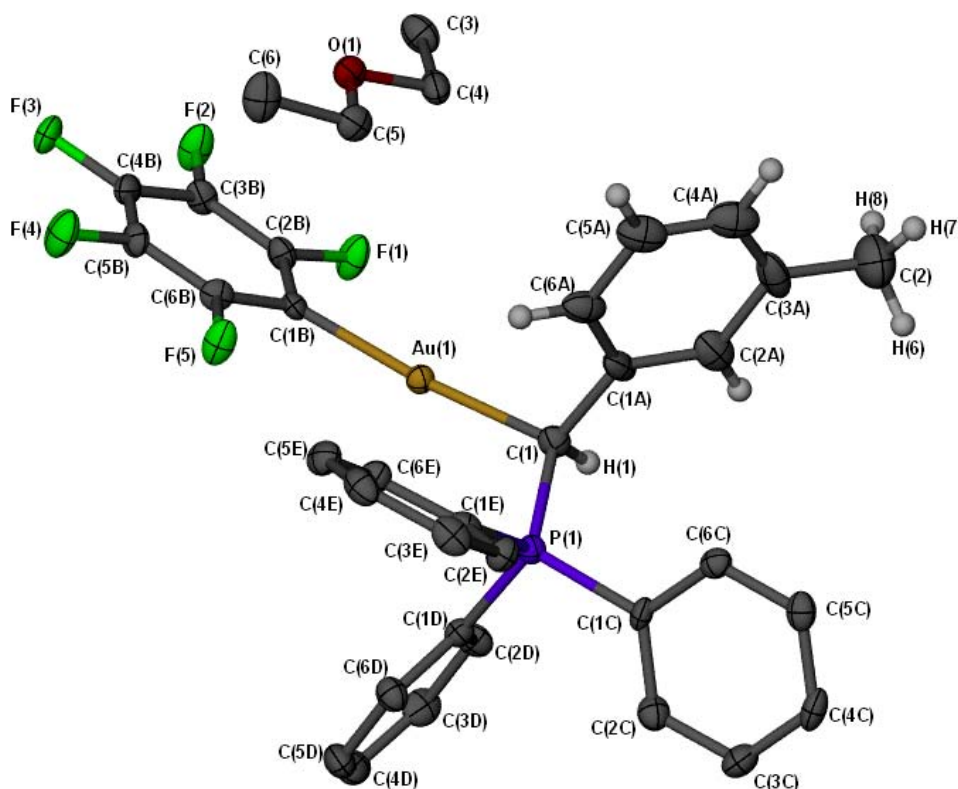


Figure 3.14 Molecular structure of **14** without hydrogen atoms on the phenyl rings of the triphenylphosphonium units and hydrogen atoms on the diethyl ether molecule that co-crystallised.

Compound **14** crystallised in the orthorhombic crystal system, space group $Pbca$. No aurophilic interactions take place and the phosphorus atom has tetrahedral symmetry, with the largest bond angle $107.9(2)^\circ$ [C(1D)–P(1)–C(1E)] and the smallest bond angle $106.0(2)^\circ$ [C(1C)–P(1)–C(1E)]. The C(1B)–Au(1)–C(1) angle is practically linear as expected for Au(I) [$174.05(16)^\circ$]. The Au(I)-aryl bond length is significantly (0.05 \AA) shorter than the Au(I)-alkyl bond length. Corresponding to the same bond lengths in other similar complexes, for example the Au(I)-aryl bond length in **IX** (Scheme 3.4) is $2.01(1)$ and the Au-alkyl bond length in **IX** is $2.09(1)$

differing significantly by 0.08 Å. The C(4A)–C(3A)–C(2) bond angle differs significantly (6.5°) from the C(2A)–C(3A)–C(2) bond angle. The short distance interactions responsible for crystal organisation between the calculated hydrogen atoms and some of the carbon, fluorine and oxygen atoms are summarised in Table 3.8 and the labelling scheme of these atoms are shown in Figure 3.15.

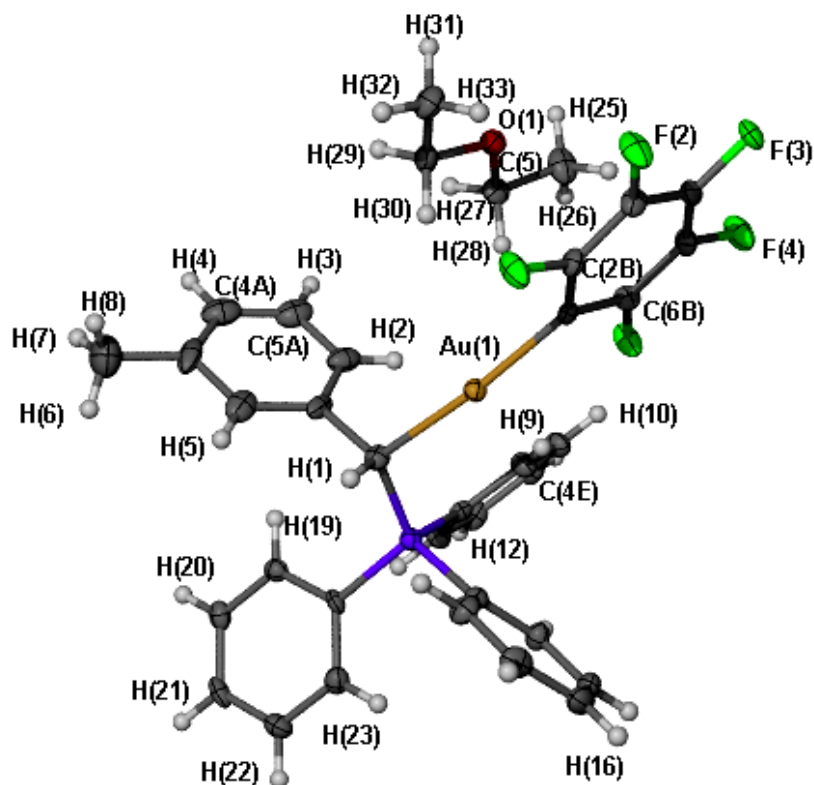


Figure 3.15 Labelling scheme of some of the calculated hydrogen atoms and the carbon, fluorine and oxygen atoms involved in short distance interactions in **14**

Table 3.8 Short distance interactions (Å) between the calculated hydrogen atoms and some of the carbon, fluorine and oxygen atoms

H(21)...O(1)	2.54	H(27)...F(4)	2.65
H(21)...C(5)	2.81	H(26)...F(3)	2.63
H(20)...C(4E)	2.89	H(31)...F(2)	2.66
H(16)...O(1)	2.49	C(6B)...H(28)	2.86
H(10)...C(4A)	2.88	H(33)...C(2B)	2.87
H(10)...C(5A)	2.87		

The geometrical parameters in the molecular structure of **14** are compared to **IX** and **X** (Scheme 3.4) as well as to **5** because of very small structural differences

and very similar bond lengths and angles. The bond lengths of **5**, **IX** and **X** are summarised in Table 3.9.

Table 3.9 Bond lengths (Å) of compounds **5**, **IX** and **X**.

	5	IX	X
C ₆ F ₅ -Au	2.05(1)	2.01(1)/ 2.05(1)	2.05(8)
Au-CH	2.10(1)	2.09(1)	2.09(7)
CH-P	1.79(2)	1.79(1)/ 1.80(1)	1.82(6)
CH-C ₆ H ₅	1.51(1)		
P-Ph ₁	1.80(1)	1.80(1)	1.81(6)
P-Ph ₂	1.82(1)	1.81(1)	1.81(6)
P-Ph ₃	1.80(1)		

All the bond lengths in **14** are in the same order of the bond lengths in **5**, **IX** and **X**. The bond angles of **5**, **IX** and **X** are summarised in Table 3.10. All bond angles in **14**, **5**, **IX** and **X** are equivalent.

Table 3.10 Bond angles (°) of compounds **5**, **IX** and **X**

	5	IX	X
C ₆ F ₅ -Au-CH	177.7(5)	177.2(5)	177.0(4)
Au-CH-C ₆ H ₄	112.5(7)		
P-CH-C ₆ H ₄	113.5(9)		
Au-CH-P	110.7(6)	107.6(5)	108.3(4)
CH-P-Ph ₁	109.4(5)	110.1(6)	111.9(4)
CH-P-Ph ₂	114.7(5)	113.9(5)	115.5(3)
CH-P-Ph ₃	109.7(5)		
Ph ₁ -P-Ph ₃	105.5(5)	105.9(6)	106.2(3)
Ph ₂ -P-Ph ₃	107.9(5)		
Ph ₂ -P-Ph ₁	109.4(5)		

Figure 3.16 and Figure 3.17 show the packing of the unit cell of **14**. All hydrogen atoms are omitted to clarify the packing pattern of the lattice. Crystal lattice arrangement is due to short distance interactions between the hydrogen atoms of the diethyl ether molecule and the fluorine atoms of the pentafluorophenyl rings

and the interaction between H(21) and O(1) (Table 3.8). The molecules arrange themselves in alternating layers along the b-axis. One layer of solvent molecules alternating with a layer of $[\text{C}_6\text{F}_5\text{AuCH}(\text{PPh}_3)(m\text{-Me-C}_6\text{H}_4)]$ molecules arranged with two neighbouring molecules directing the pentafluorophenyl rings to the same side parallel to the c-axis and the next two neighbouring molecules with the pentafluorophenyl rings to the opposite side, parallel to the c-axis.

Table 3.11 Selected bond lengths (Å) and angles (°) for compound **14**

Au(I)–C(1B)	2.041(4)	P(1)–C(1C)	1.805(4)
Au(I)–C(1)	2.095(4)	P(1)–C(1E)	1.811(4)
P(1)–C(1)	1.787(4)	C(1)–C(1A)	1.520(6)
P(1)–C(1D)	1.800(5)	C(3A)–C(2)	1.486(7)
C(1B)–Au(1)–C(1)	174.05(2)	C(1D)–P(1)–C(1C)	107.3(2)
C(1A)–C(1)–Au(1)	110.8(3)	C(1D)–P(1)–C(1E)	107.9(2)
P(1)–C(1)–Au(1)	109.2(2)	C(1C)–P(1)–C(1E)	106.0(2)
C(1)–P(1)–C(1D)	108.4(2)	C(4A)–C(3A)–C(2)	124.3(5)
C(1)–P(1)–C(1C)	113.7(2)	C(2A)–C(3A)–C(2)	117.8(5)
C(1)–P(1)–C(1E)	113.2(2)	C(1A)–C(1)–P(1)	114.7(3)

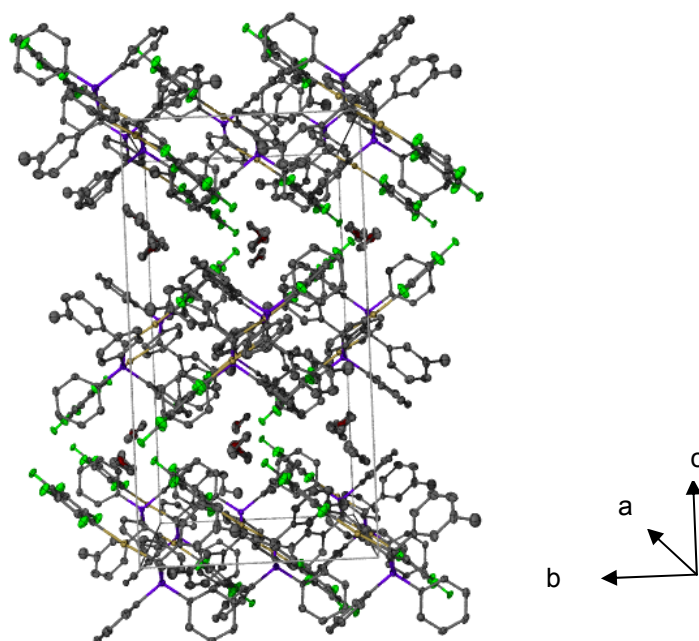


Figure 3.16 Unit cell packing diagram of **14** along the a-axis. All hydrogen atoms are omitted to clarify the packing pattern

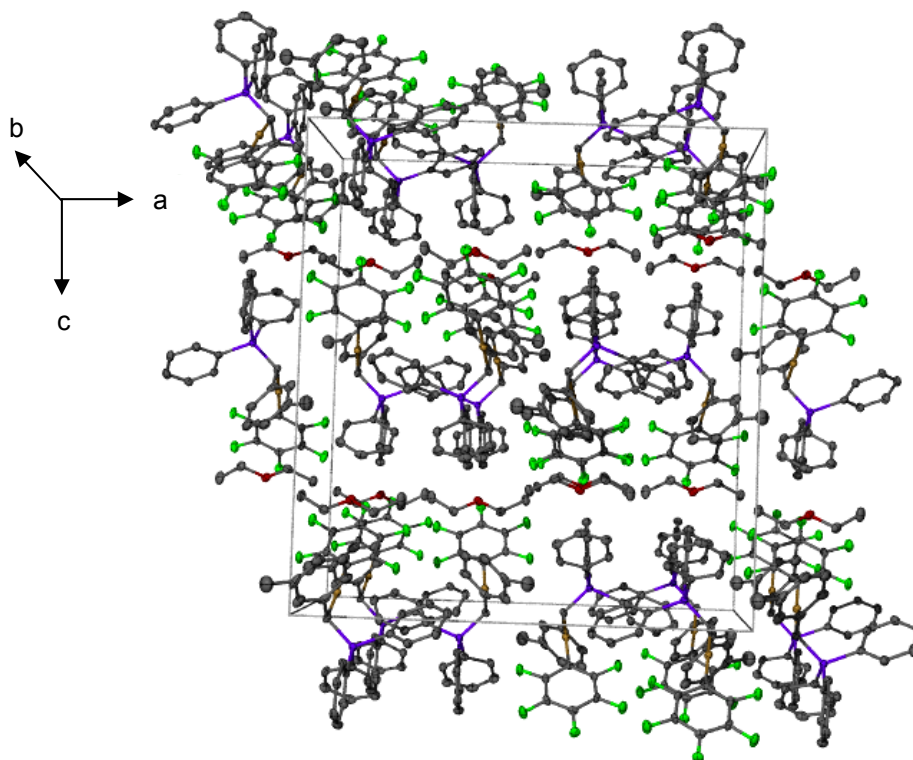


Figure 3.17 Unit cell packing diagram of **14** along the b-axis. All hydrogen atoms are omitted to clarify the packing pattern

3.2.7 Crystal and molecular structure of $[(C_6F_5)Au(SC_4H_8)]$ (**15**)

Figure 3.18 shows the molecular structure of **15** and the numbers assigned to the various atoms. The diethyl ether molecule that co-crystallised is omitted for clarity. Table 3.12 contains selected bond lengths and angles of **15**.

Compound **15** crystallised in the orthorhombic crystal system, space group *Pbnc*. Intermolecular aurophilic interactions (alternating between 3.128 Å and 3.191 Å) as well as intramolecular aurophilic interactions (3.305 Å) arrange the molecules in a polymeric chain (Figure 3.19). In this chain, pairs of neighbouring $[(C_6F_5)Au(SC_4H_8)]$ molecules lie with their pentafluorophenyl rings to one side while the next pair orientate their pentafluorophenyl rings to the opposite side. The pentafluorophenyl rings lie parallel to each other while the tetrahydrothiophene rings lie parallel to each other, but perpendicular to the pentafluorophenyl rings. The S(2)–Au(1)–C(7) and S(1)–Au(2)–C(1) angles deviate very slightly from linearity by 3.4° and 2° respectively.

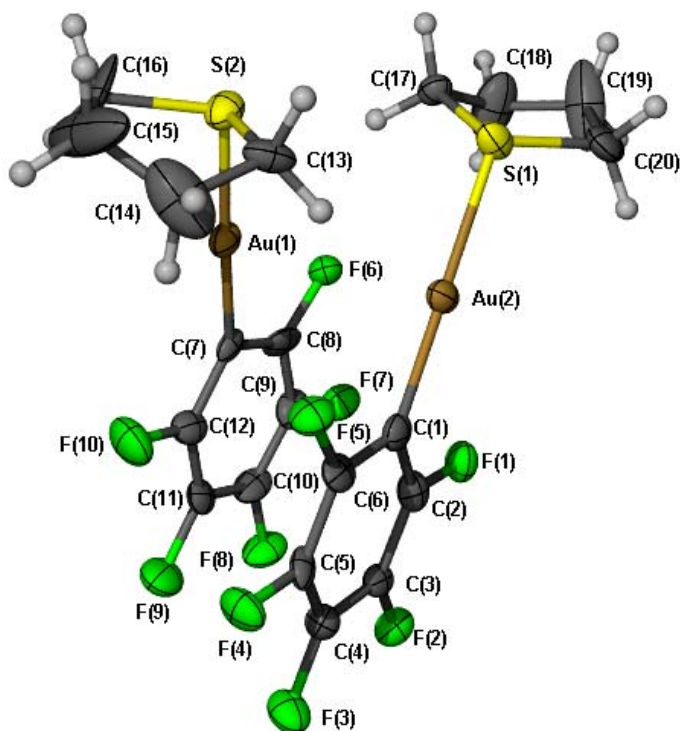


Figure 3.18 Molecular structure of **15**. The diethyl ether molecule that co-crystallised is omitted for clarity

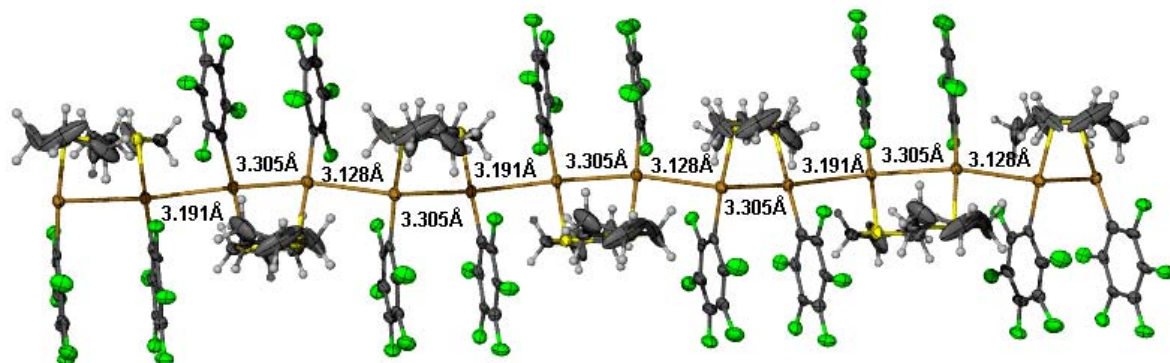
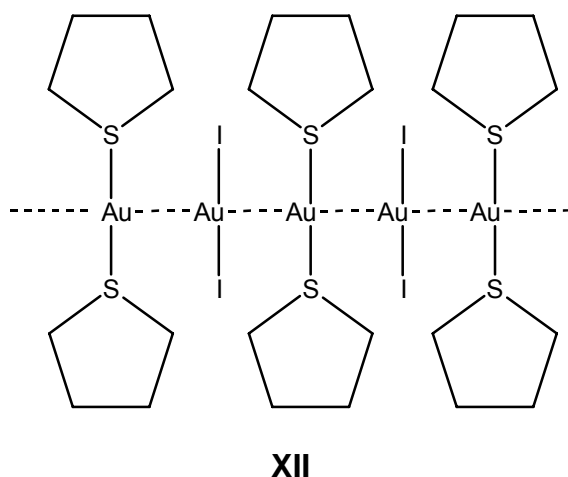


Figure 3.19 Polymeric chain formed by **15** due to intermolecular aurophilic interactions (alternating between 3.128 Å and 3.191 Å) as well as intramolecular aurophilic interactions (3.305 Å)

The molecular structure of **15** is compared to a very similar structure, **XII** (Scheme 3.6), reported by Arhland *et al.*⁹ The two gold units (AuI_2 and $\text{Au}(\text{tht})_2$) are repeated alternating with each other, throughout the structure, forming zigzag-shaped chains.

⁹ S. Arhland, B. Norén and A. Oskarsson, *Inorg. Chem.*, **24** (1985) 1330.



Scheme 3.6

The gold...gold distances within the chain of **XII** are very short, 2.967(2) and 2.980(2) Å respectively. The gold...gold distances in **15** are between 0.148 Å and 0.338 Å longer than the Au-Au distances in **XII**. In **XII**, only two different gold...gold distances occur and alternate, whereas, in **15**, three different gold...gold distances are seen to alternate (Figure 3.19). The gold(I)-sulphur bond lengths in **15** and **XII** do not differ significantly. The structural parameters of the (tht) unit in **15**, compares very well with the same unit in **XII**. The structural features of the C₆F₅-Au unit are normal.⁸

Table 3.12 Selected bond lengths (Å) and angles (°) for compound **15**

Au(1)-C(7)	2.014(9)	S(1)-C(17)	1.820 (1)
Au(2)-C(1)	2.030(1)	S(1)-C(20)	1.827(1)
Au(1)-S(2)	2.317(3)	S(2)-C(13)	1.812(1)
Au(2)-S(1)	2.321(3)	S(2)-C(16)	1.821(3)
C(7)-Au(1)-S(2)	176.3(3)	C(20)-S(1)-Au(2)	106.6(4)
C(1)-Au(2)-S(1)	178.0(3)	C(13)-S(2)-C(16)	92.8(7)
C(17)-S(1)-C(20)	93.7(5)	C(13)-S(2)-Au(1)	105.3(4)
C(17)-S(1)-Au(2)	107.4(3)	C(16)-S(2)-Au(1)	105.3(5)

Figure 3.20 shows the unit cell packing of **15**. The chains of $C_6F_5Au(tht)$ molecules lie parallel to the a-axis. There are two layers of these chains in one unit cell and the layers stack on top of each other with the tetrahydrothiophene rings of one layer on top of the pentafluorophenyl rings of the next layer. No short distance interactions between these layers occur. In the same chain, neighbouring tetrahydrothiophene rings interact through the hydrogen atoms on the tetrahydrothiophene rings and the fluorine atoms on the pentafluorophenyl rings [H(1)...F(5), 2.6 Å and H(2)...F(4), 2.62 Å]. There is no evidence of π -stacking.

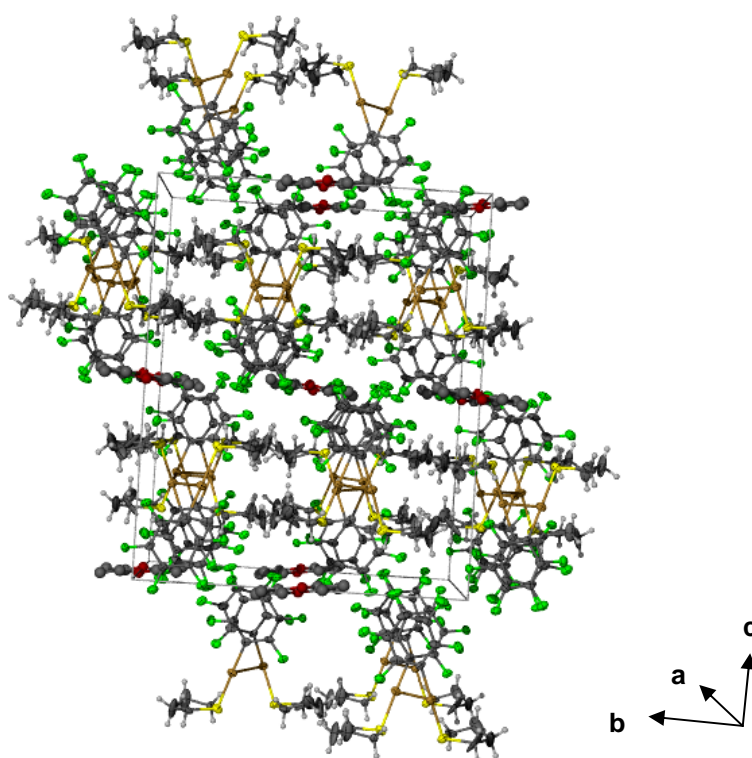


Figure 3.20 Packing of the unit cell of **15** along the a-axis

3.2.8 Crystal and molecular structure of $[C_6F_5AuC_6F_5]_2[Ph_3PCH_2(Ph)CH_2PPh_3]$ (**16**)

Figure 3.21 shows the molecular structure and numbers assigned to the various atoms in **16**. Table 3.13 contains selected bond lengths and angles of **16**.

The biscation-bisanion pair (**16**) crystallised in the triclinic crystal system, space group $P1$. No aurophilic interactions occur, and again the triphenylphosphonium

groups lie on different sides of the least-squares plane formed by the phenylenebis(methylene)-ring, leaving enough space for the aurate anions to lie almost parallel to the least squares plane through the phenylenebis(methylene)-ring. Again the presence of the aurate anions, as well as the C(1)–P(2) and C(2)–P(1) bond lengths [1.816(6), single bonds] prove that deprotonation was not effected and this could be the reason for failure of coordination of the Au(I) to the ylide carbon. The C(1J)–Au(1)–C(1K) and C(1I)–Au(2)–C(1H) bond angles have linear geometry, deviating slightly from linearity by 6°. π -Stacking of two of the pentafluorophenyl rings occur between C(5J) and C(5I) and between C(3J) and C(3I) over a distance of 3.39 Å and 3.40 Å respectively. The triphenylphosphonium phosphorus atom has tetrahedral symmetry, with the largest bond angle 110.3(3)° [C(1B)–P(1)–C(1D)] and the smallest 108.2(3)° [C(1E)–P(2)–C(1F)].

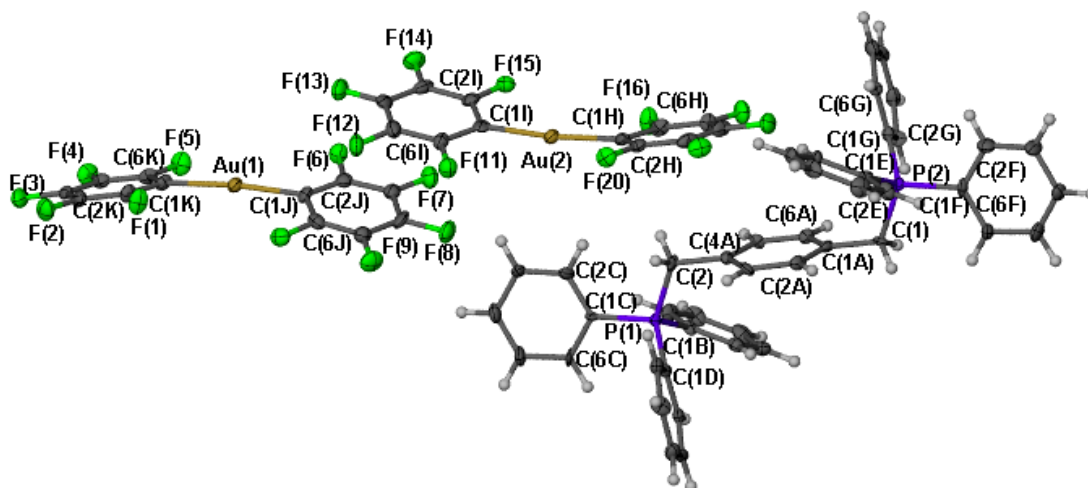
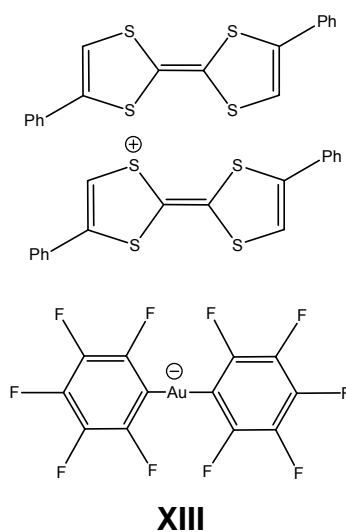


Figure 3.21 Molecular structure of **16**

The anions in **16** were reported five times in the CCD as anions to tetrakis(triphenyl-antimony)-gold(I), bis(4,4'-diphenyltetraathiafulvalenium), tetra-*n*-butylammonium, bis[*o*-phenylene-bis(dimethylarsine)] and bis[diphenyl-phosphino-{diphenylmethylphosphonio}(methanido)thiomethanethiolato]gold(III). The structure of bis(4,4'-diphenyltetraathiafulvalenium) bis(pentafluorophenyl)-gold(I) was described by Cerrada *et al.*¹⁰ (Scheme 3.7, **XIII**) and is compared to the anion

¹⁰ E. Cerrada, M. Laguna, J. Bartolome, J. Campo, V. Orera and P. G. Jones, *Synth. Met.*, **92** (1998) 245

of **16** because of the similar bond lengths and the low R-factor (1.87%). The cation in **16** is compared to **I** (Scheme 3.1) and also to the same cation in **3a**.



Scheme 3.7

Table 3.13 Selected bond lengths (Å) and angles (°) for compound **16**

Au(1)–C(1J)	2.057(7)	P(2)–C(1G)	1.776(7)
Au(1)–C(1K)	2.049(7)	P(2)–C(1E)	1.793(7)
Au(2)–C(1I)	2.034(8)	P(2)–C(1F)	1.798(7)
Au(2)–C(1H)	2.055(7)	P(1)–C(2)	1.816(6)
P(1)–C(1B)	1.781(6)	P(2)–C(1)	1.814(6)
P(1)–C(1C)	1.788(6)	C(4A)–C(2)	1.520(8)
P(1)–C(1D)	1.802(7)	C(1A)–C(1)	1.507(9)
C(1J)–Au(1)–C(1K)	174.0(3)	C(4A)–C(2)–P(1)	113.8(4)
C(1I)–Au(2)–C(1H)	174.0(3)	C(1A)–C(1)–P(2)	114.5(4)
C(1B)–P(1)–C(1C)	109.6(3)	C(1B)–P(1)–C(2)	109.4(3)
C(1B)–P(1)–C(1D)	110.3(3)	C(1C)–P(1)–C(2)	107.2(3)
C(1C)–P(1)–C(1D)	109.1(3)	C(1D)–P(1)–C(2)	111.1(3)
C(1G)–P(2)–C(1E)	109.7(3)	C(1G)–P(2)–C(1)	113.0(3)
C(1G)–P(2)–C(1F)	109.6(3)	C(1E)–P(2)–C(1)	107.8(3)
C(1E)–P(2)–C(1F)	108.2(3)	C(1F)–P(2)–C(1)	108.4(3)

The Au(1)–C(1J) and Au(1)–C(1K) as well as the Au(2)–C(1I) and Au(2)–C(1H) bond lengths in **16** are in the same order as the C₆F₅–Au bond distances in **XIII**. The C(1J)–Au(1)–C(1K) and C(1I)–Au(2)–C(1H) bond angles in **16** are 6° smaller than the C₆F₅–Au–C₆F₅ angle in **XIII** (180.0°), probably as a result of the steric requirements of the cation in **16**.

All the bond lengths and bond angles in the cations of **1**, **3a** and **16** are equal.

Figures 3.22 and 3.23 show the unit cell packing of **16**. All hydrogen atoms are omitted to clarify the lattice packing pattern. Along the a-axis and the b-axis molecules arrange themselves in alternating layers of anions and cations with the pentafluorophenyl rings on top of each other due to π -stacking.

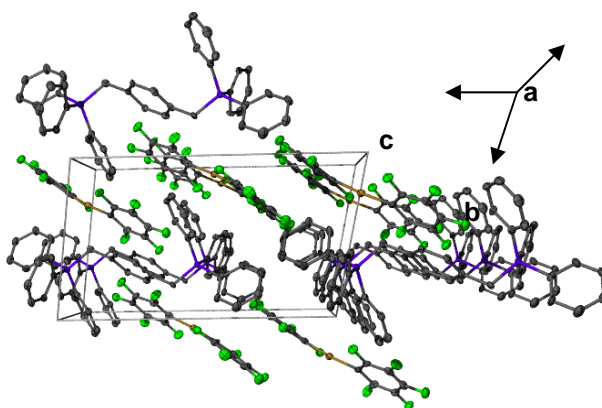


Figure 3.22 Unit cell packing diagram of **16** along the a-axis. All hydrogen atoms are omitted to clarify the packing pattern

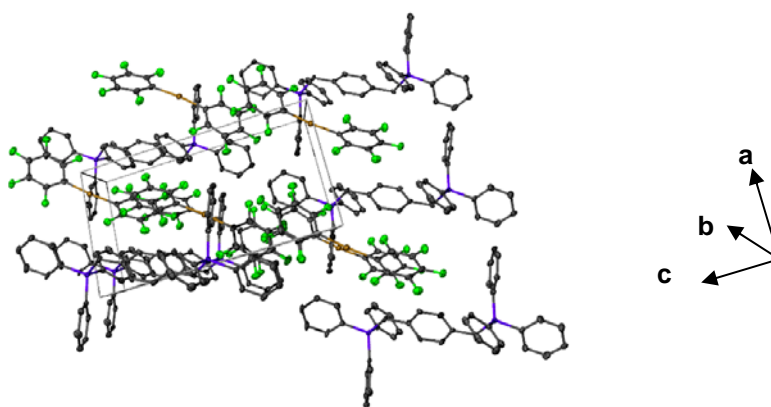


Figure 3.23 Unit cell packing diagram of **16** along the b-axis. All hydrogen atoms are omitted to clarify the packing pattern

3.2.9 Crystal and molecular structure of [(acac)(AuPPh₃)₂] (17)

Figure 3.24 shows the molecular structure of **17** and the numbers assigned to the atoms. Selected angles and bond lengths of **17** are listed in Table 3.14.

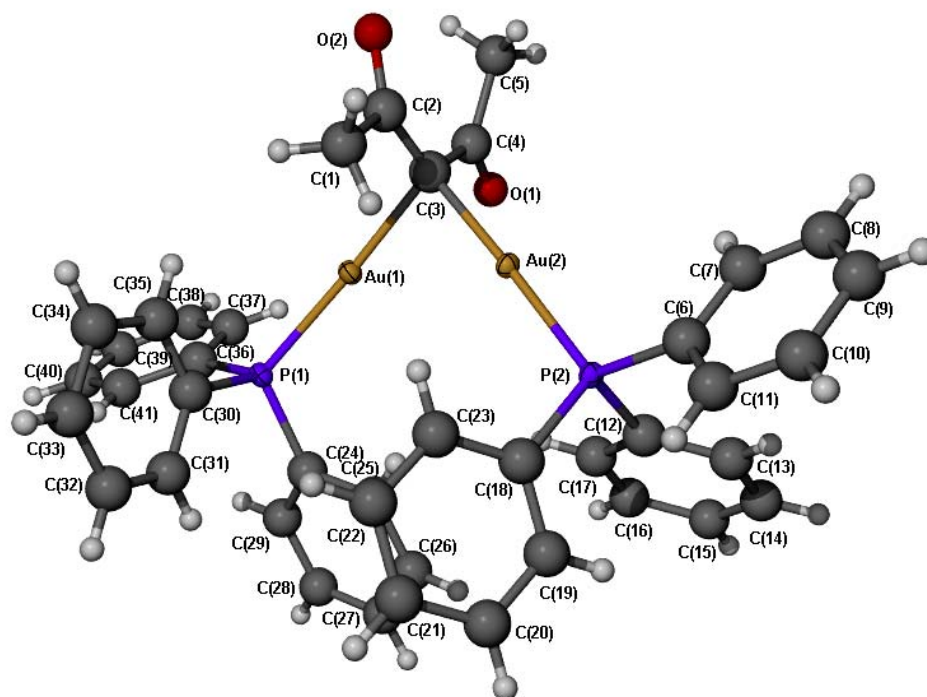


Figure 3.24 Molecular structure of **17**

Compound **17** crystallised in the monoclinic crystal system, space group $P2_1/c$. Very short, intramolecular aurophilic interactions over a distance of 2.85 Å are observed between Au(1) and Au(2). These aurophilic interactions force the Au(1)–C(3)–Au(2) angle to be very acute [84.8(2)°]. The C(3)–Au(2)–P(2) angle [177.06(17)°] and the C(3)–Au(1)–P(1) angle [173.56(17)°] are practically linear as expected for Au(I) compounds. The phosphorus atom has the usual tetrahedral configuration with the largest angle [C(6)–P(2)–C(18), 107.4(3)°] and the smallest angle [C(6)–P(2)–C(12), 104.3(3)°].

Compound **17** was recently (while this work was in progress) described by Djordjevic *et al.*¹¹ (**XIV**), with a R-factor of 2.47%.

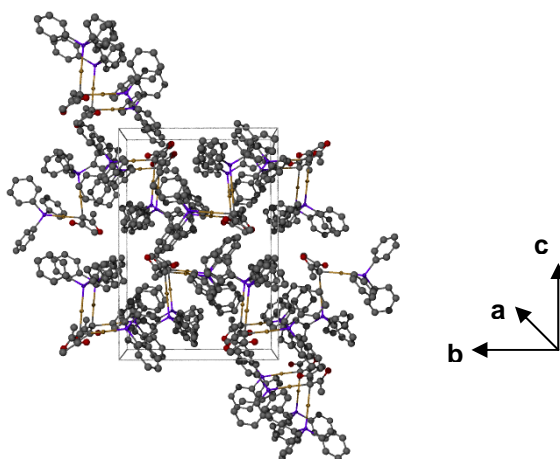
All the bond lengths and angles in **17** are similar to the corresponding bond lengths and angles in **XIV**.

¹¹ B. Djordjevic, K. A. Porter, S. Nogai, A. Schier and H. Schmidbaur, *Organometallics*, **22**, (2003), 5336

Table 3.14 Selected bond lengths (Å) and angles (°) for compound **17**

Au(1)–C(3)	2.123(6)	P(2)–C(6)	1.811(6)
Au(1)–P(1)	2.274(2)	P(2)–C(12)	1.820(5)
Au(2)–P(2)	2.267(1)	P(2)–C(18)	1.826(6)
Au(2)–C(3)	2.105(6)	P(1)–C(24)	1.811(6)
O(1)–C(4)	1.236(7)	P(1)–C(30)	1.819(6)
O(2)–C(2)	1.226(7)	P(1)–C(36)	1.821(6)
C(3)–Au(1)–P(1)	173.6(2)	C(24)–P(1)–C(30)	104.9(3)
C(3)–Au(2)–P(2)	177.1(2)	C(24)–P(1)–C(36)	104.4(3)
C(6)–P(2)–C(12)	104.3(3)	C(30)–P(1)–C(36)	106.1(3)
C(6)–P(2)–C(18)	107.4(3)	C(24)–P(1)–Au(1)	114.9(2)
C(12)–P(2)–C(18)	104.4(3)	C(30)–P(1)–Au(1)	107.6(2)
C(6)–P(2)–Au(2)	115.5(2)	C(36)–P(1)–Au(1)	117.9(2)
C(12)–P(2)–Au(2)	113.1(2)	Au(2)–C(3)–Au(1)	84.8(2)
C(18)–P(2)–Au(2)	111.3(2)		

Figure 3.25 shows the unit cell packing of **17** along the a-axis, all hydrogen atoms are omitted from the diagram for clarity. Short distance interactions between O(1) and O(2) and the hydrogen atoms of the phenyl rings in the triphenylphosphonium units arrange the lattice. The gold atoms in the neighbouring molecules are aligned and spaced 11.28 Å apart. Thus no intermolecular aurophilic interactions are present.

**Figure 3.25** Packing diagram of **17** along the a-axis without all hydrogen atoms

3.2.10 Crystal and molecular structure of $[(C_6F_4)AuPPh_3]_2$ (**21**)

The molecular structure of **21** and the numbers assigned to the atoms in the structure are shown in Figure 3.26. Selected angles and bond lengths of **21** are listed in Table 3.15.

Compound **21** crystallised in the triclinic crystal system, space group $P-1$. No aurophilic interactions are observed. The C(10)–Au(1)–P(2) bond angle deviates from linearity by 12.5° [$167.5(3)^\circ$], while the C(1)–Au(2)–P(1) bond angle is practically linear [$177.9(3)^\circ$] as expected for Au(I) compounds. The two tetrafluorophenyl rings orientate themselves to lie in different planes, but not perpendicular to each other, with a torsion angle of 63.7° through C(4)–C(7). π -Stacking of the tetrafluorophenyl rings over a distance of 3.33 Å between C(10) and C(9) in neighbouring rings and then also C(9) and C(10) in the same rings determine lattice arrangement. This probably causes the C(10)–Au(1)–P(2) bond angle to deviate more from linearity than the C(1)–Au(2)–P(1) bond angle, as the bulky triphenylphosphine groups and the tetrafluorophenyl ring not taking part in the π -stacking lie in the same plane (Figure 3.27). The phosphorus atom in the triphenylphosphonium units have the usual tetrahedral configuration with the largest angle [C(31)–P(1)–C(42), $105.8(5)^\circ$] and the smallest angle [C(31)–P(1)–C(48), $104.3(5)^\circ$]. Corresponding bond lengths and angles within **21** are equivalent.

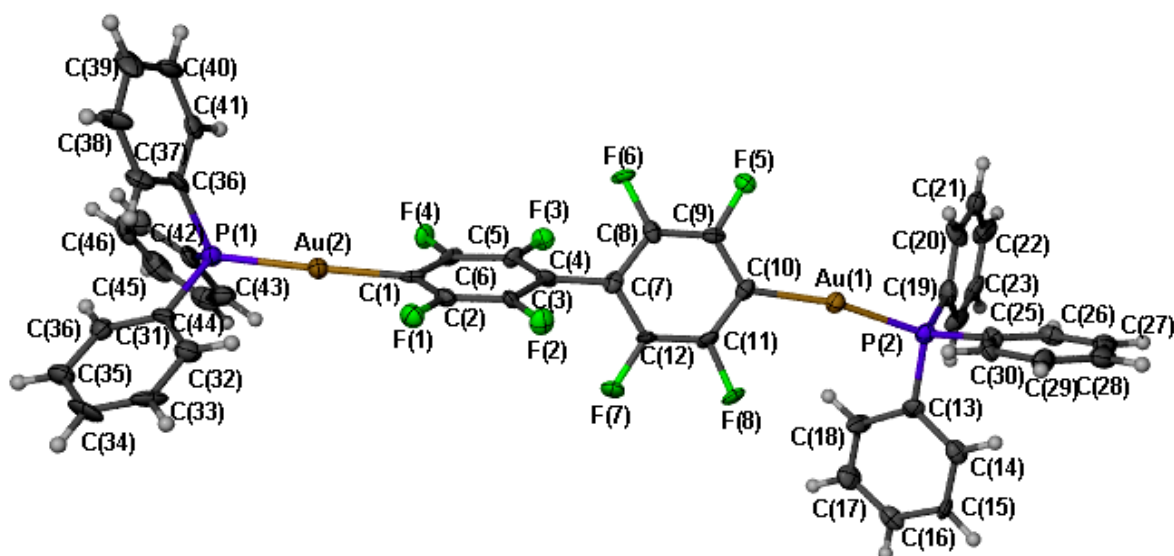


Figure 3.26 Molecular structure of **21**

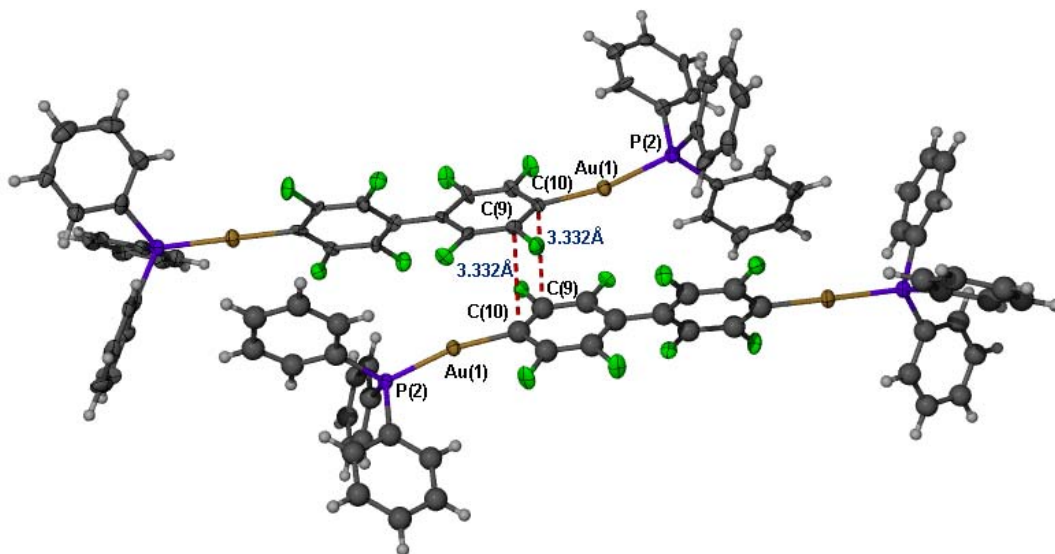


Figure 3.27 π -Stacking of the pentafluorophenyl rings through C(9) and C(10) over a distance of 3.33 Å

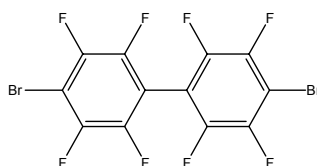
The structure of compound **21** is compared to the starting compound, 4,4-dibromooctafluorobiphenyl (Scheme 3.8, **XV**), described by Pilati *et al.*¹² The Au-PPh₃ unit in **21** may be compared to the same fragment in the structure of PPh₃-Au-C₆F₅ (**XVI**, Scheme 3.9), described by Baker *et al.*,¹³ as no gold containing structures similar to **21** could be found in the CCD.

All bond lengths in **21** are in the same order of the corresponding bond lengths in **XV**. The bond angles in **21** compared well to the bond angles in **XV**, except for the slightly smaller C(12)–C(11)–F(8) and F(4)–C(6)–C(5) bond angles in **21** (3° and 3.3° respectively), compared to the corresponding angles in **XV**.

All the corresponding bond lengths in **21** and **XVI** are equal. The C(10)–Au(1)–P(2) bond angle in **21** is 10.3° smaller than the C–Au–P bond angle in **XVI**, probably due to the steric requirements of the π -stacking of the tetrafluorophenyl rings. The C(48)–P(1)–Au(2) bond angle in **21** is 3.1° larger than the corresponding angle in **XVI**, the C(25)–P(2)–Au(1) bond angle in **21** is 7.1° larger than the corresponding angle in **XVI** and the C(13)–P(2)–Au(1) bond angle in **21** is 4.5° smaller than the corresponding Ph–P–Au angle in **XVI**.

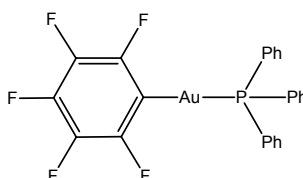
¹² T. Pilati, P. Metrangolo and G. Resnati, *Acta Crystallogr.*, **C 57** (2001) 113

¹³ R. W. Baker and P. J. Pauling, *J. Chem. Soc., Dalton Trans.* (1972) 2264



XV

Scheme 3.8



XVI

Scheme 3.9

Table 3.15 Selected bond lengths (Å) and angles (°) for compound **21**

P(2)–C(25)	1.800(1)	Au(1)–C(10)	2.030(1)
P(2)–C(19)	1.830(2)	Au(2)–C(1)	2.020(1)
P(2)–C(13)	1.830(1)	Au(1)–P(2)	2.269(3)
P(1)–C(31)	1.790(1)	Au(2)–P(1)	2.275(3)
P(1)–C(42)	1.810(1)	C(4)–C(7)	1.450(2)
P(1)–C(48)	1.830(1)		
C(10)–Au(1)–P(2)	167.5(3)	C(48)–P(1)–Au(2)	113.7(3)
C(1)–Au(2)–P(1)	177.9(3)	C(25)–P(2)–C(19)	105.1(5)
C(31)–P(1)–C(42)	105.8(5)	C(25)–P(2)–C(13)	104.8(5)
C(31)–P(1)–C(48)	104.3(5)	C(19)–P(2)–C(13)	105.0(5)
C(42)–P(1)–C(48)	105.6(5)	C(25)–P(2)–Au(1)	120.4(4)
C(31)–P(1)–Au(2)	113.1(4)	C(19)–P(2)–Au(1)	114.1(4)
C(42)–P(1)–Au(2)	113.5(4)	C(13)–P(2)–Au(1)	106.1(4)

Figures 3.28 and 3.29 show the unit cell packing of **21**. The molecules pack only on the corners of the unit cell, with an inversion centre on each corner of the unit cell. The molecules are interlocking: the triphenylphosphonium units slot into the space left by the neighbouring tetrafluorophenyl ring.

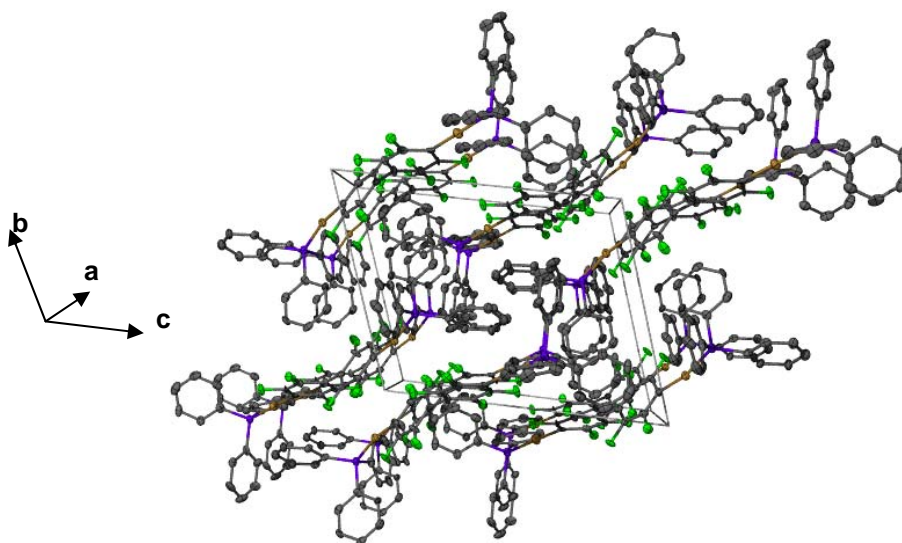


Figure 3.28 Packing diagram of **21** along the a-axis

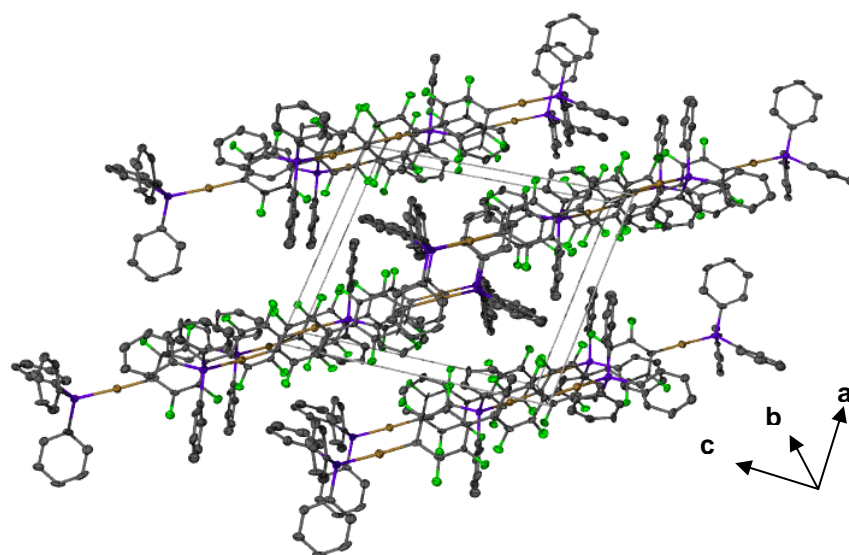


Figure 3.29 Packing of the unit cell of **21** along the b-axis

3.3 Conclusions

The molecular structures of the phosphonium salts **3a** and **4a** display very similar characteristics. The bond distances and bond angles of these two compounds do not differ significantly and their triphenylphosphonium units are orientated on the same side of the central phenyl ring. Hydrogen type bonding between the ethanol oxygen atom, the bromide ion and the triphenylphosphonium and methylene hydrogen atoms, determine the lattice arrangement.

The molecular structure of compound **5** confirmed the successful coordination of the ylide derived from benzyltriphenylphosphonium bromide to gold(I) and the same method of preparation was, therefore, used to prepare compounds **6**, **8**, and **9**. The goals for this project were achieved in the isolation and characterisation of compound **9**, as it is a novel, dinuclear gold(I)phosphonium ylide complex.

Valuable information about the reaction procedure was gained from the molecular structure of **10**, as it shows that the bromide ions present in the reaction mixture, coordinated to the gold(I) instead of coordination of the ylide. An alternative reaction procedure had to be used to coordinate the ylides to the gold(I) center.

The molecular structure of **15**, shows very interesting aurophilic interactions. This is the first example of a linear gold chain in which the intermolecular separation alternate between three significantly different distances (3.13 Å, 3.31 Å and 3.19 Å). In previously reported gold chains, these intermolecular distances are either all different or very similar to each other, or alternate between two different gold...gold distances.

Compound **21** is the first fluorobiphenyl gold(I) complex. The molecular structure of **21** revealed that one of the C–Au–P bond angles deviates from linearity by 12.5° [167.5(3)°], while the other C–Au–P bond angle is practically linear [177.9(3)] as expected for Au(I) compounds. π -Stacking of the tetrafluorophenyl rings over a distance of 3.332 Å probably causes the one C–Au–P bond angle to deviate considerably from linearity because of steric requirements of the bulky triphenylphosphonium units.

All the gold(I) bond angles are linear, with the largest deviation from linearity being 12.5° in compound **21**, due to the steric requirements of π -stacking by the tetrafluorophenyl rings. All the phosphorus atoms in the triphenylphosphonium units display tetrahedral symmetry with the smallest angle 103.4(3)° in compound **9** and the largest angle 111.2(3)° in compound **3a**, due to the orientation of the triphenylphosphonium units on either side of the central phenyl ring, facing one another on the same side of the plane formed by the central phenyl ring. Aurophilic interactions are seen only in compounds **15** and **17**. Lattice

organisation in the other compounds was determined by hydrogen bonding or π -stacking of the phenyl rings.

3.4 Experimental

The crystal data collection and refinement details for compounds **3a**, **4a**, **5**, **9**, **10**, **14**, **15**, **16**, **17** and **21** are summarised in Tables 3.16 – 3.25. All other crystallographic information of these structures is available from Prof. H. G. Raubenheimer, Department of Chemistry, University of Stellenbosch. All structure solution and refinement procedures were carried out by the author.

Crystal data for compounds **5** and **10** were collected on a NONIUS Kappa CCD-diffractometer¹⁴ using graphite monochromated Mo-K α radiation ($\lambda = 0.71073 \text{ \AA}$). The data sets were scaled, reduced and corrected for Lorenz and polarisation effects. The structures were solved with direct methods (SHELXS)¹⁵ and refined anisotropically for all non-hydrogen atoms by full-matrix least squares calculations (SHELXL-97) on F^2 . The program X-Seed¹⁶ was used as a graphical interface for structure solution and refinement using SHELX. All hydrogen atoms are placed in calculated positions. POV-Ray for Windows was used to generate the figures.

Crystal data for compounds **3a**, **4a**, **9**, **14**, **15**, **16**, **17** and **21** were collected on a Bruker SMART-Apex diffractometer using graphite monochromated Mo-K α radiation ($\lambda = 0.71073 \text{ \AA}$). The data sets were scaled, reduced and corrected for Lorenz and polarisation effects. The structures were solved with direct methods (SHELXS), except for the structure of **21**, which was solved by using the Patterson method (SHELXS). All the data sets were refined anisotropically for all non-hydrogen atoms by full-matrix least squares calculations (SHELXL-97) on F^2 . The program X-Seed¹⁶ was used as a graphical interface for structure solution and refinement using SHELX. All hydrogen atoms are placed in calculated positions. POV-Ray for Windows was used to generate the figures.

¹⁴ B. V. Nonius, "COLLECT, Data collection software" (1999) Delft, The Netherlands.

¹⁵ G. M. Sheldrick, SHELX-97. Program for crystal structure analysis, University of Göttingen, Germany, (1997)

¹⁶ a) L. J. Barbour, *J. Supramol. Chem.*, **1** (2001) 189, b) J. L. Atwood and L. J. Barbour, *Cryst. Growth Des.*, **3** (2003) 3

Table 3.16 Crystallographic data for **3a**

Chemical formula	C ₄₈ H ₅₀ Br ₂ O ₂ P ₂
Molecular weight (g.mol ⁻¹)	880.64 g.mol ⁻¹
Crystal system	Tetragonal
Space group	I4 ₁ /a
a (Å)	36.774(4)
b (Å)	36.774(4)
c (Å)	12.672(3)
α (°)	90
β (°)	90
γ (°)	90
Volume (Å ³)	17136(5)
Z	16
Calculated density (g.cm ⁻³)	1.365
Temperature (K)	173(2)
Absorption coefficient (mm ⁻¹)	2.004
2θ _{max} (°)	56.6
Crystal size (mm)	0.25 × 0.15 × 0.07
Index range	-47 ≤ h ≤ 48 -46 ≤ k ≤ 47 -16 ≤ l ≤ 13
No. of reflections collected	45612
No. of independent reflections	9442 (R _{int} = 0.1755)
Parameters	241
GooF (goodness of fit)	0.787
R ₁ (F _o > 2σF _o)	0.0729
wR ₂	0.1633
Largest peak	1.130
Deepest hole	-0.656

Table 3.17 Crystallographic data for **4a**

Chemical formula	C ₅₀ H ₅₅ Br ₂ O ₃ P ₂
Molecular weight (g.mol ⁻¹)	925.70
Crystal system	Triclinic
Space group	<i>P</i> -1
a (Å)	10.6152(7)
b (Å)	11.8454(8)
c (Å)	18.6863(13)
α (°)	98.0000(10)
β (°)	93.9380(10)
γ (°)	99.3800(10)
Volume (Å ³)	2285.6(3)
Z	2
Calculated density (g.cm ⁻³)	1.345
Temperature (K)	273(2)
Absorption coefficient (mm ⁻¹)	1.884
2θ _{max} (°)	56.5
Crystal size (mm)	0.21 × 0.27 × 0.11
Index range	-13 ≤ h ≤ 13 -15 ≤ k ≤ 15 -23 ≤ l ≤ 24
No. of reflections collected	26627
No. of independent reflections	10551 (R _{int} = 0.0343)
Parameters	519
GooF (goodness of fit)	1.043
R ₁ (F _o > 2σF _o)	0.0369
wR ₂	0.0872
Largest peak	0.786
Deepest hole	-0.324

Table 3.18 Crystallographic data for **5**

Chemical formula	C ₃₁ H ₂₁ Au ₁ F ₅ P ₁
Molecular weight (g.mol ⁻¹)	716.41
Crystal system	Orthorhombic
Space group	<i>P</i> 2 ₁ 2 ₁ 2 ₁
a (Å)	9.761(2)
b (Å)	15.390(3)
c (Å)	17.025(3)
α (°)	90
β (°)	90
γ (°)	90
Volume (Å ³)	2557.4(9)
Z	4
Calculated density (g.cm ⁻³)	1.861
Temperature (K)	173(2)
Absorption coefficient (mm ⁻¹)	5.871
2θ _{max} (°)	54.9
Crystal size (mm)	0.17 × 0.30 × 0.22
Index range	-12 ≤ h ≤ 12 -19 ≤ k ≤ 19 -22 ≤ l ≤ 22
No. of reflections collected	5842
No. of independent reflections	5842 (Data merged)
Parameters	343
<i>GooF</i> (goodness of fit)	1.327
R ₁ (F _o > 2σF _o)	0.0555
wR ₂	0.1584
Largest peak	1.476
Deepest hole	-0.977

Table 3.19 Crystallographic data for **9**

Chemical formula	C ₅₆ H ₃₆ Au ₂ F ₁₀ P ₂
Molecular weight (g.mol ⁻¹)	1354.72
Crystal system	Triclinic
Space group	<i>P</i> -1
a (Å)	13.3191(19)
b (Å)	13.5300(19)
c (Å)	14.453(2)
α (°)	104.022(2)
β (°)	107.468(2)
γ (°)	99.837(2)
Volume (Å ³)	2325.4(6)
Z	2
Calculated density (g.cm ⁻³)	1.935
Temperature (K)	100(2)
Absorption coefficient (mm ⁻¹)	6.451
2θ _{max} (°)	56.6
Crystal size (mm)	0.19 × 0.25 × 0.27
Index range	-17 ≤ h ≤ 17 -17 ≤ k ≤ 17 -19 ≤ l ≤ 19
No. of reflections collected	26436
No. of independent reflections	10599 (R _{int} = 0.0505)
Parameters	631
GooF (goodness of fit)	0.779
R ₁ (F _o > 2σF _o)	0.0430
wR ₂	0.1054
Largest peak	2.654
Deepest hole	-1.624

Table 3.20 Crystallographic data for **10**

Chemical formula	C ₅₈ H ₄₂ Au ₂ Br ₂ Cl ₄ F ₁₀ P ₂
Molecular weight (g.mol ⁻¹)	1686.41
Crystal system	Orthorhombic
Space group	<i>Pba2</i>
a (Å)	14.506(3)
b (Å)	22.083(4)
c (Å)	8.9439(18)
α (°)	90
β (°)	90
γ (°)	90
Volume (Å ³)	2865.1(10)
Z	2
Calculated density (g.cm ⁻³)	1.955
Temperature (K)	173(2)
Absorption coefficient (mm ⁻¹)	6.823
2θ _{max} (°)	55.0
Crystal size (mm)	0.13 × 0.27 × 0.19
Index range	-18 ≤ h ≤ 18 -28 ≤ k ≤ 28 -11 ≤ l ≤ 11
No. of reflections collected	60371
No. of independent reflections	6540 (R _{int} = 0.0416)
Parameters	354
GooF (goodness of fit)	1.071
R ₁ (F _o > 2σF _o)	0.0460
wR ₂	0.1306
Largest peak	1.230
Deepest hole	-2.623

Table 3.21 Crystallographic data for **14**

Chemical formula	C ₇₂ H ₆₆ Au ₂ F ₁₀ O ₂ P ₂
Molecular weight (g.mol ⁻¹)	1609.12
Crystal system	Orthorhombic
Space group	<i>Pbca</i>
a (Å)	21.4958(10)
b (Å)	12.4634(6)
c (Å)	23.3126(11)
α (°)	90
β (°)	90
γ (°)	90
Volume (Å ³)	6245.7(5)
Z	4
Calculated density (g.cm ⁻³)	1.711
Temperature (K)	273(2)
Absorption coefficient (mm ⁻¹)	4.821
2θ _{max} (°)	56.5
Crystal size (mm)	0.24 × 0.21 × 0.19
Index range	-28 ≤ h ≤ 24 -16 ≤ k ≤ 11 -30 ≤ l ≤ 30
No. of reflections collected	37140
No. of independent reflections	7450 (R _{int} = 0.0527)
Parameters	399
GooF (goodness of fit)	1.030
R ₁ (F _o > 2σF _o)	0.0371
wR ₂	0.0743
Largest peak	1.886
Deepest hole	-0.652

Table 3.22 Crystallographic data for **15**

Chemical formula	C ₂₂ H ₂₁ Au ₂ F ₁₀ O _{0.50} S ₂
Molecular weight (g.mol ⁻¹)	941.44
Crystal system	Orthorhombic
Space group	<i>Pbnb</i>
a (Å)	11.851(5)
b (Å)	18.664(8)
c (Å)	22.576(9)
α (°)	90
β (°)	90
γ (°)	90
Volume (Å ³)	4994(4)
Z	8
Calculated density (g.cm ⁻³)	2.504
Temperature (K)	100(2)
Absorption coefficient (mm ⁻¹)	11.993
2θ _{max} (°)	56.4
Crystal size (mm)	0.17 × 0.28 × 0.10
Index range	-14 ≤ h ≤ 15 -24 ≤ k ≤ 15 -29 ≤ l ≤ 22
No. of reflections collected	29015
No. of independent reflections	5819 (R _{int} = 0.1020)
Parameters	322
GooF (goodness of fit)	0.965
R ₁ (F _o > 2σF _o)	0.0515
wR ₂	0.0922
Largest peak	1.496
Deepest hole	-1.603

Table 3.23 Crystallographic data for **16**

Chemical formula	C ₆₈ H ₃₈ Au ₂ F ₂₀ P ₂
Molecular weight (g.mol ⁻¹)	1690.86
Crystal system	Triclinic
Space group	<i>P1</i>
a (Å)	9.6020(5)
b (Å)	10.3563(6)
c (Å)	16.4108(9)
α (°)	79.5810(10)
β (°)	87.1720(10)
γ (°)	63.8530(10)
Volume (Å ³)	1439.90(14)
Z	1
Calculated density (g.cm ⁻³)	1.950
Temperature (K)	100(2)
Absorption coefficient (mm ⁻¹)	5.254
2θ _{max} (°)	56.5
Crystal size (mm)	0.14 × 0.23 × 0.11
Index range	-12 ≤ h ≤ 12 -13 ≤ k ≤ 13 -21 ≤ l ≤ 20
No. of reflections collected	16622
No. of independent reflections	12598 (R _{int} = 0.0150)
Parameters	824
GooF (goodness of fit)	1.068
R ₁ (F _o > 2σF _o)	0.0208
wR ₂	0.0534
Largest peak	1.442
Deepest hole	-0.653

Table 3.24 Crystallographic data for **17**

Chemical formula	C ₈₂ H ₇₂ Au ₄ O ₄ P ₄
Molecular weight (g.mol ⁻¹)	2033.14
Crystal system	Monoclinic
Space group	<i>P2₁/c</i>
a (Å)	11.2834(7)
b (Å)	14.6283(9)
c (Å)	21.3770(13)
α (°)	90
β (°)	90.4010(10)
γ (°)	90
Volume (Å ³)	3528.3(4)
Z	2
Calculated density (g.cm ⁻³)	1.914
Temperature (K)	273(2)
Absorption coefficient (mm ⁻¹)	8.432
2θ _{max} (°)	56.7
Crystal size (mm)	0.13 × 0.28 × 0.14
Index range	-14 ≤ h ≤ 14 -16 ≤ k ≤ 18 -18 ≤ l ≤ 28
No. of reflections collected	21751
No. of independent reflections	8117 (R _{int} = 0.0330)
Parameters	426
GooF (goodness of fit)	0.857
R ₁ (F _o > 2σF _o)	0.0347
wR ₂	0.1080
Largest peak	2.062
Deepest hole	-2.169

Table 3.25 Crystallographic data for **21**

Chemical formula	C ₄₈ H ₃₀ Au ₂ F ₈ P ₂
Molecular weight (g.mol ⁻¹)	1214.59
Crystal system	Triclinic
Space group	<i>P</i> -1
a (Å)	11.935(3)
b (Å)	12.132(3)
c (Å)	15.224(3)
α (°)	107.103(3)
β (°)	97.704(4)
γ (°)	100.494(4)
Volume (Å ³)	2030.0(8)
Z	2
Calculated density (g.cm ⁻³)	1.987
Temperature (K)	173(2)
Absorption coefficient (mm ⁻¹)	7.370
2θ _{max} (°)	56.5
Crystal size (mm)	0.11 × 0.15 × 0.21
Index range	-15 ≤ h ≤ 15 -16 ≤ k ≤ 16 -19 ≤ l ≤ 19
No. of reflections collected	22406
No. of independent reflections	9203 (R _{int} = 0.0895)
Parameters	541
GooF (goodness of fit)	0.972
R ₁ (F _o > 2σF _o)	0.0574
wR ₂	0.1176
Largest peak	2.039
Deepest hole	-1.464